University of Padova

Department of Civil, Environmental and Architectural Engineering

Master Thesis in Environmental Engineering

Life Cycle Model to Address the Environmental Sustainability of Carbon Capture and Storage Systems

Supervisor
Prof. Alessandro Manzardo
University of Padova

Master Candidate
Milad Nooshadi

Student ID
2005512

Academic Year
2022-2023
02/03/2023

Acknowledgment

Prior to anything else, I would like to express my gratitude to my thesis supervisor, **Prof. Alessandro Manzardo**. In addition, I appreciate **Ing. Giovanna Paladin** for her assistance in using the Sima Pro environmental software. Finally, I wish to thank my family and friends for their support, encouragement, and understanding.

"For Woman, Life, Freedom"

Milad Nooshadi
Padova, Italy
March, 2023

Abstract

In an attempt to minimize greenhouse gas emissions and control the gradient of carbon concentration rise in the atmosphere, CO_2 capture, and storage (CCS) is gaining traction in many countries around the world. CCS refers to the capture and storage of the greenhouse gas (GHG) CO_2 in geological formations or other suitable storage places. CCS is well suited for large point sources of emissions, such as power plants and other industrial sites. Also, life cycle assessment (LCA) is a strategy that belongs to the family of lifecycle thinking approaches and is an effective instrument for assessing environmental performance which provides a more comprehensive view of environmental implications, including greenhouse gas (GHG) emissions, and allows decision-makers to quantify the trade-offs inherent in every modification to the power generation systems.

This thesis presents a life cycle assessment (LCA) on carbon dioxide capture and storage (CCS), creating a comprehensive LCA methodology for the "Gate-to-Gate" evaluation of potential CCS technologies. Life Cycle Inventory (LCI) database that represents inputs/outputs of processes at a high degree of detail, adjusts for technological and regional variances, produces LCI data in a consistent and transparent way, and has a flexible structure has been designed and organized. All CO_2 capture and storage methods will show an increase in cumulative energy demand with environmental effects and a significant reduction in greenhouse gas (GHG) emissions.

The proposed LCI models were effectively used to post-combustion chemical absorption capture, pipeline transportation, and saline aquifer storage. This study examines the LCI models for chemical absorption CO_2 capture base on empirical relationships, with the aim of introducing more parameters into the LCI model for CO_2 conditioning in post-combustion CO_2 capture. Furthermore, the designed LCI model provides a flexible framework for estimating energy consumption and emissions from CO_2 pipeline transportation and injection. Then, using LCA modeling of geological storage, calculate CO_2 distribution in the saline aquifer and evaluate multiple models of CO_2 leakage through different paths. Lastly, by Implementing a case study of a carbon capture, transportation, and storage project at the Asnaes coal power station in Kalundborg, Denmark, and the life cycle impact assessment (LCIA), a model is presented that not only quantifies the emissions from the constructed system and the relating LCA environmental impacts, but also analyzes the variation through the provided sensitivity analysis, operational conditions, reservoir characteristics, and alternative leakage pathway parameters that have a significant effect on the LCA environmental impact results.

Consequently, post-combustion chemical absorption (MEA) CO_2 capture unit captures 95% of CO_2 and emits less PM-10, SO_2, SO_3, NO_2, HCl, HF, mercury (Hg) vapor. As well, MEA production, MEA transport, CO_2 pipeline infrastructure, CO_2 capture facility infras-

tructure, and compressor infrastructure, have very modest life-cycle environmental effects. The AP, EP, GWP, HTP, and POCP are all significantly impacted by emissions into the atmosphere. Trace metal emissions to the air or soil are the primary causes of the FAETP and TETP. Also, changes in the capture rate and the required amount of energy can have a significant effect on all of the categories. In contrast, the length of the pipeline and the transport pressure do not affect the life-cycle impacts in the majority of categories. Using K PZ or KS1 to chemically absorb CO_2 has a smaller environmental impact than using MEA to achieve the same result. Lastly, the ratio of potential CO_2 leakage to total CO_2 injected is sensitive to changes in the injection period and injection rate.

Keywords: Carbon Capture, Carbon Storage, Carbon Transportation, LCA

Contents

List of Figures

List of Tables

List of acronyms

Ag ..... Silver

AMP 2-amino-2

As ..... Arsenic

Ba ..... Barium

BAT ..... Best Available Techniques

Be ..... Beryllium

CBA ..... Costs Benefit Analysis

CCL ..... Compacted Clay Liner

CCS ..... Carbon Dioxide Capture and Storage

CH_3Br ..... Methyl Bromide

CH_4 ..... Methane

Cl ..... Chlorines

CML ..... Centre of Environmental Science

Co ..... Cobalt

CO_2 ..... Carbon Dioxide

CO_2CRC ..... Cooperative Research Centre for Greenhouse Gas Technologies

Cr ..... Chromium

Cu ..... Copper

DEA ..... Diethanolamine

DMI ..... Direct Material Input

EA ..... Energy Analysis

EC ..... European Commission

ECBM ..... Enhanced Coalbed Methane

EGR ..... Enhanced Gas Recovery

EIA ..... Environmental Impact Assessment

EMS ..... Environmental Management System

ELS ..... Eco-Label Scheme

EOR ..... Enhanced Oil Recovery

EP ..... Eutrophication Potential

EPA ..... Environmental Protection Agency

EPD ..... Environmental Product Declarations

FGD ..... Flue Gas Desulphurisation

GaBi ..... GaBi LCA software

GHGs ..... Greenhouse Gases

GTL ..... Gas to Liquid

GWP ..... Global Warming Potential

H ..... Hydrogen

HCFCs ..... Hydrochlorofluorocarbons

HCL ..... Hydrochloric Acid

HEED ..... Hydroxyethyl ethylenediamine

HEI ..... Hydroxyethyl imidazolidone HF: Hydroflouric Acid

HF ..... Hydroflouric Acid

Hg ..... Mercury

HTP ..... Human toxicity Potential

IOA ..... Inpute-Output Analysis

IPCC ..... Intergovernmental Panel on Climate Change

IPP ..... Integrated Product Policy

ISO ..... International Organisation for Standardisation

KS1 ..... A kind of hindered amine developed by Japanese company Mitsubishi

K+ /PZ ..... Promoted potassium carbonate

LCA ..... Life Cycle Assessment

LCI ..... Life Cycle Inventory

LCIA ..... Life Cycle Impact Assessment

LCM ..... Life-Cycle Management

MAC ..... Main Air Compressor

MDEA ..... N-methyldiethanolamine

MEA ..... Monoethanolamine

MIPS ..... Material Intensity Per Unit Service

Mn ..... Manganese

N ..... Nitrogen

NH_3 ..... Ammonia

Ni ..... Nickel

NMHC ..... Non-methane hydrocarbon

NMVOC ..... Non-Methane Volatile Organic Compounds

NO ..... Nitrogen Oxide

NO_2 ..... Nitrogen Dioxide

NOx ..... Nitrogen Oxides

O ..... Oxygen

ODP ..... Ozone Depletion Potential

Pb . . . . . Lead

PCF . . . . . Pulverised coal fired power plant

PCFs . . . . . Perfluorochemicals

PDF . . . . . Probability Distribution Functions

PM . . . . . Particulate Matter

POCP . . . . . Photochemical Oxidant Creation Potential

POX . . . . . Partial Oxidation

PPM . . . . . Part Per Million

S . . . . . Sulfur

Sb . . . . . Antimony

SCR . . . . . Selective Catalyst NOx Reduction

Se . . . . . Selenium

SEA . . . . . Strategic Environmental Assessment

SOx . . . . . Sulfur Oxides

TDS . . . . . Total Dissolved Solids

TEA . . . . . Triethaolamine

TETP . . . . . Terrestrial Ecotoxicity Potential

Ti . . . . . Thallium

TMR . . . . . Total Material Requirement

V . . . . . Vanadium

Zn . . . . . Zinc

1

Introduction

Because of the fast rise in both technology and the population of the world, there has been a substantial increase in the usage of fossil fuels, which are only attainable in limited amounts and have a negative impact on the environment [36, 37]. Fossil fuels are accountable for around 86% of the world's energy consumption and approximately 75% of the anthropogenic CO_2 emissions that are occurring today. According to the Intergovernmental Panel on Climate Change (IPCC), the total emissions that resulted from the burning of fossil fuels and the flaring of natural gas amounted to 10 billion tons of carbon.

Several efforts have been made to reduce the negative effects that the use of fossil fuel has on the environment. These efforts have focused on enhancing the effectiveness of the processes that are now in use and inventing novel methods and technologies for the conversion of energy. In an effort to minimize greenhouse gas emissions and control the gradient of carbon concentration increase in the atmosphere, CO_2 capture and storage (CCS) is gaining traction in many nations across the world. CCS refers to the capture and storage of the greenhouse gas (GHG)

carbon dioxide in suitable storage locations, such as depleted oil and gas fields, aquifers, and other geological or ocean formations. Large point emission sources, such as power plants and other industrial facilities, such as cement and ammonia plants, refineries, petrochemical and hydrogen plants, are ideal candidates for carbon capture and storage. In these cases, it is more economically possible to capture CO_2, compress it, and transport it to a disposal location than in cases involving small or mobile CO_2 sources. CCS may theoretically be used to CO_2 emissions from biomass facilities, therefore functioning as a carbon sink. Figure 1.1 summarizes the indicated explanations.

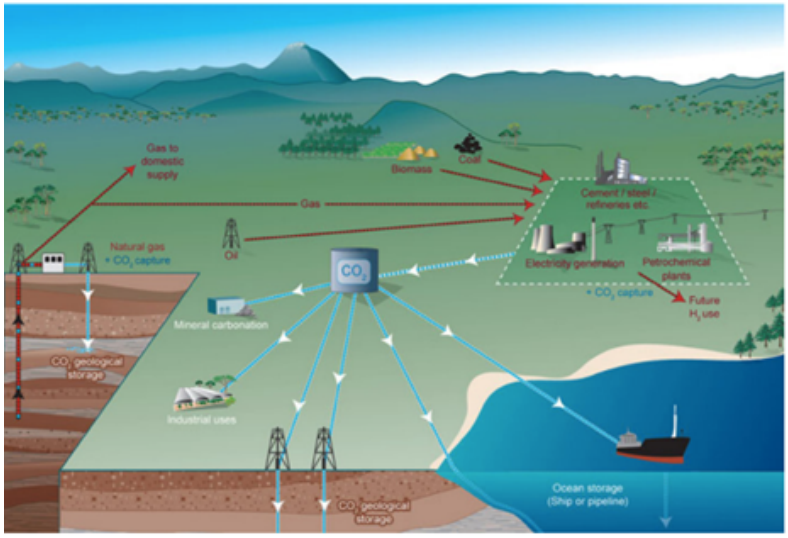

Figure 1.1: Schematic view of CCS chain [1].

Currently, the majority of existing CCS technology can absorb between 85 and 95% of a power plant's CO_2 emissions. Unfortunately, the majority of power plants with CCS systems would use more energy than those without CCS facilities. This additional energy is mostly required for CO_2 capture and compression, which provide 10–40% more energy to conventional power plants [38, 39]. According to [40], the impact of CCS technology on existing power plants shows the increased CO_2 emissions caused by CCS as well as the total net emission decrease caused by CCS. Once CO_2 is effectively absorbed and stored, CCS technology can contribute to an 80–90% decrease in total atmospheric emissions. The disadvantage of

integrating CCS technology with power plant systems is that more energy will be required; hence, there is a penalty on the energy efficiency of the power cycles. In addition, the higher consumption of chemicals needed for CO_2 capture, such as monoethanolamine (MEA), leads in an increase in both on-site and upstream GHG emissions as well as other environmental consequences per kWh generated in comparison to plants that do not utilize CO_2 capture.

The known and currently developed CCS technologies provide a variety of options with varying energy consumptions and environmental impacts. Consequently, it is essential to perform a comprehensive environmental assessment on alternative CCS options that is capable of analyzing GHG releases throughout all stages of the life cycle and providing accurate data to stakeholders to guarantee that a CCS option selected does not lead in upstream or downstream changes that raise the total release of GHGs and does not increase other environmental issues, such as the formation of solid and hazardous waste and the release of toxic compounds that negatively affect human health and ecological systems. Life cycle assessment (LCA) satisfies this principle because it not only tracks energy- and non-energy-related GHG emissions, but also numerous other environmental emissions such as common air pollutants, as well as the consumption of other resources such as water, minerals, and land.

To make sure that cutting back on greenhouse gas emissions doesn't have unintended negative consequences, LCA provides decision-makers with a comprehensive view of the potential effects of alternate energy strategies. The ISO 14040 series of LCA standards was developed by the International Organization for Standardization (ISO) in order to provide guidance on a variety of LCA-related topics, including but not limited to: system boundary definition; data collection; evaluation of environmental impacts; interpretation of results; and transparent reporting [41]. Also, it can be useful to note that in order to assist polluters in developed countries in meeting their GHG emission objectives, the Kyoto Protocol established three flexible mechanisms: emissions trading, joint implementation, and the clean development mechanism (CMD).

LCA, being a globally recognized method, provides a way to include CCS projects within

the CDM framework and assists participants of flexible mechanisms in evaluating their project proposals and confirming their emission reductions. Previous life-cycle assessment (LCA) studies have looked into alternative CO_2 capture and storage systems [42, 43, 44, 45, 46] and found that CO_2 capture can cut CO_2 emissions by around 80% across the board in the life cycle. [32] evaluated post-combustion CO_2 capture, transport, and injection using complete Life Cycle Impact categories, although the research is case specific, and the storage procedures are not fully investigated.

In order to fully characterize the environmental profiles of various CCS technologies and account for technical and geographical variations, a comprehensive and dynamic LCA model adapted to CCS is required. This thesis's research has the following primary goals:

1. Designing a full Gate-to-Gate LCA framework for evaluating CCS alternatives;
2. Creating a quantitative Life Cycle Inventory (LCI) database that represents inputs/outputs of processes at a high degree of detail, aiming at exact LCI data in a consistent and open way, and has a flexible system for long term strategic energy system planning;
3. Assessing the relative benefits of various CCS technology and to discover possibilities for making life-cycle reductions in terms of both energy and environmental impacts.

This thesis is divided into five chapters. The chapter 2 provides an overview of different CO_2 capture technologies, transportation systems, and CO_2 geological storage options. This chapter also presents the methodological framework of LCA and previous LCA applications on CCS, as well as the limitations of previous LCA applications. The chapter 3 develops a comprehensive framework for the application of LCA on alternative CCS options, which can characterize the environmental profiles of the CCS technologies at a high level of detail, account for technical and spatial differences, and quantify the uncertainty of LCA results. Life cycle inventory (LCI) modeling approach for component operations in post-combustion CO_2 capture power plants, including the LCI models of chemical absorption CO_2 capture and CO_2 conditioning units, CO_2 pipeline transportation and CO_2 injection, and the modelling of CO_2 saline storage are done in this part. The chapter 4 begins with a discussion of a case study to apply the life cycle impact assessment (LCIA). This chapter generates the consequences of direct

emissions, resource consumption, and the materials required to construct systems. In addition, the LCIA analysis, sensitivity analysis, and uncertainty analysis in terms of Post-combustion capture system, transportation, and injection, as well as the uncertainties associated with the potential CO_2 leakages in terms of CO_2 storage, are performed to identify the opportunities to reduce the environmental impacts from a life-cycle perspective. Finally, chapter 5 summarizes the study's findings, highlights its achievements, and offers suggestions for further study.

2

CCS Technology & LCA Methodology

2.1 Introduction

Since it is widely acknowledged that no single technology can fully realize the potential strategy for mitigation in any given sector, the century's energy demands will be encountered while also achieving goals for reducing greenhouse gas emissions through the use of a broad range of technologies that are either already in use or are anticipated to accomplish this in the near future [4, 47]. Carbon capture and storage (CCS) is a promising solution for mitigating global warming by removing CO_2, the most significant greenhouse gas (GHG), from the atmosphere. The CO_2 will be captured at the source, transferred to an appropriate storage location, and stored for geological time scales. The process chain is made up of three parts: CO_2 capture, transportation, and storage.

Life Cycle Assessment (LCA) is a powerful tool for evaluating environmental performance in the family of life-cycle thinking methods. With more than 30 years of development since the

LCA concept was introduced in 1969, the methodology of LCA is widely accepted and well-established [48]. CO_2 capture and storage systems require considerable quantities of energy to operate, and the CCS technologies available provide a variety of solutions with varying energy requirements and, as a result, various environmental implications. The well-established LCA method provides the necessary methodological framework to ensure that a given CCS option, in addition to reducing CO_2 emissions, does not result in a significant increase in other environmental impacts, and to identify opportunities for improved designs that minimize environmental impacts along the CCS chain. Furthermore, the application of LCA is consistent with the life-cycle thinking of present environmental laws and anticipated future legislation.

This chapter initially explains The implementation of CCS (i.e. in power plants) is comprised of three major phases. These include CO_2 separation from the power plant stream, often known as carbon capture (CC), CO_2 transportation, and CO_2 storage. In the second part are presented LCA and the LCA methodological framework, then addresses the application of LCA at the social and organizational levels, including the method's limits and current LCA development trends, also it examines prior LCA studies on CCS and discusses its shortcomings. Following that, the modeling technique of this research with representing system modeling is described.

2.2 CCS Technology

2.2.1 CO_2 Capture (CC)

Capturing CO_2 from the power plant process normally requires CO_2 to be separated from the flue gases at some stage throughout the process. Post-combustion, Pre-combustion, and Oxy-fuel combustion capture are three ways to connect CO_2 capture technology with power production systems.

The objective of CO_2 capture is to generate a stream of concentrated CO_2 that is easily transportable and storable. Diverse techniques have been developed for capturing CO_2 from

gas streams. These methodologies and their underlying assumptions are as follows: Physical and chemical absorption, Adsorption, and Membrane separation.

2.2.1.1 Post-combustion CC

This approach involves separating CO_2 from flue gases produced from large-scale fossil fuel combustion like boilers, cement kilns, and industrial furnaces. Figure 2.1 shows post-combustion CC technology in a typical layout for the absorption process. Today absorption process using chemical solvents like amine is often used in the CC from a number of power plants. The hot flue gas is cooled to temperatures between 40 and 60 °C and then introduced to the absorber, where CO_2 bonds with the chemical solvent. The CO_2-rich solvent is then pumped to a stripper where the solvent is heated for solvent regeneration between 100 and 140 °C, and CO_2 is stripped off [2, 49]. There are lots of energy requirements for operating the pumps, blower and compressors, and heating, which creates an efficiency penalty [50, 51]. The fuel type determines the CO_2 content in the flue gas, and a typical CO_2 recovery of 80–90% can be realized in the CC absorption process. Removal of nitrogen oxides NOx and sulfur oxides SOx to prevent them from reacting with the solvent, and hence maximize CC is possible [52]. Use of solid sorbents like calcium oxide, pressure swing adsorption, and membrane separation have all been studied as well for CC [53, 54].

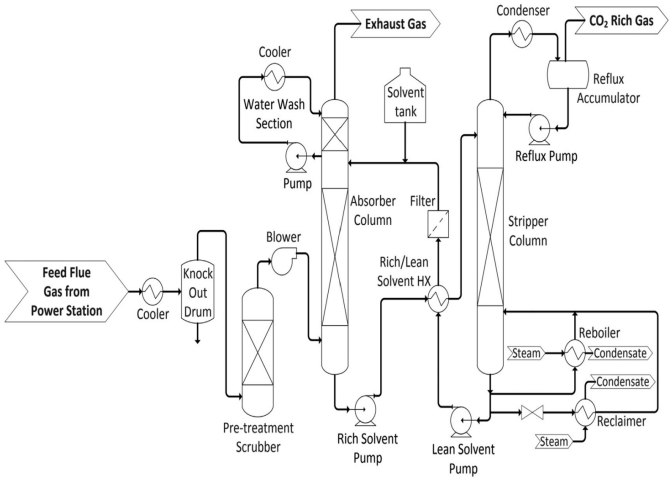

Figure 2.1: Post-combustion carbon capture process [2].

2.2.1.2 Pre-combustion CC

The pre-combustion CC involves syngas (a mixture of hydrogen H_2 and carbon monoxide CO) being produced from fuel reforming followed by CO_2 separation, as shown in Figure 2.2 Fuel reforming and partial oxidation are the major processes that lead to the formation of the synthesis gas. In steam reforming, steam reacts with fuel in a partial oxidation reaction [3]. The process also involves eliminating sulfur and particulate matter as a pretreatment to maintain catalyst operability and activity. The process net result is capturing CO_2 and hydrogen gas to be used as fuel, with water as the ultimate combustion product.

2.2.1.3 Oxy-fuel Combustion CC

The oxy-fuel combustion CC includes burning fossil fuel in pure oxygen, leading to nitrogen-free flue gas production with only CO_2 and H_2O. The flue gas condensation leads to a pure CO_2 stream being produced, as well as the elimination of NOx gases. Figure 2.3 explains the process of oxy-fuel combustion in a coal-fired power plant.

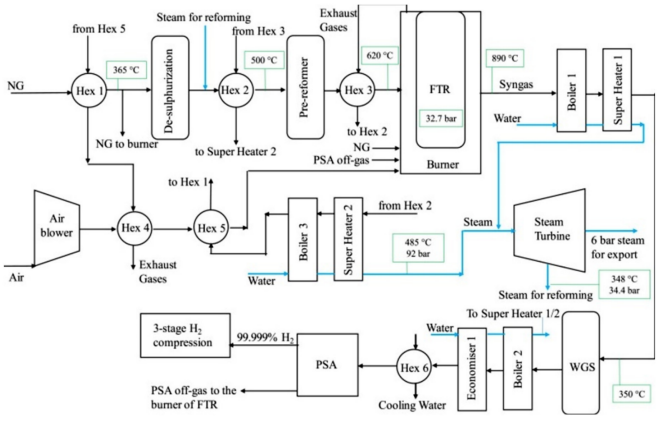

Figure 2.2: Gas reforming with carbon capture [3].

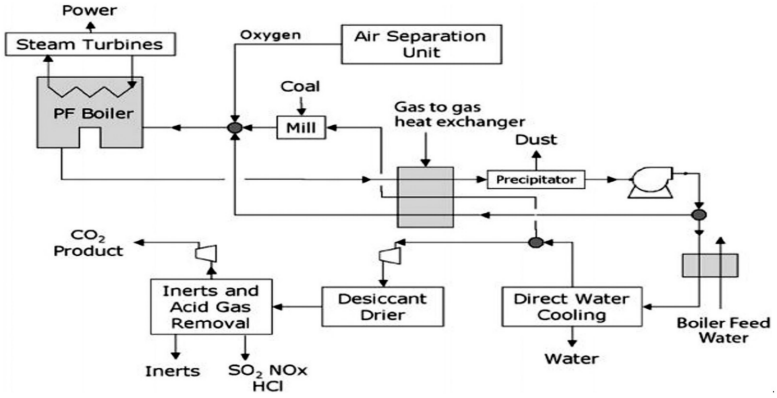

Figure 2.3: Oxy-fuel carbon capture [4].

2.2.1.4 Physical and Chemical Absorption

Carbon dioxide separation for post- and pre-combustion CC occurs in two steps; absorption and stripping process. In absorption, the gas stream is fixed physically with the solvent stream. In the stripping process, the CO_2 rich solvent is heated to regenerate the solvent and strip off CO_2 gas, as depicted in Figure 2.4 The main principle in physical CO_2 absorption is Henry's law. In the absence of any form of alteration of the chemical identities of CO_2 and the solvent, the breakdown of CO_2 in the liquid solvent is due to the electrostatic interaction or Van der Waals attraction forces [3, 55]. Physical absorption is relatively better under higher pressure but lower temperature conditions. Lower pressure and higher temperature will be ideal for

physical desorption or stripping. These conditions tend to make physical absorbents attain higher absorption characteristics compared to chemical absorbents [56].

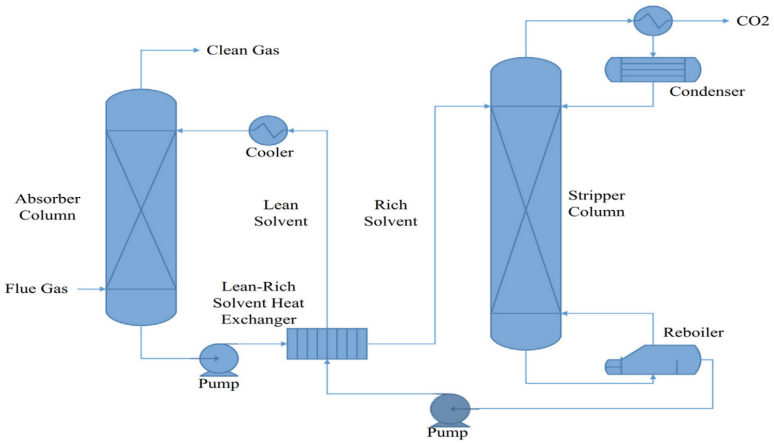

Figure 2.4: Schematic of the absorption-stripping technique [5].

2.2.1.5 Adsorption technique

The adsorption process involves forming physical or chemical interactions between the adsorbate, i.e., CO_2, and the surface of the solid adsorbent. The adsorbed CO_2 can be desorbed later either by decreasing the pressure or increasing the temperature, commonly referred to as pressure-swing or temperature-swing adsorption, respectively, in a similar approach to that of absorption. The pressure-swinging adsorption process is utilized for high CO_2 partial pressure, while temperature-swinging adsorption is often preferred when the concentration of the CO_2 being is lower. The pressure-swinging adsorption process is normally preferred because it requires a shorter time adsorbent regeneration. Some notable advantages of adsorption include high loading capacity at ambient conditions, lower energy demand, and economic regeneration. Other merits include good mechanical and chemical stability, high adsorption rate, simple operation, easy system maintenance, and tolerance to impurities in flue gas [57]. Some common types of physical adsorbents include activated carbon, zeolite, silica membrane, and metal-organic framework materials (MOF). The chemical adsorbents, on the other hand, are

made up of calcium oxide (CaO), lithium metal-based, and solid amines sorbents [58, 59].

2.2.1.6 Membrane technology

Separation with the aid of a membrane occurs via the Knudsen diffusion principle and Fick's molecular diffusion [60]. The elimination of CO_2 from natural gas is best carried out using membrane separation technology, which is ideal for precombustion capture as well, especially for high CO_2 partial pressure [61] (See Figure 2.5). In the case of CC from low CO_2 in flue gas, a higher energy penalty is imposed [49, 50].

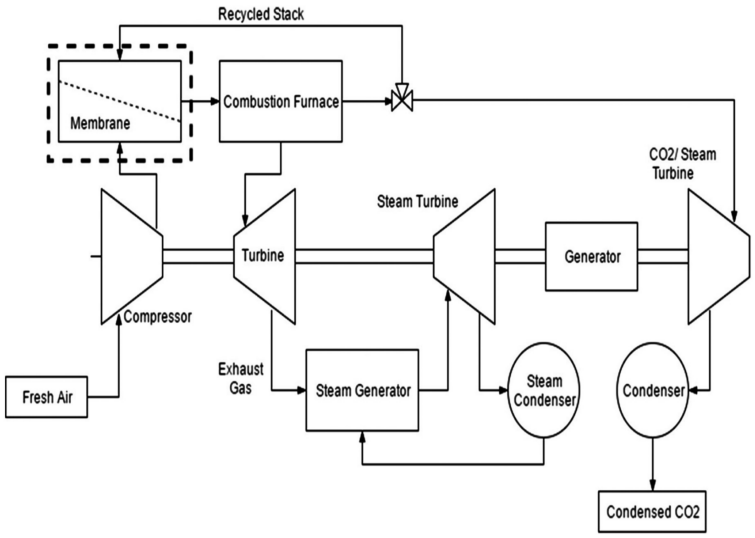

Figure 2.5: Membrane process for CO_2 capture [5].

2.2.2 Transportation

After CO_2 is separated, it must be transported to the appropriate destination. The gas must first be compressed and transported in a supercritical condition, with the critical point of CO_2 at 31 °C and 73.77 bar, where its density is 500 times that of the gaseous state [62]. To avoid the two-phase flow regime, carbon dioxide is often compressed to a pressure above 80 bar. This technique also aims to increase the CO_2's density, hence making the transportation process

easier and less expensive. It can be developed for both onshore and offshore CO_2 transport in a manner similar to that employed in the oil and gas sector. The onshore pipes are positioned at a depth of 1 meter, whilst the offshore pipelines are installed in shallow waters [63]. Among the possible transportation options are the CO_2 transport by pipeline, ship, railway or truck.

2.2.2.1 Pipeline

The transportation of CO_2 by pipeline is a proven technology. Besides, there is a high degree of experience and know-how, especially in the field of natural gas and oil pipelines that can be transferred to CO_2 transport. At present, there is globally about 3100 km of CO_2 pipelines, especially in the USA & Canada, with a transport capacity of 44.7 Mt CO_2 per year [64]. Several physical and environmental aspects must be examined and determined while designing a pipeline. The appropriate size and pressure of the pipeline are determined by the condition of the CO_2 being transferred. Other elements, such as the initial compressor station, intermediate pumping or recompression stations, section and safety valves, cathodic corrosion protection, and stations for corrosion monitoring, must be considered in addition to the piping made of high-quality carbon steel that has been coated against external corrosion and mechanical damage [65] (See Figure 2.6).

Consideration of the pressure that must always be above the critical point of 73.9 bar with a temperature of 31.1 °C is an essential part of pipeline design (cf. Annex A.I). In the literature [65], a minimum pressure of 80 bar is frequently necessary to provide a margin of safety. As a result of the friction induced by the roughness of the pipe, a pressure decrease occurs during CO_2 transit down the pipeline. To compensate for this pressure loss, compressor stations or a greater beginning pressure may be required across long distances. In the research, compressor stations are deemed necessary for routes more than 150 kilometers [29]; nevertheless, in practice, distances of 400 kilometers or more are deemed practical [4]. The key parameters that influence the pressure drop are the pipe's roughness, the mass flow, and the pipe's inner diameter.

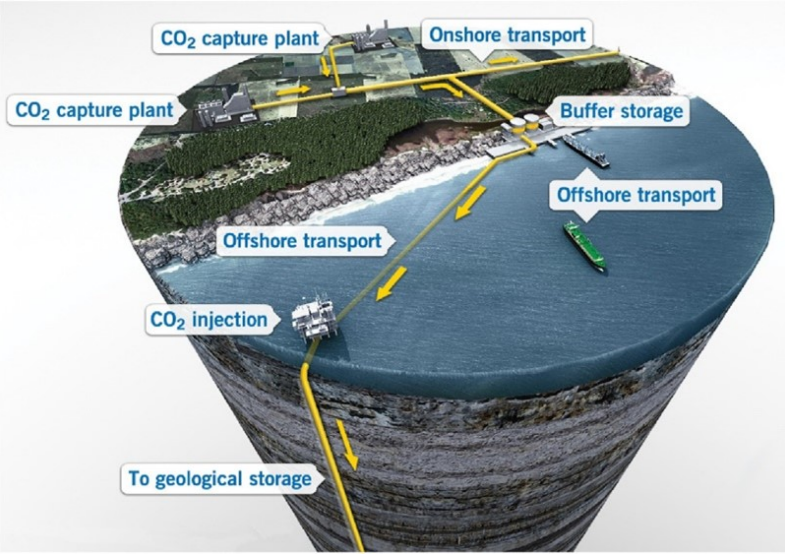

Figure 2.6: CCS transportation pilpeline [6].

2.2.2.2 Ship

Transporting CO_2 to the injection location via ship is a versatile option. However, because to its discontinuous aspect, the continually acquired CO_2 at the plant requires interim storage. Consequently, more space, materials, and energy are necessary for intermediate storage. The greater the distance, the more economical ship travel becomes. According to [4], the break-even distance for a system with a transport capacity of 6 Mt/yr is around 1000 km. However, transporting greater quantities of CO_2 pushes the break-even threshold to greater distances. The transport by ship is comparable to the transfer of LPG via ship. The creation of the ship, tank, operation, and onshore loading system for the transport of LPG can be based on current technologies. In addition, fresh concepts must be created for the unloading procedure and liquefaction plant.

There are three types of CO_2 transport ships: a) pressure type/fully pressurized operating at high pressure to prevent gas from boiling under ambient temperature conditions; b) low-temperature type/fully refrigerated ship operating at a sufficiently low temperature to keep gas as a liquid (or) under atmospheric pressure a solid; and c) semi-refrigerated type/semi-

pressurized combined conditions of temperature and pressure required to keep gas as a liquid. The semi-pressurized vessel transfers CO_2 in the liquid phase at temperatures below ambient temperature and pressures above atmospheric pressure. This design is favored by ship designers. The design parameter is roughly -54°C per 6 bar to -50°C at 7 pressure for conveying an approximate amount of 22000 m3 [4]. The completely refrigerated ship delivers CO_2 in solid form as extremely dense dry ice. However, this solution does not appear to be economically viable due to the complicated loading and unloading operations and the significant energy need for refrigeration.

2.2.2.3 Truck and Railway

Compared to pipelines or ships, transportation via truck or railroad has substantially lower transit capacity. Technically, it is possible to transport CO_2 in a liquid state at a pressure of 2 MPa and a temperature of -20 °C. These solutions are less desirable and more expensive than other choices like shipping or pipeline when it comes to long-distance and large-volume CO_2 transportation for CCS. These alternatives could be a better choice only in very small-scale situations or in situations where flexibility is crucial [4] [65].

2.2.3 Storage

Carbon sequestration refers to the process of storing carbon in a carbon storage. Biological, chemical, and physical processes remove carbon dioxide from the atmosphere in a natural manner. Physical mechanisms include those relating to biomass, ocean storage, and geological storage. This thesis analyses geological storage and its characteristics.

2.2.3.1 Carbon Dioxide Storage Mechanisms

Geological sequestration of CO_2 is the process of directly capturing CO_2 from anthropogenic sources and storing it indefinitely inside geological formations. Combinations of physical and chemical trapping techniques, such as structural and stratigraphic trapping, residual CO_2 trap-

ping, solubility trapping, mineral trapping, and adsorption trapping, can be used to collect CO_2 in geologic formations.

Structural and stratigraphic trapping refers to trapping CO_2 below low-permeability seals (caprocks), such as very-low-permeability shale or salt beds, which is the principal means to store CO_2 in geological formations. Structural traps comprise folded or fractured rocks. Faults can act as permeability barriers in some circumstances and as CO_2 leakage pathways in other circumstances [66]. **Residual trapping** refers to the process of sequestering carbon dioxide as a residual, non-wetting phase in the pore spaces of rock. When CO_2 is injected into a saline formation, it displaces the salty formation water and migrates upwards because it is less dense than the formation water. **Solubility trapping** relates to the dissolution of CO_2 in formation water or the interactions between CO_2 and water that result in the creation of carbonic acid and other aqueous carbonate species [67]. During CO_2 flooding EOR, when the injected CO_2 dissolves in the crude oil stored in the reservoir, solubility trapping also occurs [67]. In **mineral trapping**, dissolved CO_2 undergoes chemical reactions with the sodium and potassium basic silicate, or calcium, magnesium, and iron carbonate, or silicate minerals in the reservoir formation to form bicarbonate ions, and continued reaction of the bicarbonate ions with calcium, magnesium, and iron from silicate minerals such as clays, micas, chlorites, and feldspars present in the rock matrix to finally form carbonate minerals [4]. In **physical adsorption**, CO_2 molecules are immobilized on the micropore wall surfaces of coal organic matter, kerogen, or minerals at near liquid-like densities [67]. Hydrostatic pressure in the formation regulates the gas adsorption procedure [4]. Coal seams and shales are examples of physical adsorption trapping geological formations [68].

2.2.3.2 Carbon Dioxide Geological Storage Operations

For an area to be ideal for CO_2 storage, it must possess properties such as adequate storage capacity, injectivity, a good confining unit or sealing caprock, and a stable geological environment. As indicated in Figure 2.7, CO_2 can be sequestered using one of three methods. The first

has to do with utilizing both active and depleted oil and gas fields for the recovery of oil and gas, where it aids in achieving increased oil or gas recovery (EOR and EOG). Enhanced coalbed methane (ECBM) recovery involves deep, non-minable coal layers that are capable of boosting methane recovery. The last possibility is deep saline aquifers. [69].

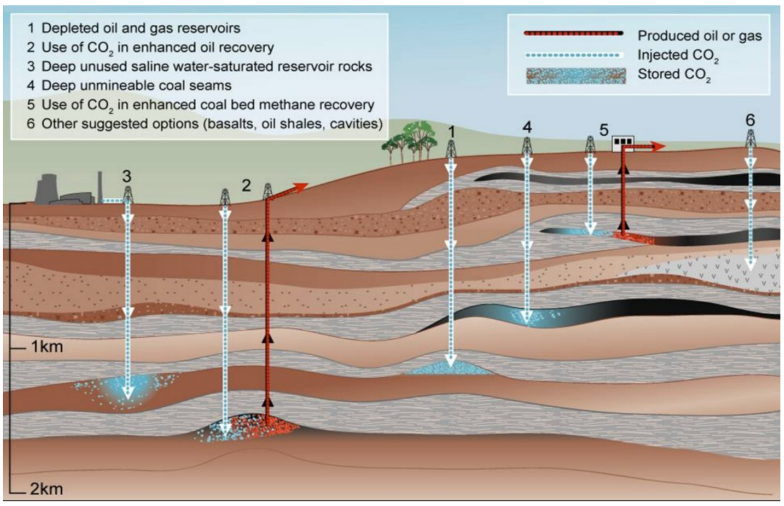

Figure 2.7: An overview of geological storage options [7].

Depleted Oil and Gas Fields

As oil and gas reserves, porous rock formations containing physically trapped hydrocarbons are deemed acceptable. Carbon sequestration in depleted oil and gas reservoirs comes into two distinct categories. The first is stratigraphic traps, which are caused by variations in rock types, and the second is structural traps. These abandoned sites are considered suitable for CO_2 storage because for millions of years they accumulated hydrocarbons. Enhance oil recovery (EOR) and enhanced gas recovery (EGR) have a low capacity compared to other CO_2 sequestration strategies, but they are well-established, with well-defined features and geological data, and are thus often favored [70]. Some of these locations have a total carbon dioxide retention rate of up to 60% [71, 72, 73]. The best location for CO_2 storage is one where structural and stratigraphic characteristics, in combination with solubility, permit the injection of CO_2 for millions of years [74]. Residual and solubility trapping techniques can be utilized for this purpose; hence, it is

crucial to implement regulatory and monitoring frameworks to verify that these approaches are being utilized properly. Because gaseous CO_2 dissolves in water to generate carbonic acid, it may remove oil from porous media and assure a drop in viscosity, which raises the injectivity index. This method of EOR is based on molecular diffusion because it allows for the mixing of CO_2 and oil at the pore level using a rate-controlling strategy that promotes the oil-miscibility. For instance, Weyburn CO_2-enhanced oil recovery (CO_2-EOR) project located in the Williston Basin (Canada) is expected to inject 23 $MtCO_2$ and extend the life of the oil field by 25 years [75].

Coalbed Methane Recovery

As CO_2 is used to enhance coalbed methane recovery (CO_2-ECBM), it is injected into the coal seam and displaces methane in the coal matrix because CO_2 has a stronger affinity for coal than methane [76]. Solid coal has a relatively large number of micropores between cleats, which allow gas molecules from the cleats to diffuse and be strongly adsorbed. Coal has fractures (cleats). Coal pore structures are made up of micropores and macropores, but not mesopores. The micropores' radius is usually lower than 2 nm and occupies nearly 70% of the total porosity of the coal matrix. On the other hand, macropores have a porosity of more than 50 nm and are usually made up of a cleat system. Coal is considered as a dual-porosity rock due to the existence of macropores and micropores [77]. Many gases, including CO_2 and methane, may be physically absorbed by coal. If coalbed methane reserves are saturated, they can absorb five times as much methane by volume as a typical natural gas reservoir of equal size [76]. Because it can store the injected CO_2 and increase methane production from the coal seam simultaneously, carbon dioxide enhanced coalbed methane recovery is potentially appealing. However, this option is not well developed, and a better understanding of the injection and storage processes in coals is required [4].

Saline Formation

Saline aquifers are permeable and porous rocks that are saturated with salt water. These types of sedimentary basin formations are abundant on land and at sea. These salt deposits are also suit-

able for the storage of carbon dioxide. The techniques that may be used to absorb CO_2 include solubility trapping, interaction with fluid and minerals to produce solid carbonates, and pore space trapping. Since the density of CO_2 is less than that of salty water, CO_2 production occurs on top of the formation layer, and caprock is necessary to prevent any leaking. The CO_2 storage capability of saline formations is greater than that of oil and gas reservoirs. Within the aquifer, the supercritical CO_2 displaces water from the saline pores. The basic CO_2 storage technique in saline aquifers involves stratigraphic, solubility, and mineral trapping, which occur across a range of periods [78, 79]. In the solubility strategy, CO_2 is dissolved in an aqueous solution, whereas the stratigraphic stage is the primary storage mechanism. The Sleipner Project in the North Sea is an example of a CO_2 storage project that makes use of saline formation.

2.3 LCA Methodology

2.3.1 LCA Definition

LCA's origins may be traced back to the late 1960s and early 1970s. Several researchers have presented the complete history of LCA [80, 81, 82]. The first LCA recommendations, known as the "Code of Practice," were released in 1993 by the Society of Environmental Toxicology and Chemistry (SETAC). The "Code of Practice" pushed LCA as a widely acknowledged concept as well as a reliable approach for assessing product environmental performance [83]. Today, the "Code of Practice" has been superseded by a set of standards created by the International Organization for Standardization between 1997 and 2006 (ISO 14040-44). Life Cycle Assessment (LCA), as defined by ISO 14040 (1997) [84], is a "compilation and assessment of the inputs and outputs, as well as the possible environmental consequences, of a product system throughout its life cycle." In general, LCA evaluates the environmental consequences associated with a product system's whole life cycle, from raw material extraction to manufacture, processing, use of the product during its function, and waste processing of the discarded product [41].

Environmental Impact Assessment (EIA), System of Economic and Environmental Ac-

counting (SEEA), Environmental Auditing, and Material Flow Analysis are just a few of the instruments available for analyzing environmental consequences (MFA). Figure 2.8 shows that only LCA covers both the life-cycle environmental impacts and the product systems (or service systems), whereas other techniques focus on regional environmental impacts, site-specific environmental impacts, policy or economic issues, or all of the above [8].

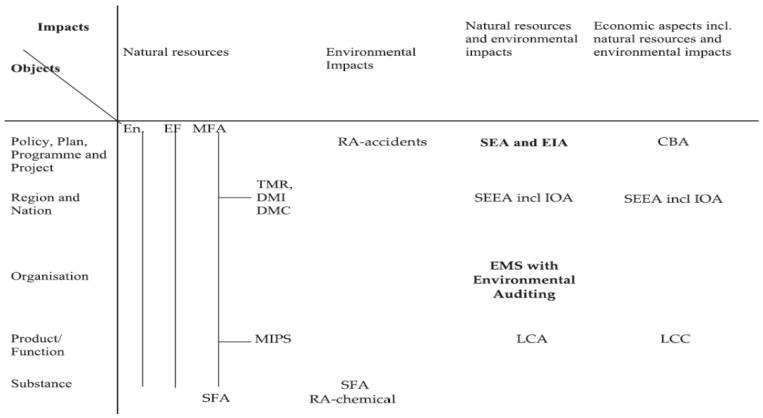

Figure 2.8: The tools are shown in relation to their focus, [8].

2.3.2 The Life Cycle Assessment Framework

In order to deal with the complexity of LCA, ISO published four international standards on the topic of LCA, which established a fixed protocol and methodological framework for performing an LCA study, including Goal and Scope, Inventory Analysis, Impact Assessment and Interpretation Figure 2.9.

Goal and Scope definition states the aim of an intended LCA study, the system boundary, the functional unit, the competing systems considered, and the breadth and depth of (or level of detail) the LCA study in relation to this aim. The functional unit is the quantified performance of a product system for use as a reference unit in an LCA study (ISO 14040,1997 [84]).

The **life cycle inventory** (LCI) is aimed at quantifying the input/output relationship and preparing an inventory of input/output data for all processes involved in the life cycle of the system(s) under study. The input/output flows to be quantified for a unit process include

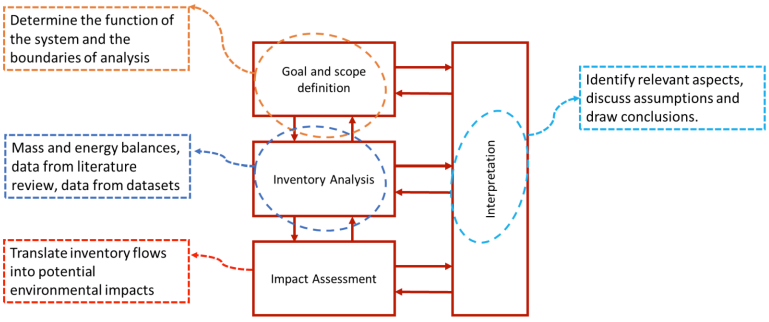

Figure 2.9: The Life Cycle Assessment Framework.

economic and environmental flows Figure 2.10. The input/output data are normally generated by following four methods: monitoring data measurement, emission factor estimations, mass balance and engineering calculations. For every unit process, LCI generates a unit process table (matrix) [9], illustrated in Equation 2.1, in which 35 variables represent the changes of economic flows or environmental interventions, relating to functional unit. The total process along the life-cycle of a product, relating to functional unit, can be represented as a set of column vectors Equation 2.1.

$$P_i = \{\Sigma\, ecf(1)...ecf(N)\ and\ \Sigma\, evf(1)...evf(N)\}\,. \tag{2.1}$$

$$P = [P_1...P_2...P_N]. \tag{2.2}$$

Where, Unit process, i, is represented as a column vector; P_i; First N_{ec} is economic flows; Next N_{ev} is environmental flows; Total process can be represented as a set of column vectors, P,with (N_{ec} + N_{ev}) rows and np columns.

Life cycle impact assessment. Here, the in- and outflows of the system are categorized and allocated to impact categories, such as global warming or acidification. After calculating the environmental effects in the different categories, optional steps are normalization, grouping and weighting. In particular, the last of them is necessarily based on subjective assumptions and

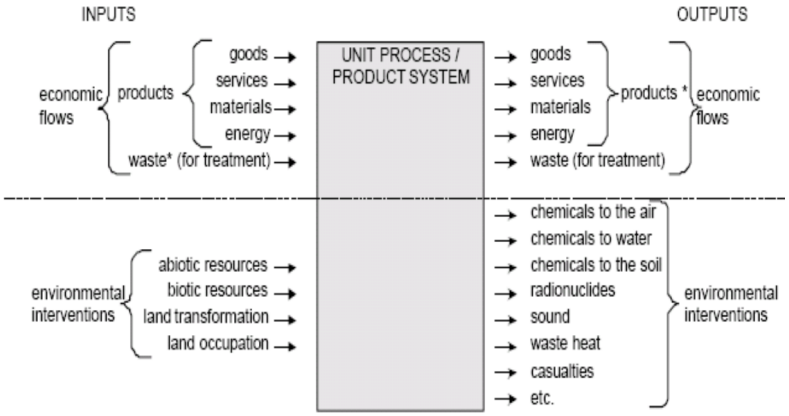

Figure 2.10: Environmental interventions and economic flows [9].

valuation.

Interpretation of the results. In the last step, results have to be summarised and discussed as a basis for conclusions and recommendations. Limitations are to be detected. Sensitivity analysis can be used as an appropriate tool for this purpose. The two key elements of an LCA are the assessment of the entire life cycle of the investigated system and the assessment of a variety of environmental impacts (ISO 14040 and 14044).

2.3.2.1 Applications of Life Cycle Assessment

Life Cycle Assessment has been utilized to support public policy-making in many nations. Based on the findings of LCA studies indicating recycling packaging is beneficial for the environment and saves energy and other resources, the Swedish Environmental Protection Agency (EPA) expanded producer's responsibility of packaging and included beverage cans and bottles to enhance the degree of recycling [85]. LCA is employed as the foundation of regulatory and permitting systems in the Netherlands, and because LCA is focused on performance rather than compliance, regulatory monitoring has been considerably decreased [86]. The European Union (EU) has various policies (for example, the Integrated Product Policy (IPP)) that are implemented using LCA [87]: Type 1, Eco-labels show the environmental performance of a

product or service across its complete life cycle; Type 2, Environmental Product Declarations (EPD) are a communication format for quantified LCA information based on independently validated regulations for the product category.

2.3.2.2 Limitations of Life Cycle Assessment

Because LCA modeling involves complex systems and is constrained by a lack of data, theoretical expertise, and the capacity to handle complexity, which causes data uncertainty, model uncertainty, and uncertainty due to choices in LCA modeling [88] [9], the uncertainty of LCA results is an acknowledged problem. The trend in uncertainty-related LCA research is toward widening and deepening LCA:

1. Broadening may include including economic and social dimensions, as well as addressing additional environmental issues [89].
2. Adding more fate and exposure mechanisms to impact assessments, creating more models for environmental impact assessments that take into account time and space, and creating LCI models that can capture the fundamental physical or empirical relationships between processes in product systems and can generate ranges for LCI data while enabling designers to incorporate more parameters into design problems are all examples of deepening [88].

2.3.2.3 Why CO_2 Capture and Storage Requires Life Cycle Assessment

The known and currently developing CO_2 capture and storage methods offer a multitude of possibilities with varying energy consumption and consequent environmental effects. CO_2 capture and storage systems demand additional energy for their operation. It is necessary to conduct a thorough environmental assessment that can track GHG from a power generation life-cycle in order to provide a representative and accurate evaluation of the alternative CCS options. This will help to ensure that the CCS option chosen won't have any upstream or downstream effects that will increase the overall release of GHGs or significantly worsen other environmental issues like resource depletion.

Life cycle assessment (LCA) analyzes energy and non-energy related GHG emissions, as well as numerous other environmental emissions (e.g., solid waste, hazardous chemicals, and air pollutants) and resource usage (e.g. minerals). This comprehensive viewpoint assists decision makers in ensuring that reducing GHG emissions using CCS does not result in major increases in other environmental consequences. Moreover, When developing CCS projects, LCA can be used to analyze the environmental effect potential of different CCS concepts in the hunt for greener choices. Throughout addition, LCA can identify which compounds have high environmental impact potentials in the CCS life cycle and assist corporations in designing environmental control measures to mitigate the effects of these substances' release. Furthermore, LCA can quantify the environmental trade-offs of every process choice throughout the CCS chain and assist businesses in minimizing the environmental impacts of the CCS life cycle by developing the most environmentally friendly component processes or setting suitable operating parameters.

The International Organization for Standardization (ISO) has also produced the ISO 14040 series of LCA standards, which include guidance on creating acceptable system boundaries, trustworthy data collecting, evaluating environmental consequences, interpreting conclusions, and transparent reporting. This 40 provides an ideal starting place for developing GHG monitoring techniques and other environmental implications. Furthermore, three flexible mechanisms (Emissions Trading, Joint Implementation (JI), and the Clean Development Mechanism (CDM)) were developed under the Kyoto Protocol to assist developed-country emitters in meeting their GHG emission targets, and these flexible mechanisms are already a reality, as the Kyoto Protocol entered into force on February 16, 2005.

2.3.3 LCA Modeling Approach

2.3.3.1 System Modelling

The essential premise that guided the development of this approach is as follows: i) Must demonstrate clearly how life cycle impacts are computed, the uncertainty associated with the

conclusions, and the extent to which every unit process's inputs/outputs have been adequately defined. ii) Models and conventions that enable for accurate comparisons of different CCS alternatives.

2.3.3.2 System Boundary

Figure 2.11 depicts the system boundaries of LCA in CCS, which include CO_2 capture options, CO_2 transportation options, and CO_2 storage options. This study focuses on modeling the processes of alternative CO_2 capture options, CO_2 transportation, and CO_2 storage in considerable detail. The system boundaries for upstream operations include the development of CO_2 capture facilities and CO_2 pipelines. Due to limited time and limited availability of resources, this research only investigated the systems relating to post-combustion carbon capture (pulverized coal-fired power generation), pipeline transport, injection and saline aquifer CO_2 storage.

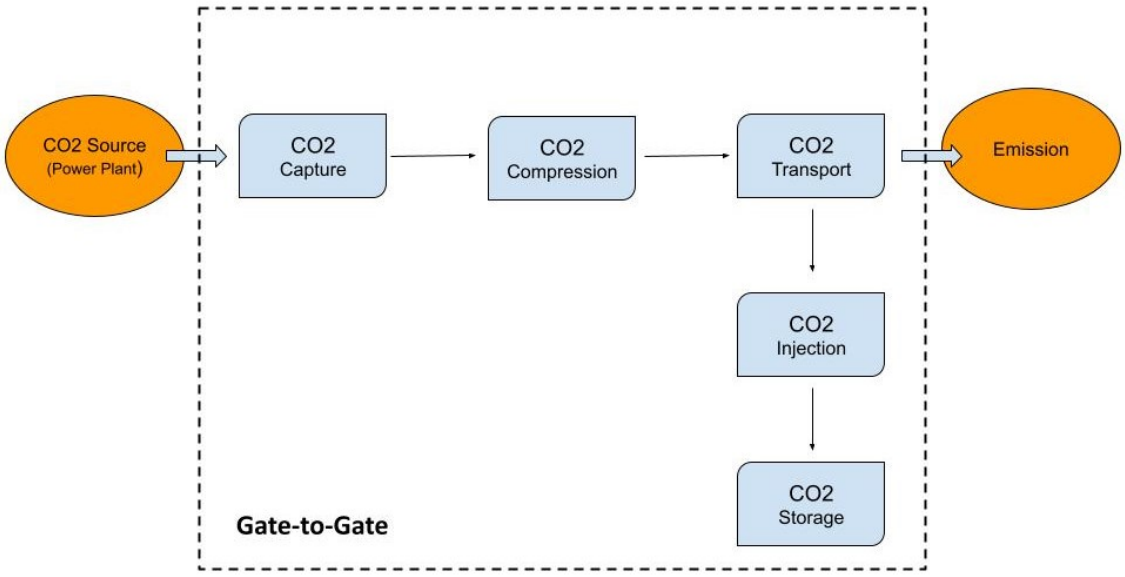

Figure 2.11: The system boundary of CCS technology.

2.3.3.3 Functional Unit

The chosen functional unit is "kg stored CO2". Here, it is considered 1000 kg CO2 stored.

2.3.3.4 Temporal Domain

As CO_2 geological storage is included in the LCA system boundaries, two further system features must be considered: the destiny of CO_2 in the storage formation and the possible leakage of CO_2 from the storage formation. This necessitates LCI modeling of CO_2 storage for thousands of years. Globally, no standard CO_2 storage performance requirements have been defined. The IPCC Special Report on CCS and CO2CRC uses a 1,000-year time period to evaluate CO_2 storage capability. Furthermore, the fundamental goal of CO_2 geological storage is to postpone present CO_2 emissions into the atmosphere for 1,000 years.

2.3.3.5 Environmental Pollutant Characterization

Pollutants discharged by a CCS system to the atmosphere, land, or water originate in the system's material or fuel inputs, usually coal and limestone. The goal of this study is to identify all elements/substances of environmental consequence from their site of input through their partition and final emission into all environmental compartments in a CCS system. The status of the following components is of major significance, as seen in Figure 2.12: i) During the combustion process, C produces CO_2, CO, and unburned carbon. The energy consumption of the unit mechanisms that create CO_2, as well as CO_2 capture and storage, is estimated. ii) During the combustion processes, S, N, Cl, and F produce SOx, NOx, N_2O, HCl, and HF. Additionally taken into account are the emissions produced by the pollution abatement technologies employed, as well as the processes that produce SOx, NOx, HCl, and HF; iii) Analyses are also done for trace elements including As, Cd, Cr, Cu, Hg, Ni, Pb, Zn, Sb, Be, B, F, Mn, Se, V, Co, Ba, Ag, and Tl, as well as their final emission to the atmosphere, water, or soil. It is crucial to note that this study only examines the CCS pollutant in the final portion, although the diagram depicts the entire process from combustion to capture.

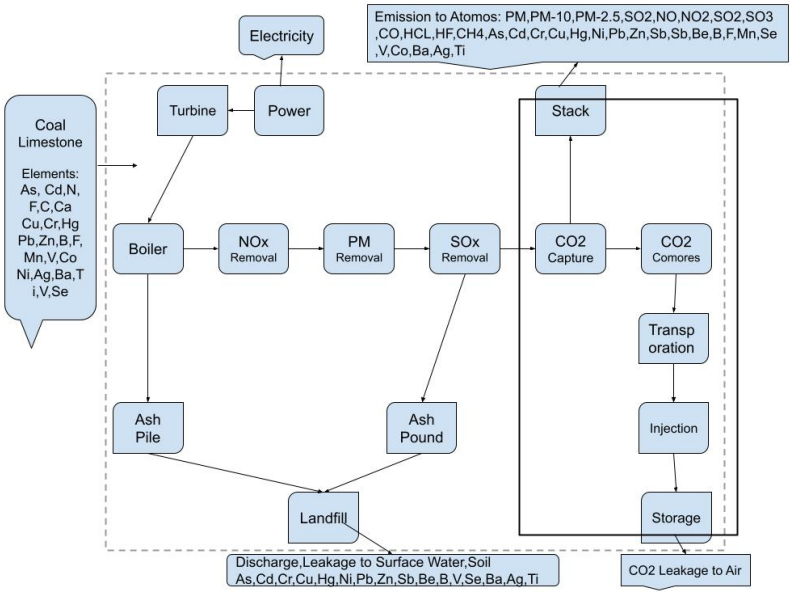

Figure 2.12: The level of detail involved in the LCA of post-combustion CCS system.

2.3.4 Life Cycle Inventory (LCI) Modelling

2.3.4.1 LCI System

A CCS in a power generation system is made up of interconnected components and interactions. The systems analysis approach is used to investigate the composition and operation of component systems. The goal of modularisation is to make complicated systems easier to understand and model exactly. Modularisation allows the LCI models to quantify the flows of materials, energy, intermediate products, or emissions in a more detailed manner, or at the component unit process level, allowing for a more accurate representation of technical, spatial, and temporal differences by modifying the parameters of component unit processes as needed [90]. By taking into account the unique operating requirements of the industrial users, this not only tackles the shortcomings of standard LCA studies that employ linear input/output coefficients for the LCI models, but also eliminates their second flaw.

2.3.4.2 Characterization of Input and Output

Wainwright and Mulligan (2004) [91] established the Gray box model as a form of unit process model for describing LCI. There are two types of models: black boxes and white boxes, and the Gray box model is in between. Only the inputs and outputs are known in a black box model, and the specifics of how the processes turn inputs to outputs are not described. A parameter or parameters characterizing the connection of outputs to inputs, such as the majority of typical LCI models, are used to model the transformation. In contrast, all parts of the physical processes that turn inputs to outputs are understood and described in a white box model.

In order to facilitate the grey box modeling technique, the input and output flows of a unit process can be further classified based on the predicted variability and uncertainty [92]: i) The uncertainties in the LCI data are usually the lowest in raw material flows, energy flows, intermediate product flows, and product flows. Process engineering models, which apply physical or chemical principles in modeling, are used to quantify these data. ii) Emissions caused primarily by chemicals present in input flows are emitted in predictable proportions to the amount of input flows. iii) Emissions produced during a unit process that change significantly depending on the physical variables present during production, such as temperature, the quantity of oxygen available, and so on. These emissions might differ by a factor of 5-10.

2.3.4.3 Accounting for Variation of Technology and Geography in CCS Applications

One of the research's differentiating elements is the incorporation of technology dependency for each CCS technology choice and type of emission; LCI models for alternative emission reduction technologies are built. LCA on CCS in energy production is used to create long-term strategic energy systems that include best available and new energy technologies. Moreover, the LCI models established recognize the value of a capture or storage plant's geographical location and account for it at the unit process level by changing the inputs or model parameters, or by substituting component unit processes. The purpose for doing this analysis; i) Installation of

emission control systems (such as carbon capture systems) has typically been gradual, after the passage of laws requiring the use of these systems to control one kind of pollution in order to achieve compliance. The amount of emissions is determined by variations in plant design and emissions control systems deployed. ii) CO_2 storage performance can differ significantly due to geological factors and the complexity of CO_2 storage locations. The variability and uncertainty of reservoir characteristics have a substantial influence on CO_2 geological storage performance projections [93].

2.3.5 Life Cycle Impact Assessment

The modeling of impact categories, category indicators, and characterization methods is determined by the goal and scope of the LCA. Guinée et al (2001) and the US EPA (2006) used the CML 2001 baseline impact categories, category indicators, and characterization methods (midpoint approach) as the standard method for LCIA to provide a comprehensive profile of environmental impacts for emissions from power generation with CCS Table 2.1.

To avoid duplicate accounting, some items, resources, or emissions may simultaneously or sequentially contribute to two or more exclusive categories. In these cases, the emission should be split or assigned to the appropriate categories. It is also conceivable that the output or outcome of an impact in one impact category might serve as the catalyst for an impact in a different impact area. Two notes: i) In order to adequately characterize the geographic differences at LCIA level, the local environmental factors and the distribution of emissions, which contribute to two or more categories of impacts, are identified; ii) Two types of analysis are used for a general environmental impact analysis, first, an average allocation of emissions among various applicable impact categories is used, allowing for the identification of all potential environmental impacts; second, only the primary emission impacts are taken into account, with the full value of a given emission being assigned to each applicable category to determine the worst-case impact.

Impact Category	Characterization Factor	Classification	Scale
Global Warming	Converts LCI data to carbon dioxide equivalents.	Carbon Dioxide (CO_2) Nitrogen Dioxide (N_2O) Methane (CH_4) Chlorofluorocarbons (CFCs) Hydrochlorofluorocarbons (HCFCs) Methyl Bromide (CH_3Br)	Global
Stratospheric Ozone Depletion	Converts LCI data to trichlorofluoromethane (CFC-11) equivalents.	Chlorofluorocarbons (CFCs) Hydrochlorofluorocarbons (HCFCs) Halons Methyl Bromide (CH_3Br)	Global
Acidification	Converts LCI data to hydrogen ion equivalents.	Sulphur Oxides (SOx) Nitrogen Oxides (NOx) Hydrochloric Acid (HCL) Hydroflouric Acid (HF) Ammonia (NH_3)	Regional Local
Eutrophication	Converts LCI data to phosphate (PO_4) equivalents.	Nitrogen Oxide (NO) Nitrogen Dioxide (N_2O) Nitrates Ammonia (NH_3)	Local
Photo-oxidant formation	Converts LCI data to ethane (C_2H_6) equivalents.	Non-methane hydrocarbon (NMHC)	Local
Ecotoxicity	Converts LC50 data to equivalents.	Toxic chemicals, including As, Cd, Cr, Cu, Hg, Ni, Pb, Zn, Sb, Be, B, F, Mn, Se, V, Co, Ba, Ag, Tl, with a reported lethal concentration to rodents or to fish	Local
Human toxicity	Converts LC50 data to equivalents.	As, Cd, Cr, Cu, Hg, Ni, Pb, Zn, Sb, Be, B, F, Mn, Se, V, Co, Ba, Ag, Tl, release to air, water, and soil.	Global Regional Local
Depletion of abiotic resources	Converts LCI data to a ratio of quantity of resource used versus quantity of resource left in reserve.	Quantity of minerals used Quantity of fossil fuels used	Global Regional Local
Land Use	Converts mass of solid waste into volume using an estimated density.	Quantity disposed of in a landfill	Global Regional Local

Table 2.1: Impact categories and characterization factors [9].

2.4 Summary

In the range of GHG reduction solutions, CCS is significant. Complex processes are involved in CO_2 capture and storage, and all available technologies produce environmental pollutants in addition to requiring additional energy and materials for operation. As a result, CCS may increase the environmental effects caused on by onsite CO_2 collection procedures or by upstream operations like coal mining or the manufacturing of solvents. Also, there are many CCS alternatives. This suggests that no straightforward model could incorporate all the environmental effects of different CO_2 capture or storage strategies. Consequently, all CCS technologies must be taken into account and modeled in a comprehensive way to benefit from the shared features of any GHG reduction strategy chosen.

The system boundaries of LCA on CCS have been established, which include CO_2 capture, CO_2 transportation, and CO_2 storage. Furthermore, in the framework of LCA, the lifetime of the project was set at 1,000 years, with a functional unit of 1000 kg CO_2 stored. Moreover, by separating the CCS systems into manageable component processes, which can be modelled based on the relevant physical or chemical principles or by using empirical relationships for component unit processes, a methodological framework for LCI modeling was developed to accommodate the technical, spatial, and temporal differences that may be experienced for different plants. Finally, By taking into account the unique operating requirements of the industrial users, which are frequently disregarded, this not only overcomes the constraints of standard LCA studies that employ linear input/output coefficients for the LCI models, but also tackles their second shortcoming.

3

Analytical Approach

3.1 Introduction

As already stated in chapter 2, because of time and resource constraints, this study focused only on post-combustion carbon capture (pulverized coal-fired power production), pipeline transport and injection, and saline aquifer CO_2 storage systems. Figure 3.1 depicts all the procedures and options, and the one chosen for this study.

This chapter focuses first on the post-combustion capture process and then develops LCI models for chemical absorption CO_2 capture with alternative solvents, based on fundamental chemical and physical principles or empirical relationships, with the goal of incorporating more parameters into the LCI models and decreasing the uncertainty of LCI results. Then, the LCI model for CO_2 conditioning in post-combustion CO_2 capture power plants is presented. Second, the chapter studies LCI models for CO_2 transport and injection. Both procedures entail substantial CO_2 movements. LCI modeling concerns energy consumption and fugitive

emissions. The LCI models account the duration of CO_2 transfer, surface temperature, and a saline aquifer's reservoir pressure, thickness, depth, and permeability. Finally, CO_2 storage is discussed. LCI modeling starts with the calculation of CO_2 movement and distribution in the saline aquifer, which is constrained by LCA geological boundaries. Then, the LCI model assesses CO_2 leakage from saline aquifer via different paths. The LCI model measures the quantity of CO_2 that spilled from the saline aquifer to the atmosphere after passing through distinct overburden geological compartments.

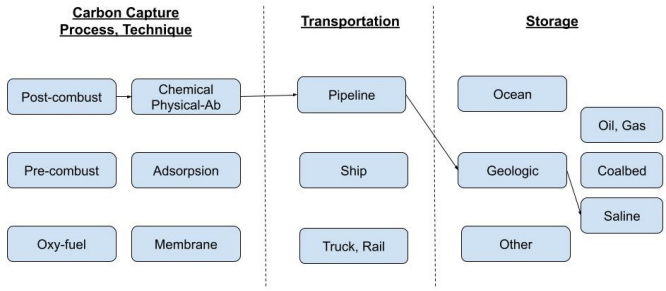

Figure 3.1: A complete CCS approach, and representing the selected techniques in this research.

3.2 Life Cycle Inventory Modelling of Post-Combustion Capture Process

Post-combustion CO_2 capture includes the removal of CO_2 from the flue gases produced by a large-scale fossil fuel or biomass-fueled combustion process. Direct burning of fuel with air in a combustion chamber has been the most cost-effective method of extracting energy from fuel (Figure 3.2). Flue gases from power production are normally at atmospheric pressure with considerable nitrogen content. Flue gas CO_2 content varies by fuel type (3% for a natural gas combined cycle to less than 15% by volume for a coal-fired plant). Flue gases from coal combustion include CO_2, N_2, O_2, H_2O, SOx, NOx, particulates, HCl, HF, mercury, trace metals, and other inorganic impurities [4]. This section describes the chemical absorption and CO_2 conditioning processes. First, chemical absorption is the primary approach for post-combustion CO_2

collection. Chemical absorption CO_2 capture is a mature technique that has been used in a variety of industrial operations, including gas treatment and ammonia manufacturing. [94, 75, 4], Secondly, post-combustion CO_2 conditioning of the capture power plant comprises of multi-stage compression and dehydration.

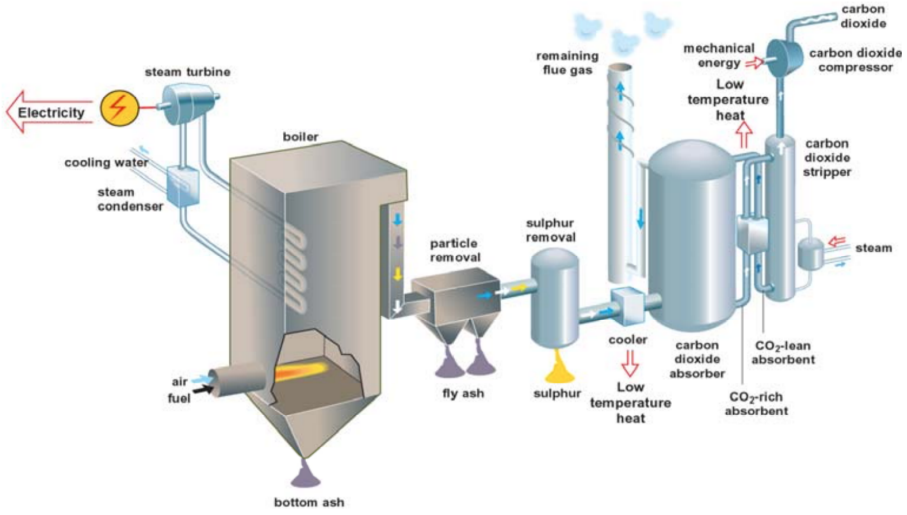

Figure 3.2: Schematic of a post-combustion CO_2 capture system in a power plant [10].

3.2.1 Modeling of Chemical Absorption Capture Technology

3.2.1.1 Basics of Chemical Absorption

Chemical absorption comprises reversible chemical interactions between CO_2 and aqueous solvents, such as alkanolamine (e.g. MEA, DEA) or potassium carbonate (K_2CO_3). Heating the result of these processes breaks the connection between the absorbent and CO_2, yielding a CO_2-enriched stream. The left-to-right reactions remove CO_2 from waste gas streams through an exothermic reaction of CO_2 with the amine functionality of the alkanolamine at low temperature (25 - 65 ^{0}C) and pressure (30 to 45 kPa). The right-to-left reactions regenerate the solvent by heating the solvent solution to 100 - 150 ^{0}C and pressure 150 to 175 kPa [95]. Table 3.1 indicates the alternatives solvent are used in capture.

Solvent Alternatives	Example of Primary Reaction	Reaction Speed	ΔH * (kcal/mole)	Corrosion & Degradation
Primary Amine (e.g. MEA, DGA) Secondary Amine (e.g DEA)	$2MEA + CO_2 <-> MEACOO- + MEAH$	Fast	20 – 22	High
Tertiary Amine (e.g. MDEA, TEA) Hindered Amine (e.g AMP)	$AMP + CO_2 + H_2O <-> AMPH + HCO_3$	Slow	10-15	Low
Potassium Carbonate (K_2CO_3)	$CO_3 + CO_2 + H_2O <-> 2HCO_3$	Very Slow	5-10	Low

Table 3.1: The alternatives solvent can be used in chemical absorption process of capture system [22].

A typical chemical absorption unit has two sections: aqueous CO_2 absorption and CO_2 stripping (Figure 3.3). In the Absorber, generally placed CO_2-lean solvent absorbs CO_2 from intake gases (e.g. MEA). Gas leaving the Absorber Column is handled. The CO_2-rich solvent is heated in the Stripper to remove CO_2 and regenerate CO_2-lean solvent. Regenerated CO_2-lean solvent is returned to the Absorber, and CO_2 is compressed. MEA solvent system employs NaOH for solvent reclamation, solid filtration, and corrosion inhibitor. Sorbent replacement is also necessary to compensate for sorbent loss during the absorption/stripping process.

3.2.1.2 Schematic Model of Chemical Absorption

In order to characterize the technical differences between various chemical absorption CO_2 capture processes, the LCI model created takes into consideration the inputs/outputs of various solvent types for chemical absorption CO_2 capture processes (refer to Figure 3.4).

*When, Monoethanolamine=MEA; Diglycolamine=DGA; Diethanolamine=DEA; Triethaolamine=TEA; Nmethyldiethanolamine =MDEA; 2-amino-2-methyl-1-propanol=AMP. ΔH: Heat for desorption [96]

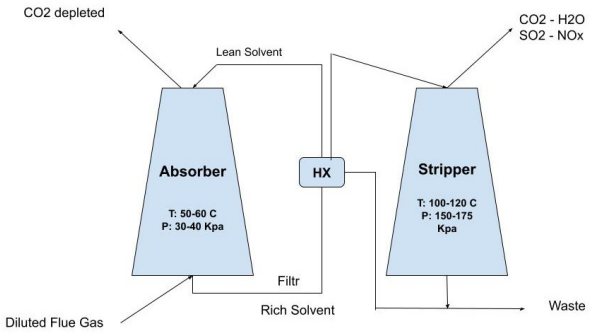

Figure 3.3: Typical aqueous absorption/stripping system for CO_2 capture.

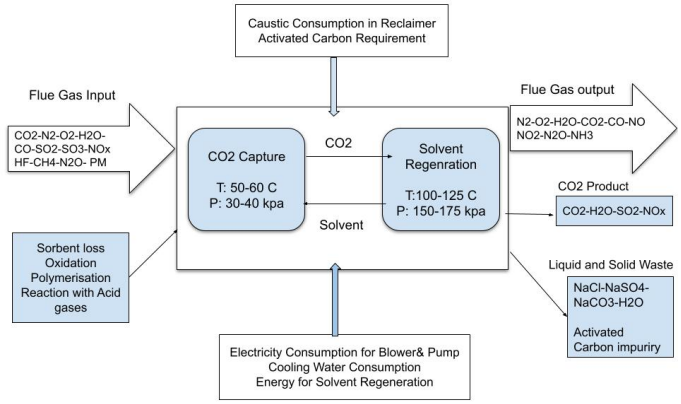

Figure 3.4: The scheme of chemical absorption CO_2 capture processes LCI model.

3.2.1.2.1 Consumption of Steam, and Heat Requirements

Solvent regeneration is energy-intensive. Heat for solvent regeneration in an aqueous absorption/stripping system is the total of CO_2 desorption heat, diluting water evaporation heat, and sensible heat to boil the solvent. Dugas (2006) found that sensible heat to raise a common MEA solvent to boiling, CO_2 desorption heat, and dilution water evaporation heat contribute for 49%, 27%, and 24% of the total heat duty. The heat needed for solvent regeneration varies from 2,200 to 6,000kJ/kg CO_2 collected, depending on the solvent type and concentration [97] (refer to Figure 3.5).

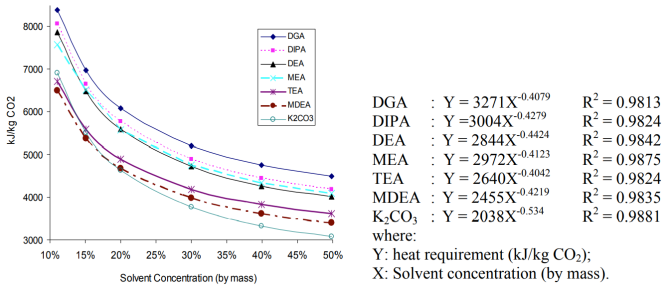

Figure 3.5: Energy consumption in chemical absorption CO_2 capture for solvent alternatives [11].

How about the Ratio of Heat-to-Electricity Equivalence? Figure 3.6 heat for sorbent regeneration is generally collected from the steam turbine as low-pressure steam and via the reboiler in coal-fired and combined-cycle gas plants. Using steam extraction instead of installing new facilities saves plant efficiency, investment cost, and space. Low pressure (LP) steam is 320 to 3700C at 60-80 kPa pressure and has 2,350 kJ/kg of heat.

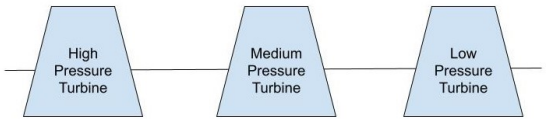

Figure 3.6: Steam extraction in power plants.

With reference to [97], the mass flow rate of steam for regeneration can be calculated as:

$$m_{steam}(tonne/hr) = Q/(\eta_{reboiler} \times h_{steam}). \tag{3.1}$$

where: h_{steam} is the heat content (enthalpy) of the steam; $\eta_{reboiler}$ is the efficiency of reboiler, which is determined by the difference between reboiler temperature and ambient temperature. The default value used for $\eta_{reboiler}$ is 0.85.

Heat-to-electricity ratio reflects power generating capacity lost due to sorbent regeneration steam extraction. The ratio of heat to electricity in a reversible thermal cycle relies on fluid temperature and pressure. Lower steam pressure and temperature reduce heat-to-electricity conversion efficiency. Heat-to-electricity ratios for LP steam vary from 0.14 to 0.25. Because of

variations in turbine and plant configuration, 0.14 is utilized for heat-to-electricity equivalence ratio in present steam turbine power plants and 0.19 in future advanced power plants. The electrical equivalence equation is [11, 98]:

$$Electricity\ equivalence = \eta_{heat-to-electricity} \times m_{steam} \times h_{steam}. \tag{3.2}$$

where: m_{steam} is the mass flow rate of steam h_{steam} is the heat content (enthalpy) of the steam.

3.2.1.2.2 Cooling Water Requirement

As CO_2 absorption in amine solvent is exothermic, low flue gas temperature is preferred. Flue gas temperature is 50-60 ^{0}C. If the flue gas originates from a wet sulfur scrubber, a direct contact cooler (DCC) may not be needed since the exit flue gas temperature is approximately 65 ^{0}C. DCC is needed for flue gas from a natural gas-fired boiler, which seldom passes through a sulfur scrubber. Typically, the circulating cooling water rate is around 110 m3cooling water per tonne of CO_2 collected from the flue gas, and a more precise estimate for the cooling water flow rate is performed using this equation [99]:

$$M_{cw} = m_{fg} \times (\Delta T_{fg}/\Delta T_w) \times (SH_{fg}/SH_w)\ tonne/hr. \tag{3.3}$$

where: Specific heat of water, SH_w = 4.2 kJ/kg oC; Specific heat of flue gas, SH_{fg}, generally around 1.0 kJ/kg C (300 ^{0}C, 75% N2, 25% CO_2); Temperature rise in the cooling water, ΔT_w, typically 15 ^{0}C; Drop in flue gas temperature, $\Delta T_{fg} = (T_{fg,i} - T_{fg})$ ^{0}C; $T_{fg,i}$ = Temperature of flue gas entering the direct contact cooler (^{0}C); T_{fg} = Temperature of flue gas exiting the direct contact cooler (^{0}C); Mass flow rate of flue gas, m_{fg}, in tonne/ hr.

3.2.1.2.3 Electricity Consumption for Blowers and Pumps

Flue gas blower power, DCC circulation pump power (if employed), and absorber wash water pump power are all inversely related to the CO_2 concentration in the flue gas and range between

0.2 and 1.3 MJ/kg CO_2 removed [100, 11]. The flue gas blower is the largest energy user over the whole spectrum of CO_2 concentrations. The following equation may be used to determine the electricity consumption per tonne of CO_2 captured [99]:

$$Electrical\ consumption\ (kW) = 9.6 + 393.6/(concentration\ CO_2 \times 100). \quad (3.4)$$

For the KS-1 system the electrical consumption is 18 kWh/ tonne CO_2.

3.2.1.2.4 Mass Flow of Acid Gases in the Flue Gases

The majority of research indicates that the CO_2 collection efficiency of amine-based systems is 90%, with a few studies claiming capture efficiencies as high as 96%. With regards to [95, 101], Due to the alkalinity of the amine solution, acid gases such as NO_2 (as HNO2/3), SOx (as H2SO3/4), and HCl will be practically entirely absorbed into the amine solution during CO_2 sorption and cause amine solvent loss. NO_2 and NO aren't substantially absorbed in amine solution and stay in flue gas. Table 3.2 shows acid gas removal parameters.

Acid Gas	Potential effects by Amines	Removal Efficiency %
SO_2	Amine absorbents react strongly	99
SO_3	Amine absorbents react strongly	100
NO_2	Not heavily absorbed; stays in flue gas	25
N_2O	Not heavily absorbed; stays in flue gas	25
NO	Not heavily absorbed; stays in flue gas	0
HCL	Amine absorbents react strongly	99

Table 3.2: Acid gases removal efficiency

The mass flow of i acid gas from the MEA capture is:

$$M_{i,acidout} = M_{i,acidin} \times (1 - \eta i, acidgas). \quad (3.5)$$

In addition, SO_2 and NOx may enter the CO_2 stream if a tiny quantity of HNO_2 and H_2SO_3

were to revert to SO_2 and NOx at the CO_2 stripper's low temperature. These S and N byproducts are anticipated to be very corrosive, particularly given the presence of moisture in the CO_2 stream [95].

3.2.1.2.5 Particulate Matter and Trace Element Removal Rate

According to Nalbandian (2004) [102], the removal effectiveness for particles bigger than 10 m is around 80% ($\eta 1$), but the removal efficiency for particles less than 10 m is 10% ($\eta 2$). Consequently, the following formulae may be used to compute the particulate matter output:

$$M_{po1} = M_{pi1} \times \eta_{p1}. \tag{3.6}$$

$$M_{po2} = M_{pi2} \times \eta_{p2}. \tag{3.7}$$

where: M_{pi1}: particulates larger than 10 μm; M_{pi2}: particulates smaller than 10 μm.

Mercury, lead, cadmium, and other hazardous metal ions react with amines to generate water-soluble complexes. In-line mist eliminators can remove non-volatile metal ion complexes from the CO_2 concentrate stream during regeneration [95].

3.2.1.2.6 Solvent Loss and Ammonia Generation Rate

Degradation, vaporization, and mechanical causes induce amine solvent loss. Solvent loss is caused by degradation of base amine molecules. Oxidation and carbamate polymerization can cause degradation. Oxidative degradation is catalyzed by iron or copper, producing oxidised particles of the solvent (e.g. Formaldehyde, Acetic Acid, Glycolic Acid) and NH_3, and is predicted to occur in the presence of dissolved O_2 in the liquid hold up at the bottom of the absorber. Secondary amines (e.g. DEA) oxidize twice as rapidly as primary amines (MEA, DGA), while hindered primary amines, tertiary amines (MEDA), the K+ salt of alanine, and combinations of MDEA with other amines deteriorate roughly one fifth as fast as primary amines [22]. Moreover, Carbamate polymerization demands high temperatures and CO_2 loading, cre-

ates large molecular weight breakdown products, and occurs at the stripper's higher temperature. Polymerization rate is extremely amine-dependent. High-amine solvents polymerize faster. Alkanolamines, tertiary amines, and hindered primary and secondary amines are not carbamate polymerizable [22].

With regards to Chapel et al., 1999 [99] and Rochelle et al., 2001 [22], the overall MEA loss owing to deterioration is conservatively approximated at 1.5 kg MEA/tonne CO_2. MEA loss due to oxidation (A) is 0.6 (1.5×0.4) kg MEA/tonne CO_2, while polymerization (C) is 0.9 (1.5×0.6) kg MEA/tonne CO_2. The rate of NH3 formation due to MEA oxidation is 0.136 kilogram NH_3/tonne CO_2. Regarding three studies [103, 104, 22], Table 3.3 depicts solvent loss and NH_3 production by degradation for alternate solvents, where A = the MEA loss by oxidation; B = NH_3 generation due to MEA oxidation; C = MEA loss by polymerisation.

Type	**Primary Amine**		**Second Amine**		**Third Amine**		**Hindered Amine**		**Potassium Carbonate**
	MEA	DGA	DEA	DIPA	TEA	MDEA	AMP	KS-1	K/PZ
Oxidation	A	A	2A	2A	0.05A	0.05A	0.1A	0.2A	0.1A
NH_3 generation	B	2B	3B	3B	0	0	3B	3B	0
Polymerisation	C	C	C	C	0	0	0	0	0

Table 3.3: solvent loss and NH_3 production by degradation for alternate solvents

Oxidative degradation products will be generated concurrently, and the actual stoichiometry of the reaction should vary between 0.5 and 2.5 moles of oxygen consumed per mole of amine oxidized [105]. Process stoichiometry is 1.5, and oxygen used by amine oxidation may be computed using the following equation:

$$\textit{Oxygen consumption by oxidation}\ (\textit{mole}) = 1.5 \times \textit{Amine loss by oxidation}\ (\textit{mole})/0.3. \quad (3.8)$$

Additionally, it is important to emphasize heat-stable salt and solvent loss here. flue gas pollutants may bind an amine molecule to produce a salt that cannot be regenerated by the addition of heat; these salts are known as Heat Stable Salts (HSS). They decrease the amine's

absorption ability and are also corrosive. Therefore, upstream SOx, NOx, and HCl units are necessary to reduce to an acceptable level the quantity of pollutants entering the amine unit. The HSS may be neutralized using sodium hydroxide (NaOH), which can free up the amine in the reclaimer that is attached to the HSS anion, but does not eliminate any pollutants from the system. Regarding [99], NaOH can't recover all HSS solvent losses. For solvent alternatives, acid gas solvent loss is evaluated using Equation 3.9, and NOx and HCl solvent losses are omitted because to their low flue gas volumes.

$$Solventloss(kgpertonCO_2) = 0.5 \times (ppmvSOXenteringtheabsorber/(CO_2concinfluegas \times 100)). \tag{3.9}$$

Finally, with reference to the papers of IEA GHG(2006) [106] and Nsakala, et al. (2001) [23], it is appropriate to include about waste stream and disposal here. A CO_2 capture system generates reclaimer waste (Table 3.4), wasted carbon from activated carbon filters, and carbon bed filter components. Flue gas composition and plant operating conditions affect the quantity of amine waste created. It's considered that wasted activated carbon equals consumption. As filter elements mostly comprise flue gas particles, the number of filter elements is considered to equal the flue gas particulate eliminated by the amine unit. Capture system waste may be incinerated and treated as solid waste.

Waste Composition	**Amount wt.%**
NH_3	0.02
NaCl	0.6
Na_2CO_3	1.7
Na_2SO_4	6.6
Total N	5.6
Total Organic Carbon	15.6
Insoluble	1.3
Amine	9.5

Table 3.4: Reclaimer waste composition [23].

3.2.2 Modeling of Post-Combustion Capture Process: CO_2 Conditioning

Figure 3.7 shows post-combustion CO_2 conditioning of the capture power plant which in most situations consists of two distinct sections like CO_2 multi-stage compression and dehydration.

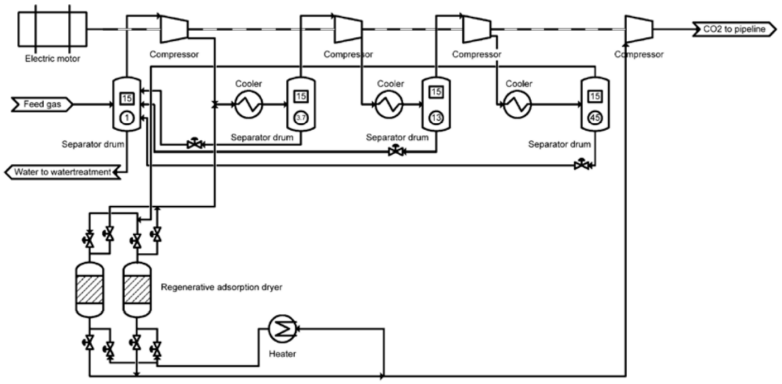

Figure 3.7: The post-combustion CO2 conditioning of the capture compressor [12].

3.2.2.1 Basics of Post-Combustion Process

Compressing the captured CO_2 to a pressure between 8 and 15 MPa is necessary to overcome frictional and static pressure decreases and deliver the CO_2 at a high enough pressure to prevent gas flashing. 13.8 MPa is the normal CO_2 compression pressure [14]. High CO_2 compression volumes need multi-stage piston or centrifugal compressors with inter-stage cooling. Based on current technology, the IEA (2002) [107] says one compressor train may be 40,000 kW. If total compression power exceeds 40,000 kW, CO_2 flow rate and total power must be separated into parallel compressor trains.

Dehydration depends on the CO_2 product's needed water content. For hydrocarbon pipes, drying the gas to 50 ppm water ensures there is no free water [108]. This may be excessively strict for CO_2 pipeline transportation. Experiments and theoretical calculations show that, for normal pipeline transit at 5 ^{0}C and 8.5 MPa, a maximum water content of 600 ppm may be adequate to avoid free water precipitation [109].

In a 3 stage CO_2 compressor, the regenerative adsorption drier is commonly on the 1st stage discharge side (or the 3rd Stage in the case of a 5 stage CO_2 compressor). The drier package has four vessels; three are in operation while one is regenerated or on standby [110]. Adsorption is the concentration of a gas or liquid on a solid surface. The dehydration adsorption system (Figure 3.8) is cyclic in nature, with an adsorption cycle followed by a regeneration cycle, allowing the adsorbent to be reused. Adsorbents include silica gel, activated alumina, and molecular sieves. As the wet CO_2 gas passes through the adsorbent bed, the adsorbent absorbs water. When the adsorbent is saturated with liquid, it is turned off and "regenerated." The liquids are absorbed by sending hot, dry gas across the adsorbent bed during regeneration. The liquids are separated when the gas is condensed. As the Regeneration Gas, a slipstream of CO_2 gas from the first stage compressor is heated. Because adsorbent bed regeneration demands a high temperature and HP steam pressure may change, a gas-fired heater is used. CO_2 entering the dryer is 32 ^{0}C [110].

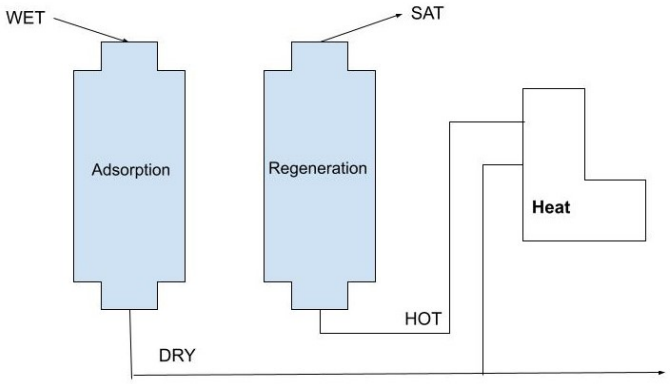

Figure 3.8: A dehydration adsorption system.

3.2.2.2 Schematic Model of CO_2 conditioning Post-Combustion Capture

In order to figure out the technical differences between CO_2 conditioning units for post-combustion capture, an LCI model is presented that quantifies the energy inputs for the compressor, heat in-

put for the dryer, adsorbent consumption for the dryer, and cooling water consumption based on engineering calculations (Figure 3.9).

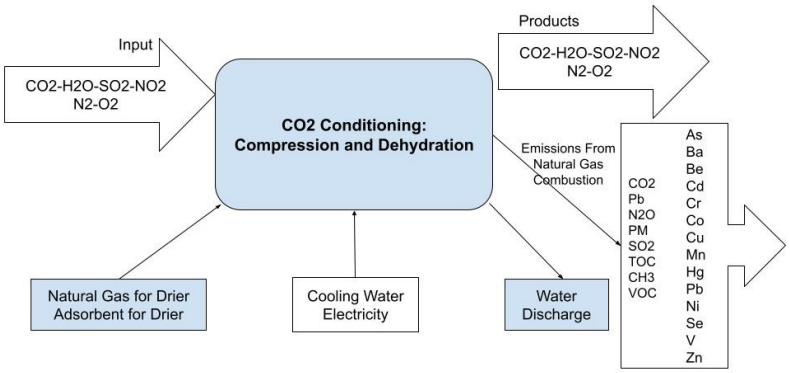

Figure 3.9: CO_2 conditioning Post-Combustion Capture Life Cycle Inventory Model.

3.2.2.2.1 Electricity for Compressor

CO_2 compression power consumption ranges from 80 to 120 kWh/ton CO_2, depending on the CO_2 product pressure, compressor performance, CO_2-rich stream composition, and integration potential. CO_2 compression is a significant energy penalty item, second only to the CO_2 collecting unit [111]. Regarding [14], CO_2 undergoes a phase transition from gas to liquid or 'dense phase' depending on its temperature when it is compressed from air pressure (0.1 MPa) to pipeline transmission pressure (typically 15 MPa). In the gas phase, a compressor is needed to compress CO_2, whereas a pump may enhance the pressure in the liquid phase. The critical pressure of CO_2, 7.38 MPa, switches a compressor to a pump. From 0.1 to 7.38 MPa, compressors are utilized, and from 7.38 to 15 MPa, pumps are employed.

Guo and Ghalambor (2005) [112] provided the equation for the ideal compression ratio (CR) for each stage of a multi-stage compressor:

$$CR = \left(\frac{P_{switch}}{P_{initial}}\right)^{1/N_{stage}}. \tag{3.10}$$

McCollum and Ogden (2006) [14] derived the following equation to determine the required compression power for each stage:

$$W_{s,i} = (\frac{m.Zs.R.T_{in}}{M\eta c})(\frac{Ks}{Ks-1})\left[(CR)^{Ks-1/Ks} - 1\right]. \tag{3.11}$$

where, P_{switch} is the pressure at which the compressor is switched to pump; N_{stage} is the number of compressor stages, typically 4 or 5; W_s is the compression power requirement (kJ); m is the CO_2 mass flow rate (kg/s); Zs is the compressibility factor; Tin is the inlet temperature (typically 313.15 K); Ks is the specific heat ratio (Cp/Cv); M is the CO_2 molar mass (44.01g/mole); R is the universal gas constant (8.314 kJ/kmol K); ηc is the is the isentropic efficiency of the compressor (typically 0.75).

With Regards to McCollum and Ogden (2006) [14], the Zs and Ks for each stage are provided in Table 3.5.

P_{switch} = **7.8 MPa**	**Stage 1**	**Stage 2**	**Stage 3**	**Stage 4**	**Stage 5**
P (MPa)	0.1-0.24	0.24-0.56	0.56-1.32	1.32-3.12	3.21-7.38
Zs	0.995	0.985	0.970	0.935	0.845
Ks		1.289	1.309	1.379	1.704

Table 3.5: Zs and Ks for each stage are provided by McCollum and Ogden (2006) [14].

To assess the pumping power required, the research of McCollum and Ogden (2006) [14] was repeated for increasing the CO_2 pressure from P_{switch} (7.38 MPa) to $P_{required}$ (15 MPa):

$$Ep = \frac{m(P_{requied} - P_{switch})}{\rho.\eta p}. \tag{3.12}$$

where, Ep is the energy consumption of pump (kJ); m is the CO_2 mass flow rate (kg/s); $P_{required}$ is the required outlet pressure (kPa); ρ is the average CO_2 density (typically 630 kg/m3); ηp is the isentropic efficiency of pump (typically 0.75).

To simplify the final equation and get the energy required in kWh/tonne CO_2 [113]:

$$E_{comp} = 51.632 + 2.785 \times ln(PCO_2 + 101.38). \quad (3.13)$$

Where, E_{comp} is the unit energy requirement for CO_2 compression (kWh/tonne CO_2); PCO_2 is the desired CO_2 product pressure (KPa).

3.2.2.2.2 Water Consumption for Inter-stage Cooling

Multi-stage compressors are water-cooled by flowing cold water to cylinder heads, inter-coolers, and after-coolers. The following equation calculates inter-stage cooling water needs (US National Institute of Standard and Technology):

$$m_{water} = (m_{CO_2}\ C_{pCo_2}\ \Delta T_{CO_2})/(C_{pwater}\ \Delta T_{water}). \quad (3.14)$$

where, m_{water} is the mass flow of the cooling water (kg/hr); m_{CO_2} is the mass flow of the compressed CO_2 (kg/hr); C_{pCO_2} is the specific heat; C_{pwater} is the specific heat of cooling water (typical value=7.56 kJ/kg ^{0}C); ΔT_{water} is the water temperature difference (15 ^{0}C is set as default value); ΔT_{CO_2} is the CO_2 temperature change (From CO_2 at suction pressure and at discharge pressure).

Guo and Ghalambor (2005) [112] calculated ΔT_{CO_2}:

$$\Delta T_{CO_2} = T_{in}\left[(P_2/P_1)Z^{(k-1)/k} - 1\right]. \quad (3.15)$$

where, Tin is the inlet CO_2 temperature at suction pressure; P_1 is the suction pressure of CO_2 (KPa); P_2 is the pressure of CO_2 at discharge point (KPa); Z is the average CO_2 compressibility, with a default value 0.845; k = (Cp/Cv) is the average ratio of specific heats of CO_2, with a default value 1.074;

In reference to Kohl and Nielsen (1997) [114] and the kind of cooling water system used to determine water loss, If the cooling water system is a closed system, then the water consumption of the compression process is equal to mwater. Water loss occurs due to evaporation, blow-

down, and drift if the cooling water system is a closed circuit and recycled to a cooling tower. Total water loss is equal to water consumption, which is equal to water replenishment (Equation 3.16).

$$Total\ Losses = Drift\ Losses + Evaporation\ Losses + Blowdown\ Losses. \tag{3.16}$$

$$Drift\ Loss = 0.15\% \times water\ flow\ rate. \tag{3.17}$$

$$Evaporation\ Loss = 0.0015 \times water\ flow\ rate \times \Delta T. \tag{3.18}$$

$$Blowdown\ Loss = Evaporation\ Loss/(cycles - 1). \tag{3.19}$$

Where, ΔT is the cooling range, with a typical value of 17 ^{0}C. Cycles refer to the cooling water circulation rate, which is typically 5 to 10.

3.2.2.2.3 Adsorbent Consumption by the Dehydration Unit

According to Abdi (2007) [13], aluminosilicate adsorbents may absorb between 13 and 22 kilograms of water per 100 kilograms of adsorbent. The equilibrium capacity of new adsorbent is expected to be about 20%, whereas the capacity of a sieve that's been used for 3-5 years would be around 13%. When determining adsorbent consumption, count all adsorption tanks. The equation for calculating adsorbent needs is:

$$S_s = (n \times m_{wt})/(0.15 C_{ss} C_t T_s 24 \times 365). \tag{3.20}$$

$$m_{wt} = m_{CO_2}(W_{CO_2} - W). \tag{3.21}$$

Where, S_s is the amount of molecular sieves used to remove the water to required level (kg); C_{ss} and C_t are correction factors, provided in Figure 3.10; Ts is the lifespan of the molecular sieve, with an average value of 4 years; n is the number of tanks; m_{wr} is the water removed; m_{CO_2} is the CO_2-rich gas flow rate (kg/hr); W_{CO_2} is the water content of CO_2-rich gas after compression; W is the required water content of the final CO_2 product.

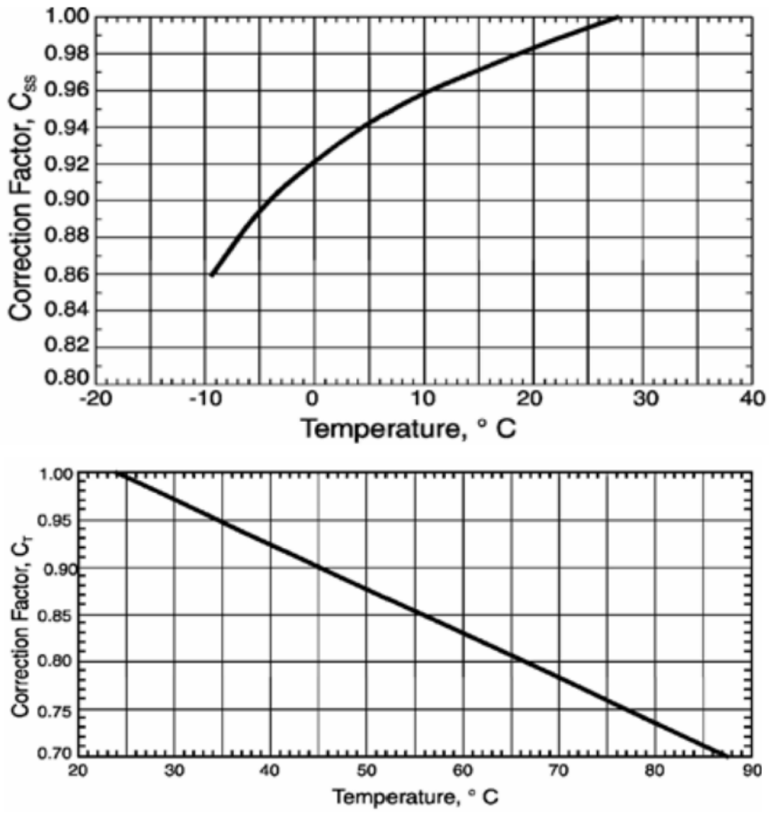

Figure 3.10: First, Molecular sieve capacity correction for unsaturated inlet gas, and second one for temperature (C_{ss} and C_t) [13].

3.2.2.2.4 Energy Requirement for Absorbent Regeneration

Abdi (2007) [13] provides the following formula for calculating the energy necessary to desorb water and heat the molecular sieve:

$$Q_w = 1706 \times m_{wr}. \tag{3.22}$$

$$Q_{si} = 0.409 \times S_s \left(T_{rg} - T_r\right). \tag{3.23}$$

$$Q_{bl} = 0.9478 \times \left(Q_w + Q_{si}\right). \tag{3.24}$$

$$Q_{tr} = Q_w + Q_{si} + Q_{bl}. \tag{3.25}$$

where, Q_w is the desorption of water heat duty (kJ); m_{wr} is the water removed by a molecular sieve (kg); Q_{si} is the duty to heat the molecular sieve to regeneration temperature (kJ); Q_{bl} is the regeneration heat loss (kJ); Q_{tr} is total regeneration heat duty (kJ); T_{rg} is the temperature of molecular sieve regeneration; T_r is the initial temperature of molecular sieve (^{0}C).

3.2.2.2.5 Natural Gas Combustion and Emissions

Combustion of natural gas provides the heat that is necessary for the process of adsorbent regeneration. Table 3.6 contains information on the emission factors caused by the internal combustion of natural gas [24]. The following equation may be used to determine the emissions resulting from combustion natural gas:

$$E_i = F_i \times Q_w. \tag{3.26}$$

where, E_i = emission of i_{th} pollutant; F_i = emission factor of i_{th} pollutant; Q_{tr} = total regeneration duty.

Emissions	Emission Factor (Kg/Mj)
CO_2	5.06E-02
Pb	2.11E-10
NO_2	9.27E-07
PM	3.20E-06
SO_2	2.53E-07
TOC	4.64E-06
CH_4	9.70E-07
VOC	2.32E-06
As	8.43E-11
Ba	1.85E-09
Cd	4.64E-10
Cr	5.89E-10
Co	3.54E-11
Cu	3.58E-10
Mn	1.60E-10
Hg	1.10E-10
Ni	8.86E-10
Se	1.01E-11
V	9.67E-10
Zn	1.22E-08

Table 3.6: The emission factors caused by the internal combustion of natural gas [24].

3.3 Life Cycle Inventory Modeling of CCS Transportation and Injection

The step that connects the CO_2 sources to the storage locations is the transport of CO_2. By taking into account the length of CO_2 transportation, surface temperature, and the features of a saline aquifer such as reservoir pressure, thickness, depth, and permeability, the LCI models

designed for energy consumption and fugitive emissions address the geological variations.

3.3.1 Modeling of Transportation

3.3.1.1 Principle of Transportation Technology

Pipeline transportation and the utilization of ocean tankers are the current procedures for long-distance movement of substantial volumes of carbon dioxide. Carbon dioxide pipelines are not new, and they currently span more than 2,500 kilometers in the western United States, transporting about 50 million tons of CO_2 yearly from natural and industrial sources to enhanced oil recovery operations [4]. A comprehensive model is figured out in the following parts.

3.3.1.2 Schematic Model of Transportation

The key processes in CO_2 pipeline transport systems, according to LCA, are pipeline transport and intermediate recompression through compressor. Figure 3.11 depicts a schematic of the LCI model created for the CO_2 pipeline transport system. The LCI model determines CO_2 density and viscosity, CO_2 pipeline diameter, CO_2 pressure drop in the pipeline, and the energy necessary for recompression. Emissions from recompression stations and pipelines are also quantified using updated emission factors.

3.3.1.2.1 Operational and Design Parameters

The first item of information required to figure out the LCA model is to get operational and design parameters. The pipeline inlet and output pressures, as well as the CO_2 temperature, are input variables in the LCI model. Table 3.7 summarizes the operating and design characteristics for CO_2 pipeline transportation discovered in the literature. According to [14], the following regression equations [3.7] can be used to compute CO_2 density and viscosity as a function of pressure and temperature.

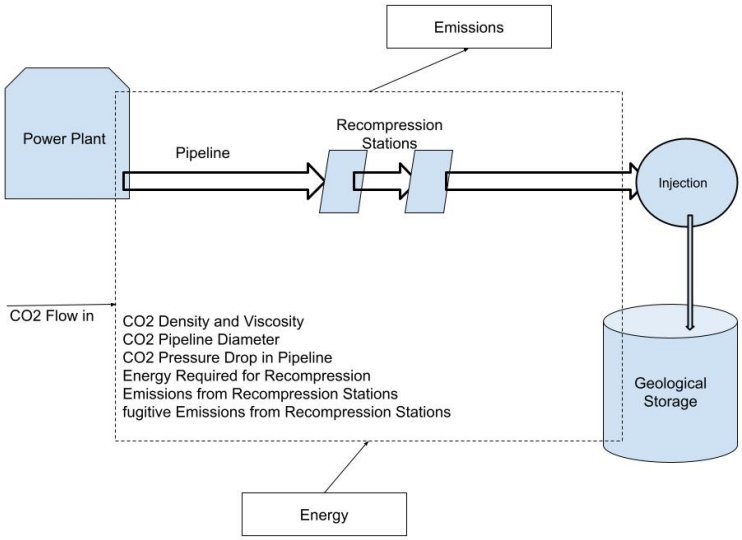

Figure 3.11: The LCI model of CO_2 pipeline transport system.

Common Design Properties	Hamelinck et al. (2001)[115]	Heddle et al. (2003)[29]	McCollum and Ogden (2006)[14]
Pipeline Inlet Pressure [MPa]	7.5	10.3-15.2	15.2
Pipeline Outlet Pressure [MPa]			10.3
CO_2 Temperature	10	25	25
CO_2 density [kg/m^3]	899	884	884
CO_2 viscosity [Pa s]	0.00008220	0.00006060	0.00006060

Table 3.7: Operational and design parameters for CO_2 pipeline transportation [14].

$$Y = ax^6 + bx^5 + cx^4 + dx^3 + ex^2 + fx + g. \tag{3.27}$$

where Y is density (kg/m3) or viscosity (Pa s); x is pressure (MPa); a, b, c, d, e, f, g are regression coefficients. For different temperatures, the regression coefficients for density (or viscosity) are provided in Figure 3.12 and Figure 3.13 .

Temperature (°C)	a (x^6)	b (x^5)	c (x^4)	d (x^3)	e (x^2)	f (x)	g
-1.1	-3.13E-07	3.25E-05	-1.44E-03	3.68E-02	-6.57E-01	1.21E+01	8.99E+02
4.4	-9.55E-08	1.98E-05	-1.41E-03	5.07E-02	-1.08E+00	1.77E+01	8.43E+02
10.0	-6.99E-07	8.56E-05	-4.41E-03	1.26E-01	-2.20E+00	2.82E+01	7.69E+02
15.6	-2.93E-07	6.57E-05	-4.75E-03	1.68E-01	-3.32E+00	4.21E+01	6.71E+02
21.1	-7.86E-06	8.73E-04	-4.03E-02	9.98E-01	-1.43E+01	1.22E+02	3.84E+02
26.7	-4.15E-05	4.44E-03	-1.95E-01	4.55E+00	-5.96E+01	4.30E+02	-5.36E+02
32.2	-1.10E-03	1.13E-01	-4.77E+00	1.05E+02	-1.26E+03	7.95E+03	-1.97E+04
37.8	-5.43E-04	5.98E-02	-2.71E+00	6.45E+01	-8.51E+02	5.93E+03	-1.63E+04
43.3	9.61E-04	-9.44E-02	3.73E+00	-7.54E+01	8.08E+02	-4.21E+03	8.42E+03
48.9	1.03E-03	-1.05E-01	4.36E+00	-9.33E+01	1.08E+03	-6.23E+03	1.43E+04
54.4	4.92E-04	-5.31E-02	2.33E+00	-5.29E+01	6.49E+02	-3.97E+03	9.61E+03
60.0	1.78E-05	-5.26E-03	3.80E-01	-1.20E+01	1.86E+02	-1.32E+03	3.61E+03
65.6	-2.01E-04	1.79E-02	-6.14E-01	9.95E+00	-7.50E+01	2.48E+02	-1.21E+02
71.1	-2.27E-04	2.18E-02	-8.26E-01	1.56E+01	-1.54E+02	7.79E+02	-1.49E+03
76.7	-1.72E-04	1.71E-02	-6.76E-01	1.34E+01	-1.40E+02	7.58E+02	-1.56E+03
82.2	-1.04E-04	1.07E-02	-4.39E-01	9.02E+00	-9.70E+01	5.47E+02	-1.16E+03

Figure 3.12: The coefficients for density calculations [14].

Temperature (°C)	a (x^6)	b (x^5)	c (x^4)	d (x^3)	e (x^2)	f (x)	g
-1.1	-3.77E-14	4.43E-12	-2.22E-10	6.35E-09	-1.20E-07	3.21E-06	9.70E-05
4.4	-4.13E-14	5.06E-12	-2.67E-10	8.10E-09	-1.60E-07	3.69E-06	8.53E-05
10.0	-1.80E-13	1.97E-11	-9.10E-10	2.33E-08	-3.71E-07	5.35E-06	7.07E-05
15.6	-3.84E-13	4.25E-11	-1.97E-09	5.00E-08	-7.54E-07	8.43E-06	5.18E-05
21.1	-9.84E-13	1.09E-10	-4.98E-09	1.23E-07	-1.75E-06	1.59E-05	2.02E-05
26.7	-4.04E-12	4.32E-10	-1.91E-08	4.46E-07	-5.88E-06	4.40E-05	-6.76E-05
32.2	2.28E-10	-2.27E-08	9.15E-07	-1.90E-05	2.12E-04	-1.20E-03	2.68E-03
37.8	9.45E-11	-9.37E-09	3.75E-07	-7.70E-06	8.44E-05	-4.58E-04	9.69E-04
43.3	4.61E-11	-4.65E-09	1.89E-07	-3.98E-06	4.50E-05	-2.50E-04	5.51E-04
48.9	2.17E-11	-2.27E-09	9.72E-08	-2.17E-06	2.62E-05	-1.57E-04	3.81E-04
54.4	1.75E-11	-1.84E-09	7.91E-08	-1.78E-06	2.18E-05	-1.33E-04	3.32E-04
60.0	1.59E-11	-1.66E-09	7.09E-08	-1.58E-06	1.93E-05	-1.18E-04	2.99E-04
65.6	1.33E-11	-1.38E-09	5.86E-08	-1.30E-06	1.59E-05	-9.75E-05	2.52E-04
71.1	9.60E-12	-9.95E-10	4.21E-08	-9.35E-07	1.15E-05	-7.10E-05	1.90E-04
76.7	4.94E-12	-5.14E-10	2.19E-08	-4.94E-07	6.23E-06	-3.93E-05	1.15E-04
82.2	8.35E-13	-9.24E-11	4.29E-09	-1.10E-07	1.66E-06	-1.17E-05	4.94E-05

Figure 3.13: The coefficients for viscosity calculations [14].

3.3.1.2.2 Composition of Product in Pipeline

The CO_2 product composition (an example Table 3.10) for pipeline transportation is not subject to any standard specifications. Under the limitations of the pipeline architecture, the CO_2 pipeline operators often set minimum standards for composition. While low nitrogen concentration is crucial for EOR, it would not be as crucial for alternative storage methods. A lower defined maximum H_2S level may be present in a CO_2 pipeline that passes through inhabited regions [4].

Compositions	Indicative Concentration (%)
CO_2	98.3
NO	0.1
SO_2	0.5
H_2S	0.2
CO	0.7
H	0.2
TOT	100

Table 3.8: Composition of CO_2 product in a pipeline [25].

3.3.1.2.3 Mass Flow Rate and Pipeline Diameter

One of the key elements that affects the pipeline diameter is the CO_2 mass flow rate from a power plant. The following equation [75] describes how CO_2 mass flow rate and pipeline diameter are related:

$$D = [m/(0.25\pi\rho v)]^{0.5}. \tag{3.28}$$

where: D = pipeline diameter [m]; m = CO_2 mass flow rate [kg/s]; ρ = CO_2 density [kg/m3]; v = flow velocity [m/s], which is typically from 2-3 m/s [14].

According to [11], For CO_2 pipes, the highest practical diameters are 1,600 mm (63 in) for land-based pipelines and 1,500 mm (59.06 in) for ocean-based pipelines.

3.3.1.2.4 Pressure Drop in the Pipeline

Regarding [11], Due to frictional forces, the pressure decreases as CO_2 moves through the pipeline. The pressure loss in a CO_2 pipeline can be calculated using the equation below for a typical CO_2 pipeline transport velocity of between 2 and 3 m/s.

$$\Delta p = \rho f(Lv^2/2d). \tag{3.29}$$

where, Δp = pressure drop (Pa); d= pipeline diameter (m); v= CO_2 flow velocity (m/s); L=pipeline length (m); $\eta = density(kg/m^3)$; f is the dimensionless pipeline friction number with a roughness of 0.5mm.

3.3.1.2.5 Energy Consumption and Emissions from Recompression and Booster Stations

Heddle et al. (2003) [29] stated that in order to achieve power consumption by booster stations for increasing CO_2 pressure during pipeline transport, recompression may be necessary at specific locations along the length of the pipeline to overcome pressure decrease. Recompression is frequently required for pipes longer than 150 km (90 miles). As a result, the energy consumed by booster stations to raise CO_2 pressure can be calculated using the following equations:

$$n_{booster} = INT(L/150). \tag{3.30}$$

$$P_{power} = n_{booster} \times (Q \times \Delta P)/(3,600,000 \times \eta). \tag{3.31}$$

Where, the number of the booster stations, $n_{booster}$; INT (number) is the function that rounds a number down to the nearest integer; L is the length of the CO_2 pipeline; P_{power} = power consumption (MW); Q = CO_2 flow rate [m3/hr]; ΔP = pressure increase in the booster (kPa); η = pump efficiency, typically 0.75.

The emission factors for natural gas-powered internal combustion engines are shown in the table below (Regarding [26]). The following equation could be utilized to compute these emissions:

$$E_i = F_i \times P_{power}. \tag{3.32}$$

where, E_i = emission of i_{th} pollutant; F_i = emission factor of i_{th} pollutant (from Table 3.9); P_{power} = power consumption (MW), calculated using last Equation.

Pollutants	Emission factors(kg/MW)
Nox	3.42E+00
CO	5.76E+00
CO_2	1.70E+02
SO_2	9.10E-04
TOC	5.54E-01
CH_4	3.56E-01
VOC	4.58E-02
PM	1.47E-02

Table 3.9: The emission factors for natural gas-powered internal combustion [26].

3.3.1.2.6 Pipeline and Booster Station Fugitive Emissions

Fugitive emissions are those caused by leaks in pressurized equipment, and these leaks typically occur through valves, flanges, seals, connections, open end lines, or similar equipment [30]. The IPCC's preset emission factors are used in facility level emission computations (2006) (and Table 3.10). The fugitive CO_2 emissions from the capture site to the storage site can be estimated as follows:

$$E_{fCO_2} = (L \times F_p + n_{booster} \times P_{power} \times F_b)/Plant\ capacity. \tag{3.33}$$

where, E_{fCO_2}= total fugitive emissions (tonne/yr); L= length of the CO_2 pipeline (km); F_p= fugitive emission factor of pipeline (tonne/km/yr); F_b= fugitive emission factor of booster station (tonne/MW/yr); $n_{booster}$= number of booster station. P_{power} = power consumption (MW),

The fugitive emissions of other gases included in the CO_2 product are computed as follows:

$$E_f = E_{fCO_2} \times C_{gas}/C_{CO_2}. \tag{3.34}$$

where, E_f = total fugitive emissions (tonne/yr); C_{CO_2} = the concentration of CO_2 in the CO_2 product; C_{gas} = the concentration of the gas (e.g. NOx, SOx, etc.) in the CO_2 product.

Type	Low	Medium	High	Unit
Pipeline	0.23	2.32	23.24	Tonne/km/yr
Booster	6.97	23.24	116.2	Tonne/MW/yr

Table 3.10: Emission factors from the [27].

On the other hand, the equipment level emission model can be utilized if comprehensive information on pipeline components, such as the number of valves, flanges, or connections, is available. The emission factors for these equipment level shown in Table 3.11. Also, the fugitive CO_2 emissions from a pipeline equipment are provided by [24, 27]:

$$E_{CO_2} = \Sigma F_i \times N. \tag{3.35}$$

where, E_{CO_2} = Emission rate of CO_2; F_i = Applicable average emission factors for the major equipment type; N = Number of pieces of equipment in the process.

Equipment Type	Emission Factor (kg/hr/source)
Valves	7.47E-03
Pump Seals	3.98E-03
Connectors	3.32E-04
Flanges	6.47E-04
Open-ended Lines	3.32E-03
Drains	5.31E-02

Table 3.11: The emission factors for fugitive emissions from pipeline equipments [28].

3.3.2 Modeling of CO_2 Injection

3.3.2.1 CO_2 Injection System

The number of injection wells and the CO_2 surface injection pressure are governed by the CO_2 mass flow rate and CO_2 storage reservoir parameters such as pressure, thickness, depth, and

permeability, which effect the number of injection wells and the CO_2 surface injection pressure. The CO_2 injection system usually includes of wellheads, distribution manifolds at the end of transport pipes, distribution pipelines to wells, extra compression facilities, monitoring and control systems, and injection wells Figure 3.14.

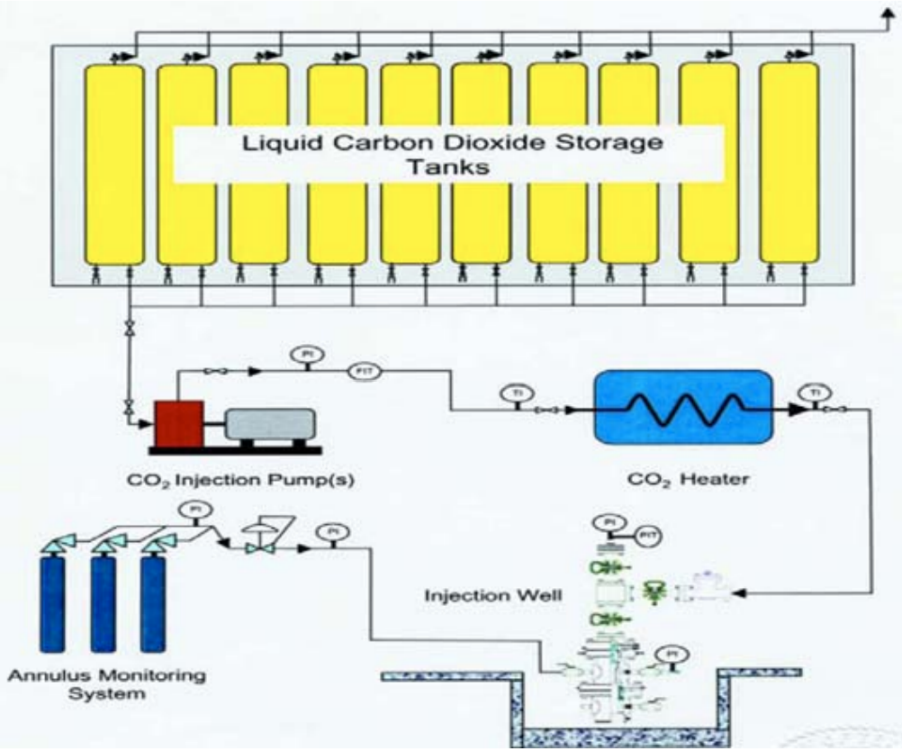

Figure 3.14: A CO_2 injection system for CO_2 saline aquifer storage [15].

3.3.2.2 Schematic Model of CO_2 Injection

The maximum allowable bottomhole injection pressure, the CO_2 injectivity, the number of injection wells, the energy needed for the injection pumps and the CO_2 heater, the emissions from the injection pumps and the CO_2 heater, and the fugitive emissions from the CO_2 injection surface facilities are all calculated using the LCI model. A schematic of the LCI model for a CO_2 injection system is shown in Figure 3.15.

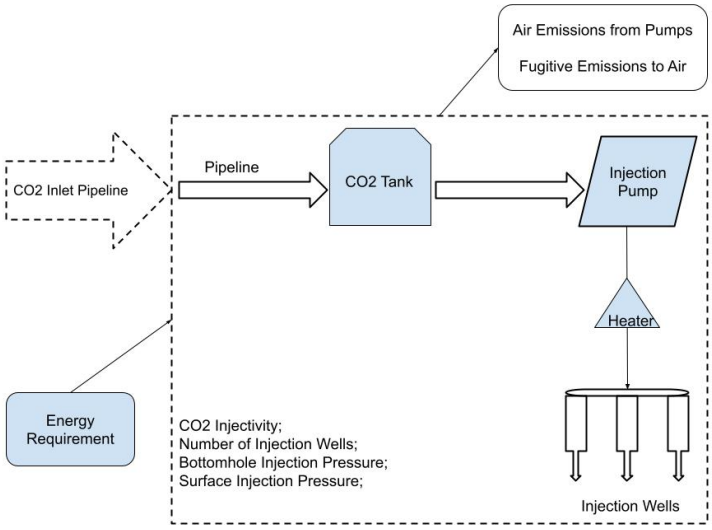

Figure 3.15: The LCI model of CO_2 Injection.

3.3.2.2.1 Maximum Allowable Injection Bottomhole Pressure

In consideration of [116, 117], The injection bottomhole pressure (BHP) is the CO_2 pressure at the injection well's bottom. To minimize uncontrolled fracturing of the reservoir rock, the top limit of injection BHP (or maximum permitted BHP) is established at the fracture pressure of the reservoir rock. Thanks to such research, the fracture pressure of the reservoir rock may be calculated using the equations below.

$$G_f = \gamma - \beta e^{-\alpha d}. \tag{3.36}$$

$$P_f = G_f d. \tag{3.37}$$

where P_f is the fracture pressure at depth (Pa), G_f is the fracture gradient (Pa/m), d is depth, and α, β and γ are coefficients with the values: 4.36 × 10-4 m -1, 9.24 kPa/m, and 22.62 kPa/m respectively.

3.3.2.2.2 CO_2 injectivity and wells number

Herzog et al. (2003) [29] investigated injectivity and defined it as the injection rate divided by the excess pressure above the reservoir equilibrium pressure driving the injection, whereas CO_2 injectivity represents the mass injection rate of CO_2 (q) that can be injected per unit of reservoir thickness (h) and per unit of downhole pressure difference.

$$I = q/(BPH - P_{res})h. \tag{3.38}$$

where, q is the injection rate (m^3/s); BHP is the bottomhole pressure (MPa); Pres is the reservoir pressure (MPa).

Law and Bachu's [118] empirical relationship is used to quantify CO_2 injectivity, where CO_2 mobility is the CO_2 mobility in the reservoir and may be determined by [29]:

$$CO_2\ injectivity = 0.0208 \times CO_2\ mobility. \tag{3.39}$$

$$CO_2\ mobility = k_a/\mu_{inter}. \tag{3.40}$$

where μ_{inter} represents the CO_2 viscosity in the reservoir near the bottom of the injection well (Pa.s), k_a is the absolutely permeability of the reservoir and can be calculated from the following equation [118]:

$$k_a = (k_h \times k_v)^{0.5}. \tag{3.41}$$

where k_h and k_v are the horizontal and vertical permeabilities of the reservoir respectively (mD).

According to McCollum and Ogden (2006), if the reservoir temperature (T_{res}) is unknown, the following equation can be used to estimate the reservoir temperature (T_{res}).

$$T_{res} = T_{sur} + d \times (G_g/1,000). \tag{3.42}$$

where T_{sur} is the surface temperature, and G_g is the geothermal gradient with a typical value of 25 o C/km.

Finally, the CO_2 injection rate per well is calculated by the following equation [15]. Additionally, the quantity of injection wells (N) is determined by the rate of CO_2 delivery to the injection site (M_f) as well as the rate of injection per well.

$$Q_{well} = (CO_2\ injectivity) \times h \times (BHP - P_{res}). \tag{3.43}$$

$$N = M_f/Q_{well}. \tag{3.44}$$

where Q_{well} is the injection rate per well (kg/s), h is the thickness of the reservoir, and Pres is the reservoir pressure.

This study applies the parameters of CO_2 storage reservoirs in the United States presented by Herzog (2003) [29] in saline aquifers to reflect a real analysis (Table 3.12).

Parameter	Unit	Typical Aquifer	Aquifer
Pressure	Mpa	8.4	5 – 11.8
Thickness	M	171	42 – 703
Depth	M	1239	694 – 1784
Permeability	md	22	0.8 – 585

Table 3.12: The parameters of CO_2 storage reservoirs in the United States [29].

3.3.2.2.3 Carbon Dioxide Injection Surface Pressure

Carcoana (1992) [119] developed the equation for the CO_2 injection surface pressure (Ptf) when:

$$P_{wf}^2 = P_{tf}^2 exp(s) + (1.57 \times 10^8 \times (SG)q^2 TZf(MD)\,[exp(s) - 1])/Sd^2. \quad (3.45)$$

where, P_{tf} = tubing flowing pressure (kPa); P_{wf} = the injection bottomhole pressure (kPa); q = average CO_2 injection rate (MMm^3/day); SG = CO_2 specific gravity; Z= CO_2 deviation factor, Z=0.56 is assumed to be practically; D = reservoir depth (m); d = Well tubing inside diameter (cm); MD = measured depth, which is the TVD; n = tubing roughness; T = average temperature in the tubing; f = friction factor; S = 0.0375(SG)(TDV)/TZ;

3.3.2.2.4 Energy Consumption and Emissions from the Injection Pumps and Heater

The CO_2 injection pumps are used to compress the CO_2 to the needed pressure if the CO_2 pipeline output pressure is less than the required CO_2 surface injection pressure. The injection pumps' energy consumption and emissions can be computed using Equation $P_{power} = n_{booster} \times (Q \times \Delta P)/(3,600,000 \times \eta)$, which was originally proposed for CO_2 pipeline transportation.

It could be necessary to put a CO_2 heater between the injection pumps and the insertion point. The CO_2 heater energy consumption and associated emissions model is created as an alternative. The CO_2 heater's goal is to maintain the CO_2's temperature at around 21 °C [15]. The heater will be set to the required temperature in order to control the CO_2's discharge temperature. The CO_2 heater's energy consumption can be determined using:

$$E_{ch} = n \times Q_{well} \times SH_c \times (T_{c,o} - T_{c,i})/\eta. \quad (3.46)$$

where: E_{ch} = the energy requirement for CO_2 heating (kJ); η = the efficiency of the heating devices, typical value 0.8; n = number of injection wells; Q_{well} = CO_2 injection rate per well (kg/s); $(T_{c,o} - T_{c,i})$ = the increase in CO_2 temperature (^{0}C); $T_{c,o}$ = Temperature of CO_2 entering the CO_2 heater (^{0}C); $T_{c,I}$ = Temperature of CO_2 exiting the CO_2 heater (^{0}C); SH_c = specific heat of CO_2 at required injection pressure (kJ/kg ^{0}C) and SH_c = 17.14P-0.5275 , this P is the CO_2

Source	Amount	Unit
Storage Stations	2.86E-02	tonne CO_2/station-hr
Distribution Pipelines	7.25E-05	tonne CO_2/km-hr
Heaters	7.62E-05	tonne CO_2/heater-hr
Wellheads	2.99E-05	tonne CO_2/well-hr
Injection Pumps	3.52E-04	tonne CO_2/compressor-hr

Table 3.13: Fugitive emission factors for gas transmission and storage equipment [30].

pressure at the outlet of the CO_2 heater (MPa) (NIST).

3.3.2.2.5 Fugitive Emissions

To estimate the fugitive emissions from CO_2 injection plants, a facility level emissions technique might be utilized. The natural gas emission factors are changed to get the adjusted emission factors [27]. The same equations used in the transportation section are used to compute the fugitive CO_2 emissions during injection. Table 3.13 shows emission factor in case of facility level approach.

3.4 Life Cycle Inventory Modelling of CO_2 Storage

As stated before, this research takes into account only saline aquifer of geological storage. Saline aquifers are reservoir rocks that are porous and permeable and hold saline water in the pore space between the rock grains (Figure 3.16).

3.4.1 Principle of Saline Aquifer

Saline aquifers can be sandstone or limestone formations with good size, depth, porosity, and caprock stability. The reservoir must be large enough to be able to store the life time CO_2 emissions from the planned emission source. Porosity and permeability must be high enough to give adequate pore space for CO_2 storage and allow CO_2 input. Moreover, more than 800

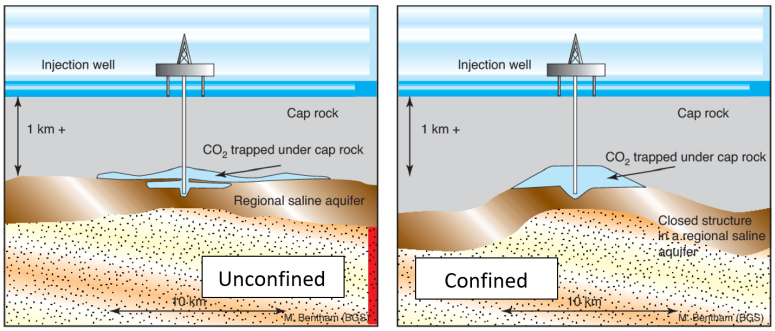

Figure 3.16: Saline Aquifer of CO_2 Storage [16].

meters below sea level is necessary for CO_2 storage because at that depth, CO_2 is in its dense phase and takes up significantly less pore space than it does in its gaseous form. Additionally, due to its lower density than brine, injected CO_2 must be prevented from migrating vertically by an impermeable caprock that lies on top [16]. Finally, it's also vital to note that the four major methods by which injected CO_2 is stored in the storage reservoir are immobilization under traps, dissolving in salt water, capillary trapping, and geochemical reaction in the pore spaces.

On the other hand, it's important to look at the patterns of migration and distribution in the saline aquifer. CO_2 can be stored in aquifers both confined and unconfined (Figure 3.16). Gas storage methods are equivalent to CO_2 storage schemes in confined aquifers. The free phase CO_2 is confined by structural and/or stratigraphic features, and the injection ends before the gas reaches a spill point. If the reservoir structure is understood, migration paths and the form of the injected CO_2 plume may be reasonably predicted. CO_2 storage in unconfined aquifers entails injecting CO_2 into vast regional aquifers that lack major structural or stratigraphic closures. CO_2 migration paths in unconfined aquifers are more complicated than in confined aquifers.

During the CO_2 injection, when CO_2 reaches a given distance laterally, the lateral flow velocity slows and buoyancy becomes apparent. The buoyancy causes the free phase CO_2 plume to float to the formation's top. In aquifers with high vertical permeability, buoyancy causes the injected CO_2 to move upwards along the most permeable pathway until it hits the impermeable

caprock, where it forms a thin free phase CO_2 layer under the caprock's top (Figure 3.17, first one). While, buoyancy has a negligible impact on aquifers with low vertical permeability, and during the injection time, moving CO_2 does not reach the top of the formation (Figure second one).

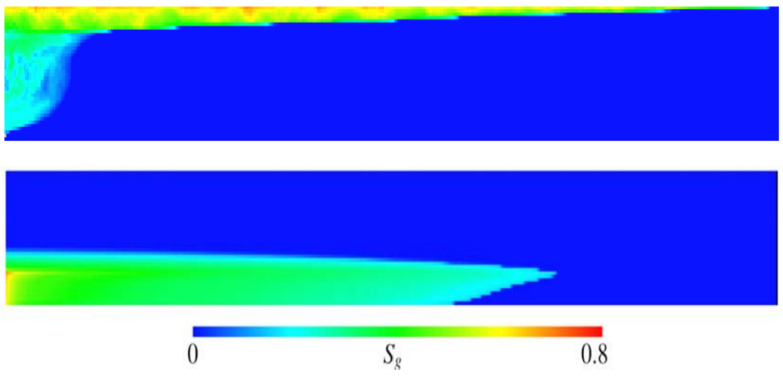

Figure 3.17: CO_2 saturation distribution [17].

3.4.2 Schematic Model of Saline Aquifer Storage

Examining the studies of Ennis-King and Paterson (2002) [120] and Sarapalli and McGrail (2002) [121] helps define the LCI model of saline aquifer storage. The LCI model divides the system into compartments and tracks the migration of injected CO_2 in the saline aquifer, since this establishes the geological boundaries and time period of the CO_2 storage system. Quantifying the CO_2 plume, the thickness of the CO_2 layer, the time it takes for the CO_2 plume to reach the top of the formation, the dissolution, capillary trapping, CO_2 lateral movement after injection ceases, and finally modeling the alternative leakage pathways interconnecting the caprock are all necessary to achieve this goal.

It is significant to note that the dispersion of dissolved CO_2 in groundwater and surface waters is not examined by this LCI model, which only determines the quantity of CO_2 reaching the atmosphere. If CO_2 leaks out from the storage aquifer, buoyancy will cause it to move via various areas of the overburden, such as water-saturated porous zones, surface water, or unsaturated soil zones, to shallower layers. Finally, the barrier between the atmosphere and the

land may be overcome by the CO_2 flow. Moreover, the LCI model's temporal horizon is 1,000 years, and figure 3.15 summarizes all that has been stated.

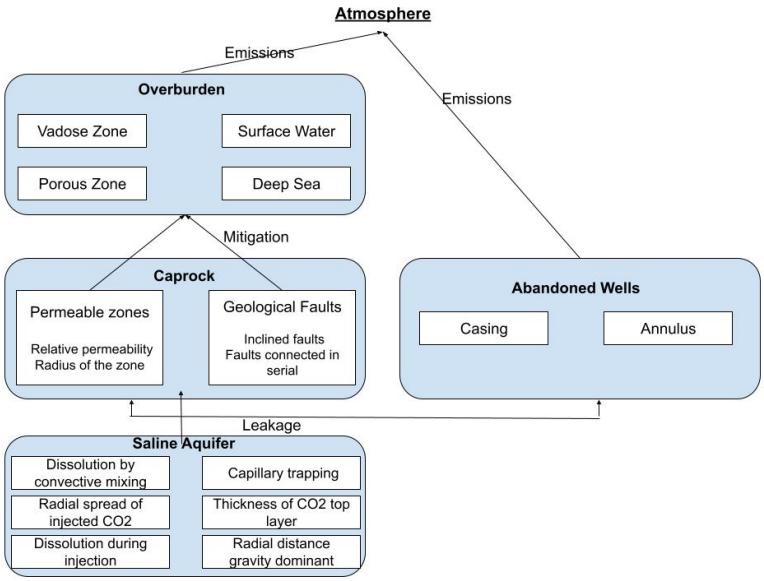

Figure 3.18: The LCI Model of Saline Formation Storage.

3.4.2.1 CO_2 Distribution around the Wellbore during Injection

Buckley-Leverett theory, with constant injection rate, uniform formation characteristics, and no gravity effects, may be used to determine the radial distribution of CO_2 around the injection well (Equation 3.47).

$$\pi r^2/t = (q/\varphi\rho_g h_i) \times (d\Phi/dS). \tag{3.47}$$

where, r is the radial distance; t is time (s); q is the mass injection rate of CO_2 (m^3/s); ρ_g is the gas density (kg/m3); φ is porosity (%); h_i is the height of the well completion interval (m); S is water saturation (%); and $\Phi = (k_{rw}/\mu_w)/(k_{rw}/\mu_w + k_{rg}/\mu_g)$ where, k_{rw} and k_{rg} are the relative permeability to water and to free phase CO_2, and μ_w and μ_g are the corresponding viscosities (Pa·s).

In terms of Saripalli and McGrail (2002) [121], An application of the Brooks-Corey relative permeability relationship may be used to simplify the equation for Φ, where the two phase relative permeabilities in granular porous media are written as:

$$k_{rw}/k_{rg} = S_w^e/(1 - S_w^e)(1 - S_w)^2. \tag{3.48}$$

3.4.2.2 The Lateral Extent

Ide et al. (2007) [18] proved that when the lateral flow rate is slow, the density difference between free-phase CO_2 and brine can be big enough to produce a gravity effect. Ennis-King and Paterson (2002) [120] estimated the radial extent where the gravity is dominant (Equation 3.49).

$$L^2 = (h_t.\mu_g.R^2.q)/(k_v.k_{rg}.\Delta\rho_g.\pi.\varphi.\rho_g.h_i). \tag{3.49}$$

Where, L is the radial extent; h_t is the thickness of the saline aquifer; μ_g is the free phase CO_2 viscosity (Pa·s); R is the dimensionless front radius; k_v is the vertical permeability (mD); q is the mass injection rate of (m^3/s); k_{rg} is the relative permeability to water and to free phase CO_2 respectively (%); ρ_g is the gas density (kg/m^3), φ is porosity (%); hi is the height of the well-completion interval (m).

3.4.2.3 Dissolution of CO_2 during and after Injection

One the one hand, because CO_2 is minimally soluble in water, it is reasonable to assume that the gas phase and formation water are locally in equilibrium. Next, Ennis-King and Paterson (2002) [120] provided the fraction of the injected gas that is dissolved in the formation water as follows:

$$P = (R_2 - 1)/(R_2 - 1 + \rho_g/(\rho_w.X_c)). \tag{3.50}$$

Where, R is the dimensionless front radius; ρ_g is the density of the CO_2 phase (kg/m3); ρ_w is the density of the aqueous phase (kg/m^3); and X_c is the mass fraction of dissolved carbon dioxide in the aqueous phase at saturation.

One the other hand, after the cessation of CO_2 injection, free-phase CO_2 can still dissolve through the convective mixing effect under three different mass transport frameworks: pure diffusive transport initially, rapid infinite-acting convective mass transport afterwards, and slow finite-acting convective mass transport afterwards [122]. The rate of dissolution in the diffusive regime is influenced by molecule diffusion and decreases quickly with time. Mass transfer overall is proportional to to.5. Fresh, Unsaturated brine is pushed upward to the CO_2-brine interface during the infinite-acting convection, whereas plumes of CO_2 saturated brine with higher density migrate downward. Convection speeds up the CO_2's disintegration. At the termination of infinite active convection, the dissolution fraction might exceed 50%. After the plume tips of CO_2 saturated brine have reached the bottom of the reservoir, finite-acting convection finally takes place, and convection dramatically slows down. According to Riaz et al. (2006) [123] and Hesse et al. (2006a) [122], convective transport must happen before the dissolved CO_2 diffusive boundary layer reaches a threshold thickness. The following equation represents the crucial period for the initiation of convection:

$$t_c = 146 \times (\varphi.\mu_w^2 D)/(Kg\Delta\rho_{gw})^2. \tag{3.51}$$

where, t_c is the crucial period for the initiation of convection; Where φ is the porosity (%); μ_w is the viscosity of the brine (Pa·s); D is the diffusivity (m^2/s); K is the absolute permeability; g is the gravitational acceleration and $\Delta\rho_{gw}$ is the density difference between the CO_2 saturated and the unsaturated brine with a typical value of 5 kg/m^3.

The transport time from the first to the second regime (t_{on}), the transport time from the second to the third regime (t_{slow}), and the time required for the brine in the reservoir to become entirely saturated with dissolved CO_2 (t_{sat}) are all taken into account. (T_{sat}) is attained in practice when the reservoir is 95% saturated. with reference to Hesse et al. (2006a) [123], the

equations for these times are:

$$t_{on} = 6251 \times (\varphi.\mu_w^{11/5}.D^{6/5})/(K_v \Delta\rho_{gw} g)^{11/5 H1/5}. \tag{3.52}$$

$$t_{slow} = 15 \times (\varphi.\mu_w.H)/(K_v.\Delta\rho_{gw}.g). \tag{3.53}$$

$$t_{sat} = 230 \times (\varphi.\mu_w.H)/(K_v.\Delta\rho_{gw}.g). \tag{3.54}$$

Where, φ is the porosity (%); μ_w is the viscosity of the brine (Pa·s); D is the diffusivity (m^2/s); k_v is the vertical permeability (mD); g is the gravitational acceleration and $\Delta\rho_{gw}$ is the density difference between the CO_2 saturated and the unsaturated brine with a typical value of 5 kg/m^3.

The permeability of prospective storage aquifers can range from 1mD to 3D, and the critical timeframes can range from a few days (tc 10 days) in a high permeability aquifer to a few thousands of years (tc 2,000 years) in a low permeability aquifer. As a result, CO_2 dissolution will be an important trapping mechanism in high permeability aquifers, where occurrence is usually rapid and the dissolution rate is high, whereas in low permeability aquifers dissolution trapping will not significantly reduce mobile CO_2 before the critical time, that might be several hundred years after convection begins, and the dissolution rate will be low [122].

3.4.2.4 CO_2 Capillary Trapping in the Aquifer

Ide et al. (2006) explained about cpillarry trapping which is residual trapping and occurs when a wetting phase (like water) is becoming more saturated while a non-wetting gas phase is becoming less saturated. Gravity takes over after CO_2 injection stops, causing free phase CO_2 to move to the aquifer's surface. Then the gas saturation of the zones where free gas CO_2 is migrating out diminishes. This drop in saturation might cause capillaries to break off, and trapping CO_2. Capillary trapping can therefore be utilized to immobilize the quantity of free gas phase CO_2 that might leak from the aquifer in CO_2 storage. Moreover, timing of capillary trapping and

fraction of CO_2 trapped by capillary trapping are related to N_{gv}, given by [18]:

$$N_{gv} = (K_v.L.\Delta\rho_{gw}.g)/(H.u.\mu_{brine}). \tag{3.55}$$

Where k_v is the vertical permeability (mD), L the aquifer length (m), $\Delta\rho_{gw}$ the density difference between formation water and free-phase CO_2 (kg/m^3), g the acceleration of gravity, H the aquifer height (m), u the total average Darcy flow velocity (m/s), and □brine is the viscosity of brine (Pa·s).

Here, the relationship between capillary trapping rate and N_{gv} is demonstrated via a diagram (Figure 3.19). The free gas phase CO_2 that is present in the thin layer beneath the caprock cannot be trapped because there is no mechanism to reduce the gas saturation there, and systems with stronger gravitational forces have higher CO_2 saturation in the uppermost zone and consequently have less gas available to trap somewhere else. As a result, an aquifer with high N_{gv} has much less trapping [18].

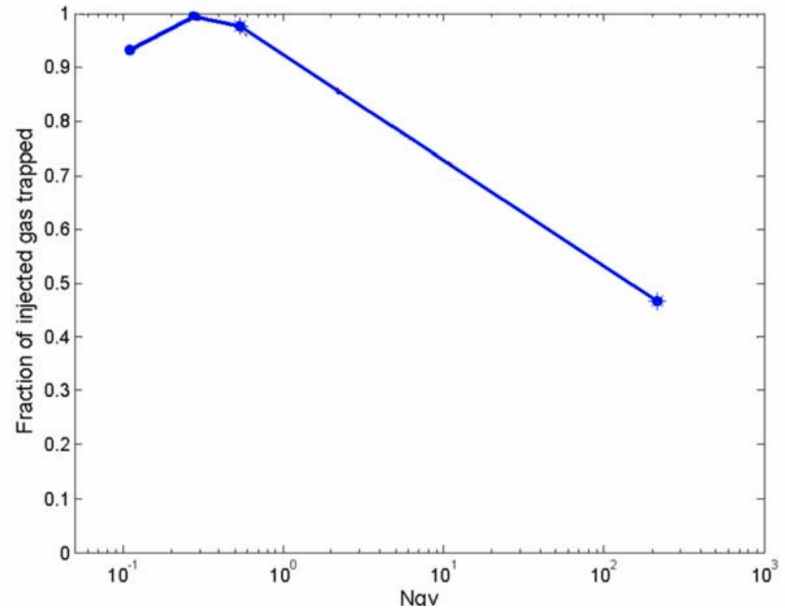

Figure 3.19: The last proportion of injected CO_2 that was trapped against N_{gv} [18].

3.4.2.5 CO_2 Leakage Calculation

There are three possible scenarios in which the leakage might occur: a permeable zone in the caprock, the fractures in the caprock, the abandoned well.

First, regarding Daddy's law, If the caprock has considerable permeability zones, free phase CO_2 in contact with the permeable zones will move to the top because of buoyancy. Moreover, when the free phase CO_2 flow through a permeable zone, the CO_2 fluid is single phase flow. Because caprock is commonly found at depths more than 1,000 m and CO_2 remains is supercritical phase while leaking through the caprock, the hypothesis of single phase flow is reasonable. The hydrostatic assumption means that the buoyancy of free-phase CO_2 floating beneath the top layer of the saline aquifer provides the force moving CO_2 upwards. According to [124], the free phase CO_2 flow through a permeable zone is calculated by equation:

$$Q = \left[k_{zone}.k_{rg}.\pi.r_{zone}^2/\mu_c\right] \times \left[(\rho_w - \rho_c).gh_c/l_{zone}\right]. \tag{3.56}$$

Where, k_{zone} is the intrinsic permeability (mD); k_{rg} is relative permeability to CO_2 (%); h_c is the thickness of free-phase CO_2 floating beneath the top layer (m); μ_c is the viscosity of the CO_2 (Pa·s); ρ_w,ρ_c are the density of brine and free phase CO_2 respectively (kg/m^3).

Sencondly fracture, With regards to [125], CO_2 could leak through faults in the caprock. If the faults connect to the atmosphere, the CO_2 leakage could be released directly into the atmosphere. A fault is characterized in this study as two smooth, parallel plates embedded in caprock with negligibly low permeability. For free phase CO_2 to enter a fracture, The CO_2 floating under the top aquifer layer causes the following vertical buoyancy pressure on the top aquifer layer:

$$P_b = (\rho_w - \rho_c)gh_c. \tag{3.57}$$

where, P_b is vertical buoyancy pressure; h_c is the thickness of free-phase CO_2 floating (m); ρ_w,ρ_c are the density of brine and free phase CO_2 respectively (kg/m^3); g is gravitational accel-

eration (m/s^2).

For CO_2 to open the fracture, P_b must exceed the capillary pressure (P_c), thus h_b (the thickness of free phase CO_2 layer that can open the fracture) is needed to satisfy the equation below, where, σ is the CO_2-brine interfacial tension, and the CO_2 fluid movement between the fracture and surrounding caprock is small enough to be neglected.

$$h_b \geq 2\sigma/(\rho_w - \rho_c)gd. \tag{3.58}$$

Besides, calculation of CO_2 flow rate by the aquation of [125]:

$$Q = (wd^3/12\mu_c) \times (\Delta P/L). \tag{3.59}$$

Where, w is the width of the fracture (m); d is aperture of the fault (m); L is the length of the fracture (m); ΔP is the pressure drop across the fracture (Pa) which is $(\rho_w - \rho_c)gh_c$.

Additionally, it is crucial to note that in this study, last equation is based on the assumption that the fracture is confined by two smooth, and parallel plates. As a result, d is considered as a real apeture of the fault. Also, this aquation is under the consideration that CO_2 moves as a single-phase. This is feasible when the faults only contact the caprock, because caprock is commonly found at depths greater than 1,000 m, and CO_2 remains in supercritical phase while leaking through the caprock at this depth [126].

Final case, CO_2 leakage from abandoned wells is the most direct CO_2 leaking channel to the surface and can happen more faster than others. Due to deterioration and corrosion, CO_2 can leak through several paths in a wellbore. The cement fill, cement plug, the interface between the cement fill and the formation rock, and the interface between the cement fill and the well casing are all conceivable paths. These potential leakage paths are depicted in Figure 3.20 given by Celia (2006) [127].

Before determining the CO_2 flow rate of an abandoned well leaking, it is important to remember that the CO_2 fluid is single phase; the leakage pathways initially contain water and

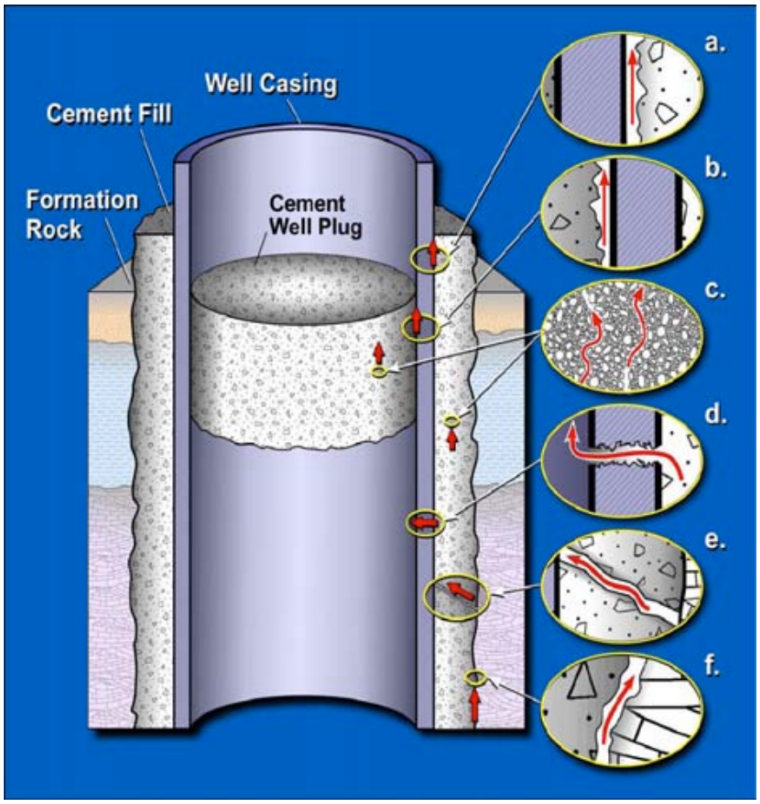

Figure 3.20: The potential CO_2 leakage paths from abandoned well.

initial conditions are hydrostatic; and the optimal way for CO_2 to migrate up along the central wellbore once it reaches the open wellbore is to do without leaking into the annulus and the formations around the wellbore. According to Brown (2000) [126], Nicot et al. (2006) [125], and Poiseuille's Law, the three forms of the CO_2 flow rate are computed with the following equations as gas channel, fracture, and microannulus respectively:

$$Q = (\pi R^4/8\mu_c) \times (\Delta P/L). \tag{3.60}$$

$$Q = (wd^4/12\mu_c) \times (\Delta P/L). \tag{3.61}$$

$$Q = (\pi R^3/8\mu_c) \times \left[(1-\kappa^4) - (1-\kappa^2)^2/Ln(1-\kappa)\right] \times (\Delta P/L). \tag{3.62}$$

where, Q is the flow rate of CO_2 (m^3/s); ΔP is the pressure drop across the channel or fracture or microannulus (Pa); R is the radius of the channel or mcroannulus (m); L is the length of the channel or fracture or microannulus (m); μ_c is the viscosity of supercritical CO_2 (Pa.s); d is the aperture of the fracture (m); κ is the ratio of internal to external radius of the microannulus.

At the end of this part, it could be advantagous to take an eaxmple of typical parameters for microannulus, fracture and gas channel from the study of [31]:

Leakage pathway geometry	**Value (μm)**
Gas channel radius	110
Fracture aperture	30
Microannulus thickness	12

Table 3.14: An example of typical parameters for microannulus, fracture and gas channel [31].

3.4.2.6 CO_2 Migration and Attenuation in different Zones

Migration and Attenuation of CO_2 are characterized into four Parts and will be discussed such as water-saturated porous zone, unsaturated soils above water table, surface water, and deep sea respectively.

First one, CO_2 can migrate upwards as small individual bubbles if the CO_2 leakage flow from the source zone, such as fractured rock or permeable zones, is minimal. This is especially true in coarse and highly permeable porous media. When the flow is substantial, however, a linked channel of CO_2 gas can emerge between the leading edge of water displacement and the source of CO_2 leakage [19]. The Corapcioglu et al. (2004) [128] approach may be used to calculate the bubble flow's velocity. In exceptionally coarse gravels, the bubble flow in the porous medium can reach a maximum velocity of around 18 cm s-1, but it is much slower

in normal sediments. While, The multiphase flow mechanism that controls the channel flow regime can be modeled using a reservoir engineering strategy, such as the model offered by Silin et al (2006)[124]. CO_2 rises roughly vertically in porous media with volumetric flux, F (m/s), determined by:

$$F = (k_v.k_{rg}/\mu_c)\Delta\rho_{gw}.g. \tag{3.63}$$

Where, k_v is the vertical absolute permeability (mD); k_{rg} is relative permeability (%); μ_c is the CO_2 viscosity (Pa·s); $\Delta\rho_{gw}$ is the density difference of CO_2 and water (kg/m^3).

A fraction of the leaking CO_2 will dissolve into surrounding water when CO_2 migrates upwards through the porous zone [125]. Before CO_2 leakage through the water-saturated porous zone, the whole water column (between the CO_2 source zone and the water table) exposed to the CO_2 plume would have to achieve maximum solubility concentrations of CO_2 [129]. Therefore, if there is not enough leakage, the CO_2 might completely dissolve into the groundwater. According to Nicot et al. (2006) [125], the attenuation rate of CO_2 resulting from CO_2 dissolution in water-saturated porous zone may be approximated as follows:

$$R_a = v_w.C_w.V_w/M_c. \tag{3.64}$$

$$V_w = \varphi.H.S. \tag{3.65}$$

Where, M_c is the CO_2 leakage rate (kg/s); v_w is the groundwater horizontal velocity (m/s); C_w is the solubility of CO_2 in water (kg/m^3); V_w is the volume of water on top area of leak (m^3); φ is the porosity of the water-saturated zone (%); H is the thickness of the water-saturated zone (m); S is the horizontal cross-sectional area of the CO_2 plume (m^2).

Secondly, with regards to Altevogt and Celia (2002) [130]; Oldenburg (2003) [129], if concentrated CO_2 is discharged to unsaturated soil via a fractured rock, leaky abandoned well, or other similar pathway, the buoyancy driving force is reversed because CO_2 is denser than

soil gas, and CO_2 migration will be governed by advective and diffusive transport processes. Pressure gradients cause the CO_2 to migrate higher and cause advective fluxes. Concentration gradients induce diffusive fluxes, which diffuse CO_2 laterally into the soil zones nearby. The density contrast is easily overcome by pressure gradients, resulting in CO_2 discharge near the ground's surface. However, the unsaturated soil zone can reduce seepage and near-surface CO_2 concentrations and attenuate CO_2 leakage by permeability trapping, and solubility trapping by infiltration or residual water. The seepage flux and near-surface gas concentrations are most significantly governed by the leakage rate and the radius of the leaking source zone.

It could be helpful to note that certain CO_2 leakage rates were utilized in the study by Altevogt and Celia (2002) [130] to assign the CO_2 attenuation rates of a typical unsaturated soil zone, as follows table below:

CO_2 **leakage per** m^2 $(kgm^{-2}s^{-1})$	**Attenuation rate (%)**
≤10-8	96
10-8÷10-7	66
10-7÷q0-6	19
≥10-6	1

Table 3.15: The CO_2 attenuation rates of a typical unsaturated soil zone

At the third stage, according to Oldenburg and Lewicki (2006) [19], If concentrated CO_2 leaks into surface water via a fractured rock, a leaky abandoned well, or another pathway, CO_2 transport tends to be by ebullition for relatively high leakage flux and/or deep water bodies, and diffusion or dispersion for relatively low leakage flux and/or shallow water bodies. During migrating across surface waters, a portion of CO_2 will be dissolved and dissociated in water. The transfer of dissolved CO_2 in surface waters is dependent on aqueous phase diffusive and dispersive mechanisms. Dispersion and mixing will expose surface water to the atmosphere on a regular basis, where it can possibly equilibrate with atmospheric CO_2, resulting in an efficient out-gassing that will eventually release the majority of dissolved CO_2 to the atmosphere. As a result, CO_2 storage, rivers, lakes, estuaries, and continental shallow ocean water are ineffective

in mitigating CO_2 leakage and seepage fluxes. Furthermore, during CO_2 migration in surface water, the dissociated portion of CO_2 is low.

In the last phase that CO_2 leaks into the deep sea, regarding Figure 3.21 due to the high hydrostatic pressure, CO_2 is in the liquid or supercritical phase and has a greater solubility than in shallow water. The supercritical or liquid droplets of the leaking CO_2 float higher due to buoyancy, changing from supercritical to liquid and eventually to gas. Large droplets typically break off into smaller ones due to instability [131].

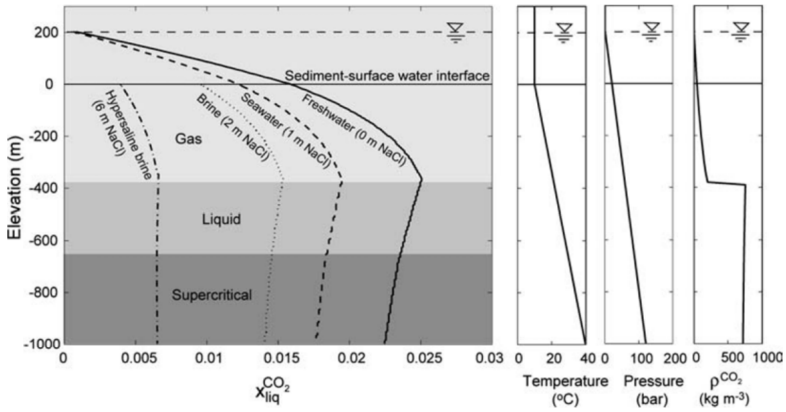

Figure 3.21: CO_2 solubility in relation to depth [19].

Due to the high solubility of CO_2 and slow velocity, a significant portion of CO_2 that is rising through the deep sea dissolves into the water. The dissolved CO_2 will spread throughout the water, and the seawater that has been saturated with CO_2 and is more dense may result in sinking plumes [132]. This approach significantly attenuates CO_2 leakage flow and can be thought of as a CO_2 disposal method. So CO_2 that finally enters the atmosphere is regarded as an air emission.

By reviewing the study of Brewer et al. (2002) [132], the radius and mass change of a CO_2 droplet induced by dissolution while moving through the deep sea may be derived:

$$(r_t - r_0) = -V_m.\Gamma.(t - t_0). \tag{3.66}$$

$$(m_t - m_0) = -4/3 \times \pi(r^3 - r_0^3) \times \rho_{CO_2}. \tag{3.67}$$

Where, t is time (s); t_0 is the initial time (s); r_0 is the initial radius of the droplet (m); r_t is the radius of the droplet at time t (m); Γ is the dissolution rate ($mol/m^{-2}s^{-1}$), which equals to 3 $\mu mol/m^{-2}s^{-1}$; V_m is the specific volume of the droplet (m^3mol^{-1}); m_0 is the initial mass of the droplet (kg); mt is the mass of the droplet at time t (kg); ρ_{CO_2} is the density of CO_2 (kg/m^3).

3.4.2.7 The Free-phase CO_2 Lake's Outlook

Finally, CO_2 injection, CO_2 dissolution, capillary trapping, and CO_2 leakage influence the fate of the saline aquifer's free-phase CO_2 pool. The progressive reduction of the thickness of the CO_2 layer floating under the caprock due to capillary trapping, dissolution by convective mixing, and leakage is considered to be nearly equal to the rate of reduction of free-phase CO_2 mass in the pool. As a result, the overall mass balance equation of free-phase CO_2 in the reservoir may be completed as:

$$dM/dt = F_i - F_d - F_c - F_o. \tag{3.68}$$

where, M is the mass of the free-phase CO_2 in the reservoir, t is time, F_i is the flow rate of CO_2 injected in the reservoir, F_d is the rate of dissolution, F_c is the rate of capillary trapping, F_o is rate of leakage.

3.5 Summary

Depending on the kind of solvent utilized, solvent regeneration in chemical absorption CO_2 capture methods takes substantial energy to operate. Particulate matter, trace metals, and acid gases can be eliminated from flue gases using a chemical absorption technique. Depending on the solvent employed, the chemical absorption process produces NH_3. Solvent loss is also caused by oxidative degradation, carbamate polymerisation, absorber emission, and solvent reactivity with acid gases. The LCI models use empirical relationships to calculate the energy

consumption for solvent regeneration and solvent loss by reaction with acid gases; electricity consumption and the use of cooling water and process water; and acid gas removal rates, particulate matter and trace element removal rates, solvent loss due to oxidative degradation and carbamate polymerisation, solvent emission via absorber, heat stable salts generation, and activated carbon consumption. Finally, using engineering calculations, the CO_2 conditioning LCI model created quantifies compressor energy usage, heat input for the drier, adsorbent use for the drier, and cooling water consumption.

The created LCI model offers a flexible structure for calculating energy consumption and emissions from CO_2 pipeline transport, taking into consideration the mass flow rate of CO_2 to be carried, pipeline length, inlet/outlet CO_2 pressure, and temperature. The CO_2 injection LCI model developed accounts for the CO_2 storage reservoir features that influence the maximum permissible injection bottomhole pressure, CO_2 injectivity, and the number of injection wells utilized in calculating the energy consumption and emissions from the CO_2 injection system. Using modified emissions factors, fugitive emissions from the CO_2 pipeline and recompression boosters, and injection plant can be computed at the facility or equipment level.

By quantifying the radial extent of the CO_2 plume, the thickness of the thin CO_2 layer, the time it takes for the CO_2 plume to reach the top of the formation, the dissolution, capillary trapping, and the lateral movement of free gas phase CO_2 after injection ceases, the LCI model of a CO_2 storage in saline aquifer examines the migration of injected CO_2, which determines the geological boundary and the timeframe of the CO_2 storage system. The model also determines the possibility for CO_2 leakage from CO_2 storage by simulating other leakage paths, such as porous caprock zones, fractures, and abandoned wells that cross the caprock. The final CO_2 flux that crosses the land-atmosphere boundary and enters the atmosphere is calculated by the model, which also analyzes the mitigation of leaked CO_2 out of the saline aquifer upwards through various compartments within the overburden, including the water-saturated porous zones, surface water, or unsaturated soil zones.

4

Life Cycle Impact Assessment & Case Study

4.1 Introduction

This chapter provides the research results on the environmental impacts of post-combustion CO_2 capture, transportation and injection, and storage in a specific power plant case study. The LCI models described in chapter 3 are programmed here in this chapter as Excel spreadsheets, Sima pro, and Gabi software. LCI models of power plants with alternative post-combustion CCS options can be constructed by selecting various LCI models and connecting them together. The LCI model of the Asnaes coal power plant in Kalundborg, Denmark, with post-combustion capture using MEA, transport and injection, and saline storage of the Havnsø structure is used to show the possibilities of the created models in this chapter. To begin, this method simulates the emissions from the constructed capture system, transportation, and injection, as well as the corresponding life cycle assessment (LCA) environmental impacts. It also analyzes the significance of technical, operational, and geographical variations using the

sensitivity analysis presented. Moreover, the significance of uncertainty and variability in the input parameters for each component unit process is assessed by way of an uncertainty analysis. This analysis makes use of the LCI model input data parameters, which are listed in the tables, figures, and appendix that are presented in the following sections. Lastly, in the portion about storage, the model is utilized to determine which operational characteristics, reservoir qualities, and the parameters of alternate leakage paths have a substantial influence on the LCA environmental impact outcomes.

4.2 Case Study

The Danish case study for SACS and GESTCO projects focuses on the possible capture and storage of carbon dioxide emissions from the coal-fired power station Asnaes in the Danish city of Kalundborg [20]. Asnaes Power Station is situated near the city of Kalundborg on the northwest coast of Zealand in eastern Denmark (Figure 4.1). It is the largest power plant in Denmark, with four operational units and an installed capacity of 1,757 MW. In addition to generating electricity for the grid, the power plant also generates district heat for Kalundborg and process steam for the nearby industrial sector. This power plant's technical characteristics are shown in Table 4.1.

It is essential to realize that the remaining lifetime of the current units is limited, as the SACS and GESTCO projects only account for units 5 and 6, which are base load plants. Therefore, in this thesis, the case study of the LCIA scenario is constructed according to the combined capacity of units 5 and 6, which is 1,340 MW.

On the other hand, considering the storage location for Kalundborg, the GESTCO regional study has already evaluated the potential for underground CO_2 storage in Denmark [20, 133]. Initially, two sites were selected for the Kalundborg case study. Both are domal closures on the Gassum Formation in the Kalundborg region (Figure 4.2). In both structures, the reservoir unit consists of shoreface sandstones of the Gassum Formation and marine mud-

Figure 4.1: Asnaes Power Station is situated near the city of Kalundborg.

Data		Unit 2	Unit 4	Unit 5	Unit 6
Electrical output	MW	147	270	640	700
District heat output	MJ/s	100	-	150	-
Steam output	MJ/s	144	50	158	-
Electrical Efficiency	%	40.0	40.3	39.9	48.0
Fuel input	MJ/s	368	670	1604	1458
Flue gas (dry, 6% O_2)	Nm^3/s	132	240	575	523
Flue gas (wet, act. O_2)	Nm^3/h	443,927	809,307	1,913,644	1,708,181
Max. CO_2 capture	kg/s	31	57	137	125
Operation mode		Peak load	Closes 2008	Base load	Base load
CO_2 emissions	tons/year	188,528	-	3,401,143	3,391,500
CO_2 capture	tons/year	169,675	-	3,061,029	3,052,350

Table 4.1: The power plant's technical characteristics.

stones of the Fjerritslev Formation as cap rock. Based on the preliminary screening and comparison of the two structures (Table 4.2), the Havns structure was selected for supplemental case study investigation which covers around 160 km_2 and is 15 km away from the source plant [20].

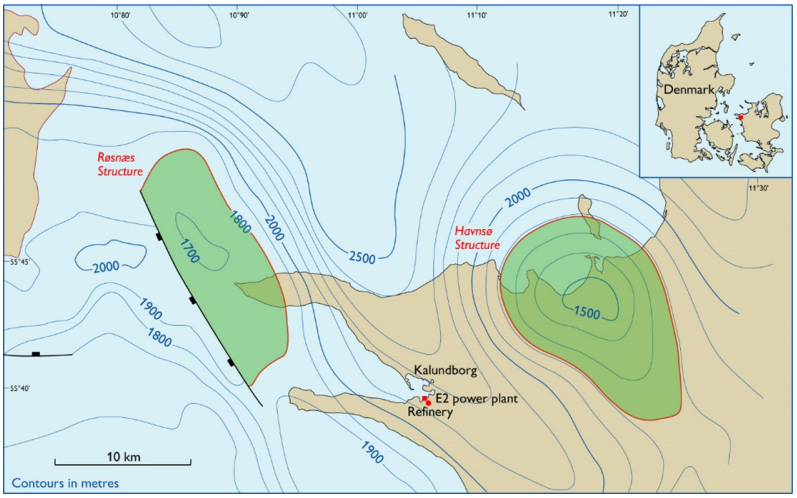

Figure 4.2: Depth structure map of the Havnsø and Røsnæs closures [20].

Economic/Risk evaluation	Havnsø	Røsnæs
3-D seismic	High costs	Low costs
DRILLING	Low costs	Medium costs
Transport	Onshore pipeline	Offshore pipeline
Monitoring	Wells	Seismic
Permission requirements	National and local authorities	OSPAR/ National and local authorities
Risk project	High seismic costs	Fault sealing capacity
Risk humans	Low	None
Risk environment	Low	Low

Table 4.2: The Characteristics of Havns and Røsnæs structure.

4.3 Post-combustion CC, Transportation, and Injection

Asnaes Power Station is a coal-fired facility with a capacity of 1,340 MW with post-combustion capture, conditioning, transportation, and injection systems. Table 4.3 shows the main features of the base case scenario in regards to the technology used for the entire system, the operational

conditions, and the geographical establishment in relation to the fuel used, the distance to the storage site, and the depth of the storage formation used as an illustration of the model's capability.

Base Case Scenario	**Post-combustion CO_2 capture, conditioning, transport and injection in the 1,340 MW plant**
CO_2 capture energy consumption (MW/1,340 MW)	1,250
Chemical absorption CO_2 capture technology	MEA
SOx removal rate	95%
NOx removal rate	0.8%
CO_2 capture rate	95%
Compression pressure (MPa)	13.80
Pipeline distance (Km)	15
Storage formation depth (m)	1,500

Table 4.3: The Base Case Scenario for The Asnaes Power Plant.

The Sima Pro LCA program calculates the LCI data for the upstream processes indicated in the figures of Appendix 1 with the relevant characteristics were presented as tables. Also, the final LCI model has been provided in Figure 4.3, and it is important to note that the coal combustion process with some removal processes (NOx, PM, SOx) are presented there, but only for initial calculations of direct emissions and trace metals, as this is required for the implementation of the case study; otherwise, this research does not account for their LCIA. In addition, this scenario examines the following characteristics and capabilities of the model generated for a final system:

1. Direct emissions and resource consumption;
2. Life cycle environmental impacts;

3. Sensitivity analysis (the effect of post-combustion CC, transport, and injection on the LCIA);

4. Uncertainty analysis (the influence of LCI input data uncertainty on emission/resource consumption estimates and the LCIA).

Upstream processes consist of (excluding the plant combustion process) Post-combustion capture system, MEA production, MEA truck transport, ammonia production, ammonia truck transport, CO_2 pipeline infrastructure, CO_2 capture facility infrastructure, compressor infrastructure, and injection system. Sources of upstream LCI data used as references in this study are listed in the tables below. They are based on the research of Koornneef (2008) [32], Emmenegger et al., (2007)[33], Althaus et al., (2007) [35] and Röder et al., (2004) [34].

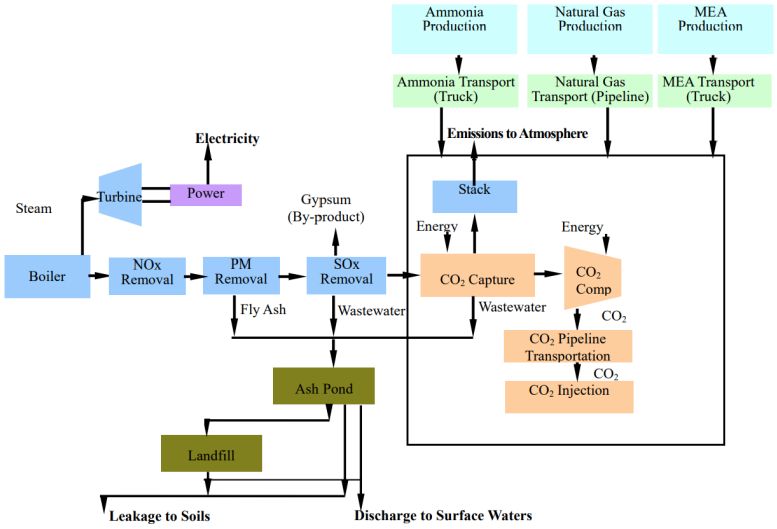

Figure 4.3: The component LCI model of the case study power plant.

4.3.1 Direct Emissions and the Fate of Air Emissions

Significant direct emissions are not produced by the SCR (Selective Catalyst NOx Reduction), ESP (Electrostatic Precipitators PM), FGD (Flue Gas Desulphurisation SOx), CO_2 capture, CO_2 conditioning, CO_2 pipeline transport, or CO_2 injection unit. Almost all emissions are

initially produced by the coal combustion process; however, coal combustion is not considered in this study because the CCS system is the only objective. Even so, in some cases, such as the investigation of direct emissions and trace metals, coal combustion is analyzed with SCR, ESP, and FGD, because these processes occur before to the CCS processes.

Concerning air emissions in power generation with post-combustion CCS include CO_2, PM-10, SO_2, SO_3, NO, NO_2, HCl, HF, and Hg. These air emissions are initially produced by the coal combustion process and are subsequently eliminated in full or in part by pollution control units such as SCR, ESP, FGD, and the CO_2 capture unit. The LCI models assess the removal rate of air emissions of concern throughout the flue gas treatment processes, taking into account that pollution control units affect each other and can affect many types of emissions.

Figure 4.4 shows that the CO_2 capture unit removes 95% of CO_2 without affecting other pollution control units. ESP removes 99.7% of PM-10, while FGD, CO_2 capture device, removes 0.11%. The CO_2 capturing unit (MEA) removes 0.02% of SO_2 after FGD removes 95%. SCR, ESP, FGD, and CO_2 capture unit eliminate SO_3 emissions (MEA). SCR can only reduce NO emissions to 23.08%. SCR with CO_2 capture unit (MEA) reduces NO2 emissions by 17.31%. FGD and CO_2 capture unit (MEA) decrease HCl and HF emissions to 0.05% and 0.15%, respectively. ESP, FGD, and CO_2 capture unit (MEA) decrease mercury vapour by 1.97%. Pollution control units limit CO emissions [24].

4.3.2 Trace Metals

After coal combustion, the trace metals are partitioned and released to the environment through different routes: with air emissions, MEA captures solid wastes, FGD wastes, gypsum, fly ash or bottom ash. The LCI models developed successfully calculate the partitioning of 17 trace metals across the flue gas treatment chain in a power plant with CO_2 capture [24].

Figure 4.5 illustrates that the most of emissions of antimony (Sb), cadmium (Cd), chromium (Cr), cobalt (Co), lead (Pb), manganese (Mn), nickel (Ni), copper (Cu), thallium (Tl), vanadium (V), barium (Ba), and silver (Ag) are found in bottom ash. During combustion, the ma-

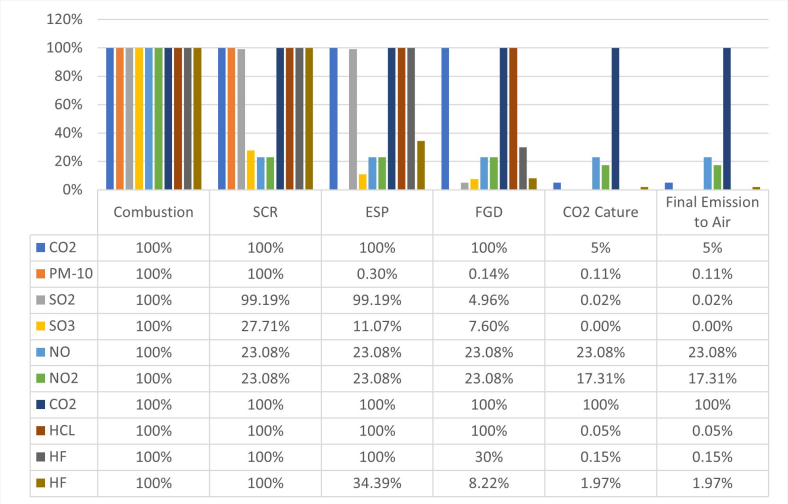

	Combustion	SCR	ESP	FGD	CO2 Cature	Final Emission to Air
CO2	100%	100%	100%	100%	5%	5%
PM-10	100%	100%	0.30%	0.14%	0.11%	0.11%
SO2	100%	99.19%	99.19%	4.96%	0.02%	0.02%
SO3	100%	27.71%	11.07%	7.60%	0.00%	0.00%
NO	100%	23.08%	23.08%	23.08%	23.08%	23.08%
NO2	100%	23.08%	23.08%	23.08%	17.31%	17.31%
CO2	100%	100%	100%	100%	100%	100%
HCL	100%	100%	100%	100%	0.05%	0.05%
HF	100%	100%	100%	30%	0.15%	0.15%
HF	100%	100%	34.39%	8.22%	1.97%	1.97%

Figure 4.4: The fate of air emissions after the pollution control units of a 1340 MW power plant with carbon capture.

jority of Arsenic (As), Beryllium (Be), and Zinc (Zn) are vaporized and mostly found in fly ash. Notable is the fact that 3.95% of mercury is discharged to the environment as a vapour. Approximately 51.40% of mercury is found in the gypsum byproduct of the FGD process, 12.52% in the MEA solid wastes, and 31.08% in the fly ash.

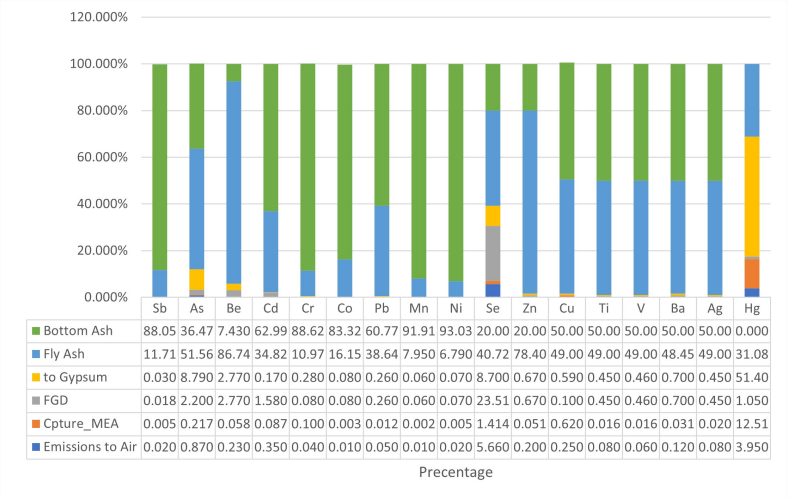

	Sb	As	Be	Cd	Cr	Co	Pb	Mn	Ni	Se	Zn	Cu	Ti	V	Ba	Ag	Hg
Bottom Ash	88.05	36.47	7.430	62.99	88.62	83.32	60.77	91.91	93.03	20.00	20.00	50.00	50.00	50.00	50.00	50.00	0.000
Fly Ash	11.71	51.56	86.74	34.82	10.97	16.15	38.64	7.950	6.790	40.72	78.40	49.00	49.00	49.00	48.45	49.00	31.08
to Gypsum	0.030	8.790	2.770	0.170	0.280	0.080	0.260	0.060	0.070	8.700	0.670	0.590	0.450	0.460	0.700	0.450	51.40
FGD	0.018	2.200	2.770	1.580	0.080	0.080	0.260	0.060	0.070	23.51	0.670	0.100	0.450	0.460	0.700	0.450	1.050
Cpture_MEA	0.005	0.217	0.058	0.087	0.100	0.003	0.012	0.002	0.005	1.414	0.051	0.620	0.016	0.016	0.031	0.020	12.51
Emissions to Air	0.020	0.870	0.230	0.350	0.040	0.010	0.050	0.010	0.020	5.660	0.200	0.250	0.080	0.060	0.120	0.080	3.950

Precentage

Figure 4.5: Trace metal segregation across the pollution control units of the Asnaes power plant's CO_2 capture system.

4.3.3 Life Cycle Impact Assessment (LCIA)

In section Appendix II, the emissions from the 1340 MW base case power plant scenario with post-combustion capture, transport, and injection, as well as the upstream processes, such as MEA production, MEA transport by truck, ammonia production, ammonia transport by truck, CO_2 pipeline infrastructure, CO_2 capture facility infrastructure, and compressor infrastructure, are presented. This study implements the impact category for the case study concerning GWP (Global Warming Potential), AP (Acidification Potential), EP (Eutrophication Potential), POCP (Photochemical Ozone Creation Potential), HTP (Human Toxicity Potential), FAETP (Freshwater Aquatic Ecotoxicity Potential), and TEPT (Terrestrial Ecotoxicity Potential).

4.3.3.1 GWP (Global Warming Potential)

Figure 4.6 depicts the total GWP of the case study power generation scenario with just capture, transport, and injection components considered. 78% of this impact is due to post-combustion carbon. Other upstream processes, such as MEA production, Ammonia production, and transportation infrastructure, account for 11%, 6%, and 4% of the GWP, respectively. This chart also demonstrates that the primary emissions causing GWP are CO_2, CH_4, and NO.

4.3.3.2 AP (Acidification Potential)

Figure 4.7 demonstrates that the majority of acidification potential (AP) is caused by CO_2 post-combustion MEA from power generation, which represents for 98% of the total. The manufacture of MEA amounts for 1.48% of AP, whereas the other processes contribute less than 1%. Figure 4.7 further shows that the primary sources of AP are emissions to the air (such as NO, NO_2, NOx, SO_2, NH_3, and NH_4) and to fresh water (such as HCl, HF, and H_2SO_4). The primary source of NO, NO_2, and NH_3 emissions is electricity generating with CO_2 capture. Specifically, the NH_3 emissions result from the MEA capture process.

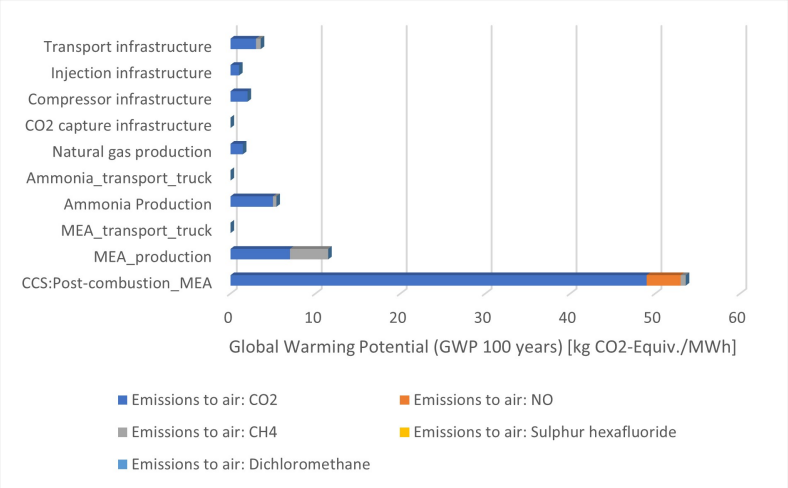

Figure 4.6: Global warming potential for the base case.

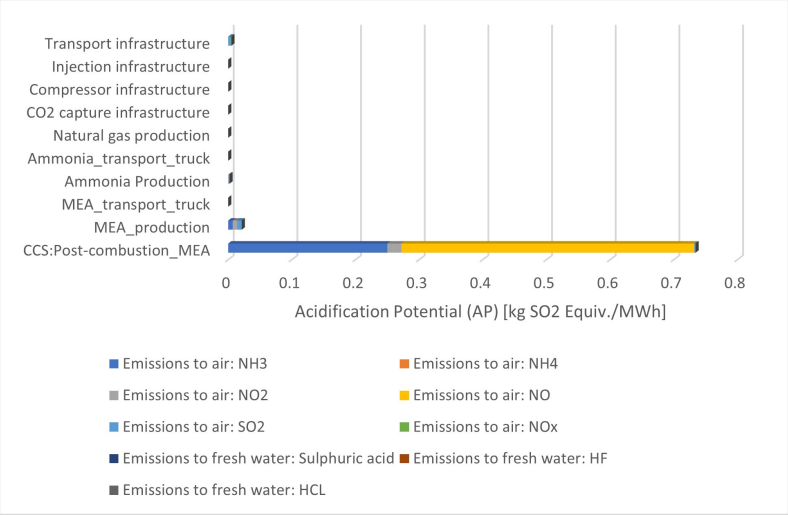

Figure 4.7: Acidification potential for the base case.

4.3.3.3 EP (Eutrophication Potential)

Figure 4.8 demonstrates that the majority of Eutrophication Potential (EP) is attributable to post-combustion CO_2 and MEA generation, accounting for 81% and 16% of EP, respectively. The main areas of eutrophication consequences are emissions to air, emissions to fresh water, and emissions to soils, according to an analysis of the data on life cycle impacts. NO, NO_2, and NH_3 emissions are mostly caused by power generating with CO_2 capture. MEA production

processes result in emissions to fresh water, including nitrate, total organic bounded carbon, and chemical oxygen demand (COD).

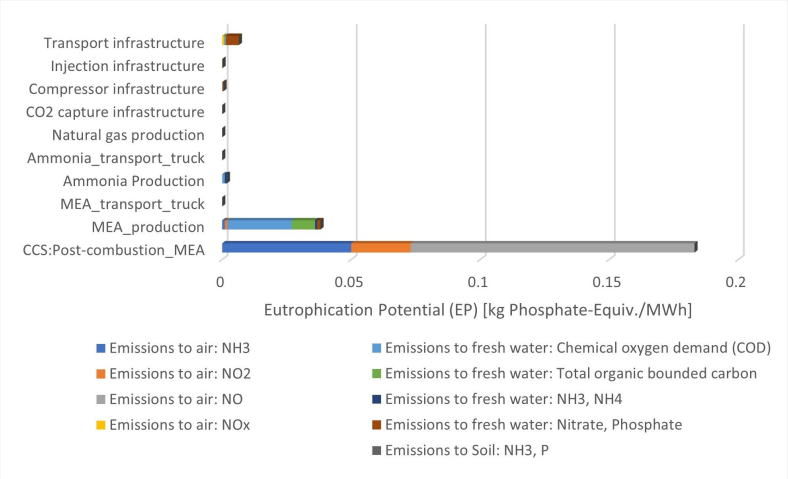

Figure 4.8: Eutrophication potential for the base case.

4.3.3.4 POCP (Photochemical Ozone Creation Potential)

Figure 4.9 depicts the Photochemical Ozone Creation Potential (POCP), which is mostly caused by capture post-combustion. The total value of the POCP is negative because the emissions of nitrogen monoxide from power generation and capture have a negative effect on the POCP, as measured by a characterization factor of -0.427 kg Ethane equivalent. Nitrogen oxide, carbon monoxide, NMVOCs (non-methane volatile organic compounds), and nitrogen dioxide represent the majority of these emissions.

4.3.3.5 HTP (Human Toxicity Potential)

Figure 4.10 shows that MEA production accounts for the vast majority (92%) of HTP. In addition to emission, post-combustion of capture system contributes 7.7% to HTP. ethylene oxide emissions to air and to freshwater, exclusively from MEA production, dominate the HTP, accounting for 53.39% and 39.09% respectively. Post-combustion capture system emissions include Arsenic (to the air) and Selenium (to air and soil).

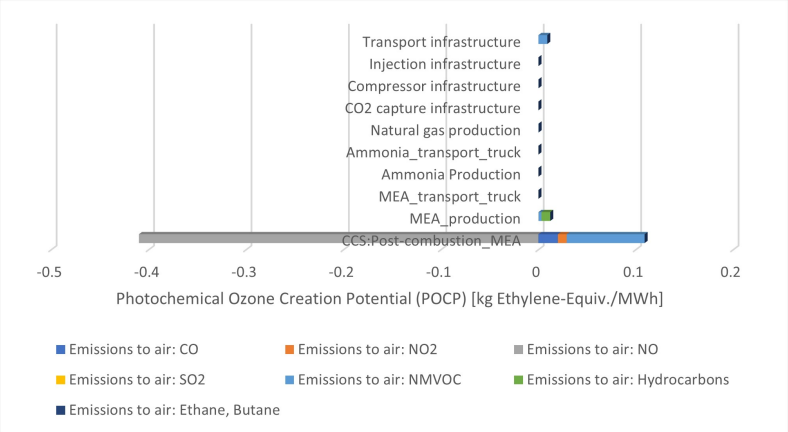

Figure 4.9: Photochemical Ozone Creation Potential for the base case.

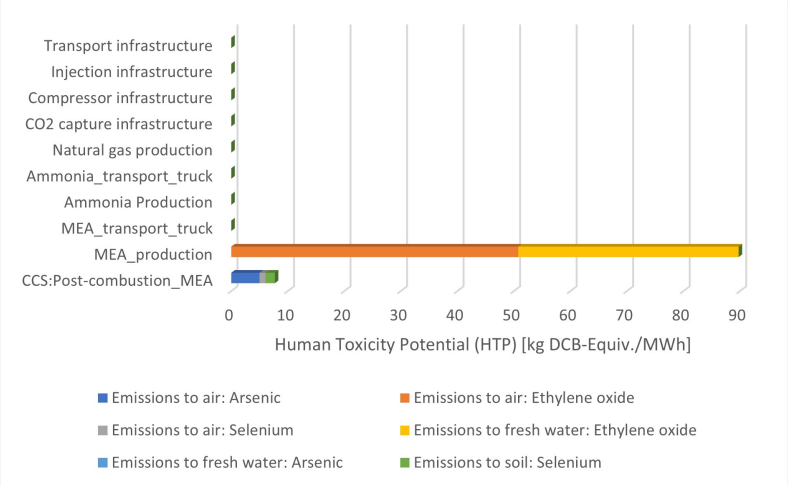

Figure 4.10: Human Toxicity Potential for the Base Case.

4.3.3.6 FAETP (Freshwater Aquatic Ecotoxicity Potential)

Figure 4.11 illustrates that the majority of Freshwater Aquatic Ecotoxicity Potential (FAETP) is accounted for by upstream activities such as capture post-combustion, MEA production, pipeline transport infrastructure, and compressor infrastructure, accounting for 68%, 15%, 10%, and 5%, respectively. Vanadium, selenium, and beryllium emissions to the atmosphere account for 13.8% of FAETP. Approximately 28.4% of all emissions include barium, copper, vanadium, ethylene oxide, and nickel are in the fresh water. Three elements account for 57.8%

of FAETP soil emission: selenium, vanadium, and beryllium.

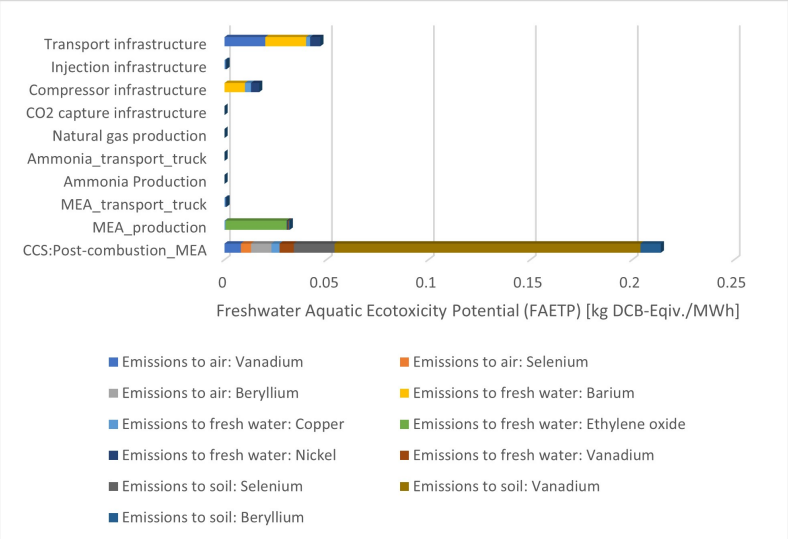

Figure 4.11: Freshwater Aquatic Ecotoxicity Potential for the base case.

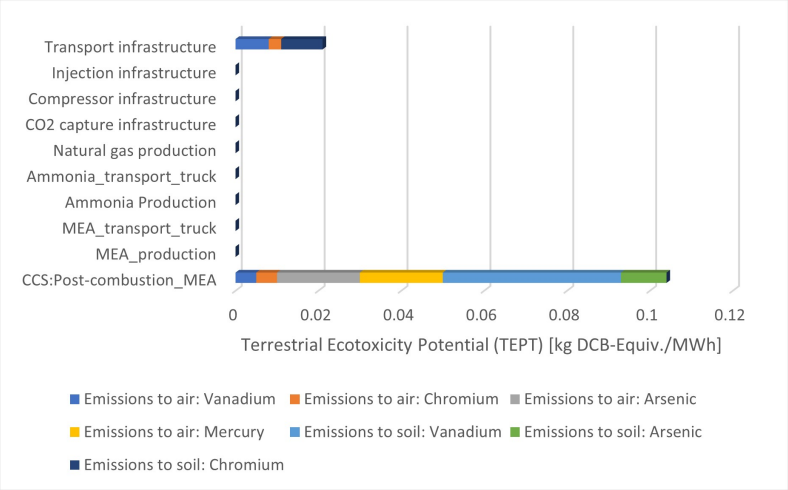

Figure 4.12: Terrestrial ecotoxicity potential for the base case.

4.3.3.7 TEPT (Terrestrial Ecotoxicity Potential)

Figure 4.12 demonstrates that the majority of the Terrestrial Ecotoxicity Potential (TETP) is attributable to CO_2 post-combustion and transportation infrastructure, accounting for 83.2%

and 16.8% of the TETP, respectively. A comprehensive examination of the life cycle impact data reveals that TETP is mostly caused by air and soil metal emissions. Specifically, the post-combustion system consists of 41% vanadium and 10% arsenic in the soil, as well as 20% mercury, 19% arsenic, and 5% chromium. Additionally, transportation infrastructure produces vanadium and chromium emissions into the atmosphere at rates of 50% and 17%, respectively, while only 33% chromium is released into the soil.

4.3.4 Sensitivity Analysis

The scenarios studied in this part cover post-combustion CO_2 capture, conditioning, transport, and injection scenario selections to evaluate the relevance of technological, operational, and geographical options on the overall system life cycle environmental effect performance. The LCI model built at the unit process level provides an examination of the choices that may be considered when reviewing or constructing a power generating post-combustion capture, transport, and injection scenario. The use of LCI model parameters in regard to these alternatives enables the practitioner to depict technical, operational, and geographical variances in the environmental evaluation of power production systems.

It is crucial to remember that chapter 3 has all of the necessary LCI input data, formulas, and parameters discussed in detail. Table 4.4 also illustrates how each characteristic relates to a certain section of chapter 3 and highlights this connection.

This study would give correct information for planners to verify that a CCS option chosen does not result in upstream or downstream changes that would raise the total environmental consequences of the system. The selections for the base case scenario (Table 4.4) are utilized as a benchmark for all categories of parameters other than the one being analyzed. The changes in LCA environmental effect indicator scores are provided in the following paragraphs, beginning with technological alternatives and continuing with operational aspects. According to research, significant design variables, such as the kind of chemical absorption capture technology used, could also affect the environmental impacts of the post-combustion capture system, transport,

and injection during its entire life cycle.

Types	Characteristics	Base Case Scenario	Sensitivity analysis alternatives	Research Reference	Chapter 3 Reference Part
Technology Option	Chemical Absorption Capture	MEA	KS1 ,K+/PZ	[32, 134, 135]	3.2.1
	CO_2 Capture Energy Consumption (MW)	1250	60 100%	[32, 136]	3.2.2
Operational Option	CO_2 Capture Rate	95%	55 99%	[32, 137]	3.2.2
Geographical setting	Compression pressure (MPa)	13.8	10.8 16.8	[138, 139]	3.2.2
	Pipeline distance (Km)	15	2.5 20	[140, 135]	3.2.1

Table 4.4: Base case scenario and sensitivity analysis options for the case study.

4.3.4.1 Chemical Absorption Capture System

Figure 4.13 demonstrates that FAETP, GWP, POCP, and TETP are about 10% lower for post-combustion capture with K_PZ or KS1 than for capture with MEA. The considerable reduction in HTP is due to the lower create requirements of capture with K_PZ or KS1 compared to capture with MEA, which reduces HF emissions from KS1 manufacturing, the major source of HTP. Since K_PZ does not create NH_3, post-combustion capture reduces EP and AP significantly. KS1 post-combustion capture creates more NH_3 than previous methods, increasing EP and AP.

4.3.4.2 CO_2 Capture Energy Consumption

According to Figure 4.14, a 10% decrease in the amount of energy consumption by the CO_2 capture process results in a reduction of around 2% in the GWP, AP, EP, and POCP as well as

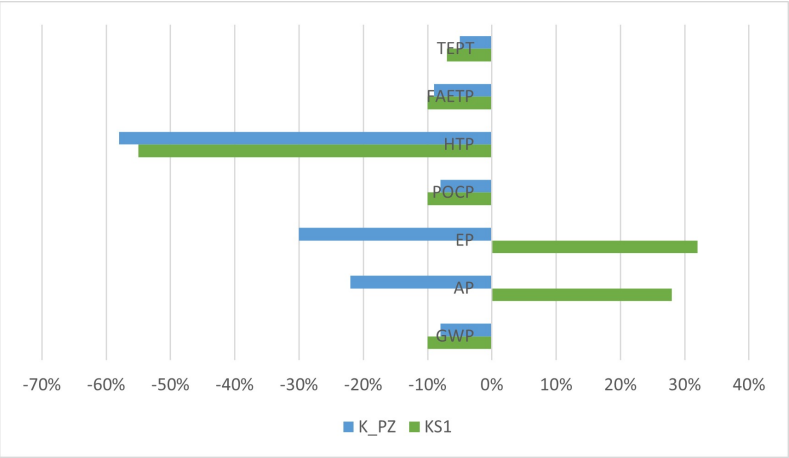

Figure 4.13: Life-cycle level comparison of chemical absorption capture technologies and their environmental impacts in post-combustion CO_2 capture.

approximately 1% in the FAETP, TETP, and HTP.

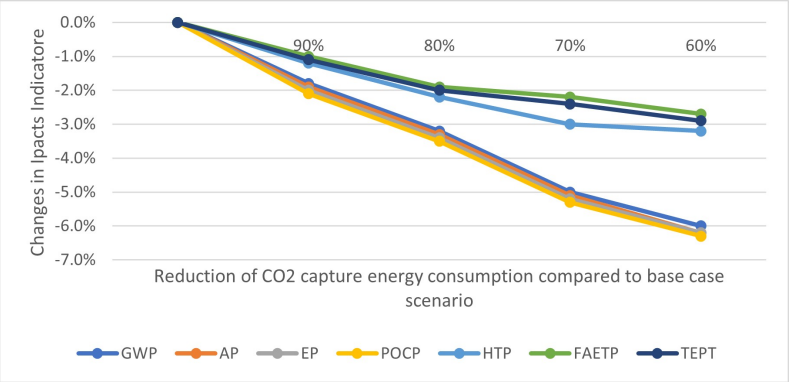

Figure 4.14: The effects of energy efficiency and CO_2 capture on the environmental impacts.

4.3.4.3 CO_2 Capture Rate

By ignoring a portion of the flue gas, power plant managers can run at varied CO_2 capture rates during post-combustion CO_2 capture. Figure 4.15 indicates that when the CO_2 capture rate increases, the GWP reduces considerably, but other environmental consequences increase somewhat. Since any change in the CO_2 capture rate has a direct impact on energy consumption by CO_2 capture, CO_2 conditioning, CO_2 transportation, and CO_2 injection processes, it

is evident that POCP, EP, and AP are more sensitive to a change in the CO_2 capture rate than the other impact categories, with the exception of the GWP.

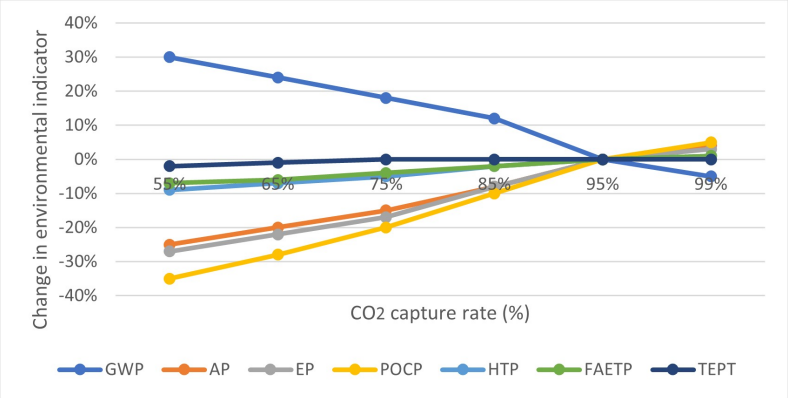

Figure 4.15: The effect of CO_2 capture rate on the environmental impacts.

4.3.4.4 Compression Pressure

Figure 4.16 demonstrates that the outlet pressure of the CO_2 conditioning unit has a negligible impact on the life-cycle environmental impacts of power generation with CO_2 capture, transport, and injection, as its proportion of energy consumption is relatively small in comparison to other parameters involved in these processes.

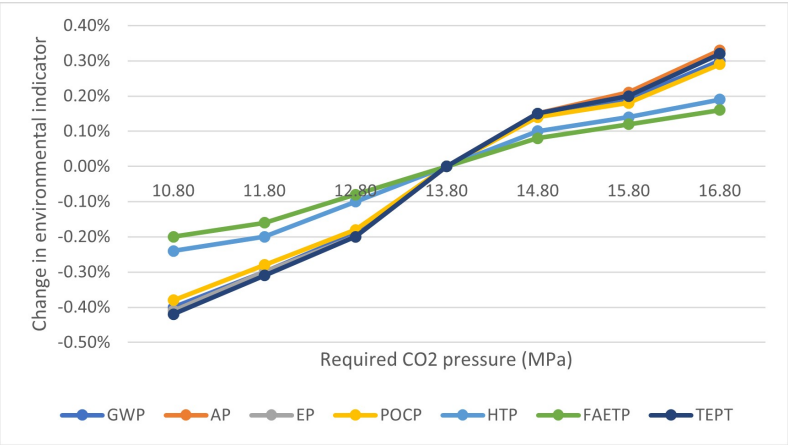

Figure 4.16: The effect of compression pressure on the environmental impacts.

4.3.4.5 Pipeline Transport Distance

Figure 4.17 demonstrates that a 2.5km change in the length of the transport pipeline leads in a 0.5% change in FAETP, a 0.4% change in TETP, and a GWP. These changes reflect the pipeline infrastructure, natural gas consumption for CO_2 compression, and CO_2 fugitive emissions from the CO_2 pipeline.

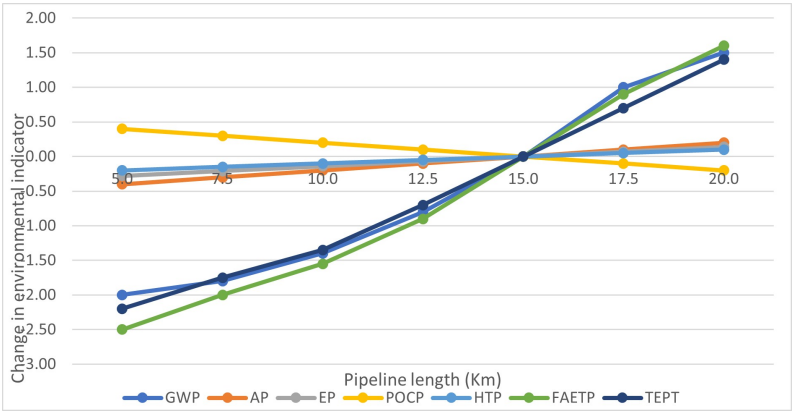

Figure 4.17: The effect of pipeline transport distance on the environmental impacts.

4.3.5 Uncertainty Analysis

This section quantifies the uncertainty associated with each environmental impact and emission source using the Monte Carlo simulations of the LCA program GaBi. In section Appendix III, the input parameters specified for each unit process component in power generation with post-combustion CO_2 capture have been detailed, along with their respective ranges. Monte Carlo simulation determines output statistical features like mean, median, standard deviation, and different level of confidence regarding these categories: major compounds direct air emission, and direct life cycle environmental impacts. The base case scenario described in Table 4.3 is used for the uncertainty evaluation for the Asnaes power plant.

4.3.5.1 Major Compounds Direct Emission

The outcomes of the uncertainty analysis for main compound direct air emissions are displayed in Figure 4.18 (section Appendix III contains the appropriate statistical measurements). Standard deviations for CO, NH_3, NO, NO_2, N_2O, and CO_2 emissions are less than those for HF, HCl, SO_2, and SO_3, because these gases are impacted by fewer pollution management mechanisms, as shown . Variability in CO_2 capture rate is the source of emission uncertainty.

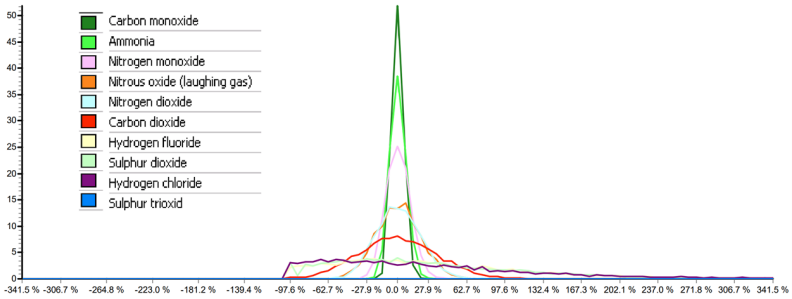

Figure 4.18: Monte Carlo analysis of air emissions at direct emission level for the base case.

4.3.5.2 Direct Life Cycle Environmental Impacts

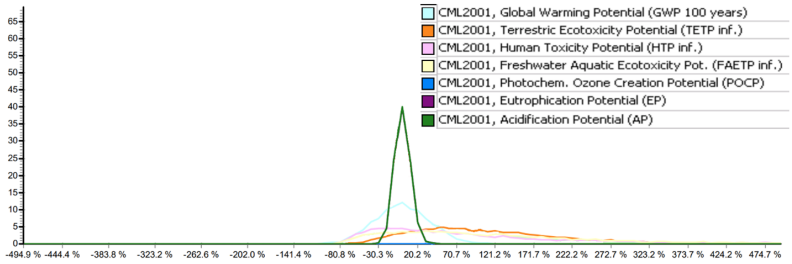

Figure 4.19: Monte Carlo analysis of the environmental impacts at direct emission level for the base case.

Life cycle environmental impacts of power generation including post-combustion CO2 capture using MEA, CO_2 transport, and injection can be seen in histogram form in Figure 4.19 (The statistical outputs are provided in section Appendix III). Because AP, EP, GWP, and POCP are all dependent on air emissions, which have lower uncertainty than the emissions of

trace metals that dominate TETP, FAETP, and HTP, the results reveal that the uncertainty of AP, EP, GWP, and POCP is smaller.

4.4 CO_2 Storage Scenario

Why the Havnsø structure was chosen for this case study was discussed at the beginning of this chapter. Therefore, this section examines the specifics of this structure, including its characteristics and geological schematic, input LCA factors, inventory model and impacts assessment, leakage parameters, and sensitivity analysis.

Figure 4.20 depicts that at depth around 1,500 – 2,000 m, the saline aquifer of the Havns structure is created by porous sandstones of the Gassum Formation and sealed by marine mudstones of the Fjerritslev Formation, which operate as caprock. A reasonable guess put the amount of CO_2 that might be stored at close to 900 million tonnes. Table 4.5 has a full description of the Havns structure.

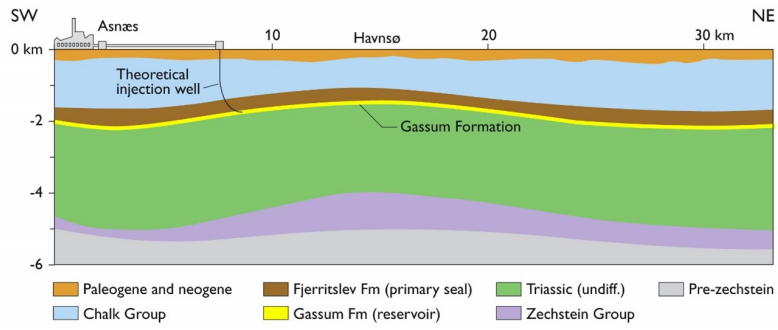

Figure 4.20: Schematic geological cross-section through the Havnsø structure [20]

Characteristics	Values
Reservoir	Gassum
Lithology	Siliciclastic sandstone
Onshore/offshore	2/3 onshore, 1/3 offshore
Depth	1500 m
Thickness	150 m
Permeability	500 mD
Porosity	22%
Pressure	150 bar
Pore volume	$3,670 km^3$
Temperature	50 ºC
Storage capacity	923 Mt
Seal	Fjerritslev Formation
Lithology	Marine mudstone
thickness	500 m
Area of closure	$166 km^2$

Table 4.5: The Characteristics of the Havnsø structure.

4.4.1 LCI Model Parameters

In Table 4.6, the LCI model parameters and input data are displayed. It is expected that CO_2 is injected into the aquifer using a vertical injection well 8 kilometers from the south-east boundary of the formation, as seen in Figure 4.20 and Figure 4.21, respectively. Figure 4.21 depicts the well in greater detail. The well is perforated 1,750 m below sea level with a well-completion gap of 150 m. Larsen et al. (2007) [20] suggest that the geological characteristics of the Havnsø reservoir will permit injection of 200 kg CO_2/sec, or roughly 6 Mt/year, for more than a century.

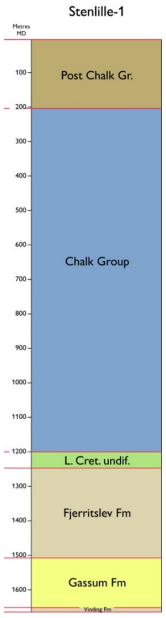

Figure 4.21: Stratigraphic depth section of the well showing the lithostratigraphic units and their thickness [20].

4.4.2 Inventory Model Result of the Havnsø structure

For the purpose of analyzing the CO_2 leakage behavior, it is supposed that a permeable zone, a fault, and an abandoned well are positioned adjacent to the CO_2 injection well (Table 4.7, [21]). In accordance with Akervoll et al. (2006), the CO_2-water relative permeability curves developed for the Sleipner project are applied for reservoir modelling (Figure 4.22).

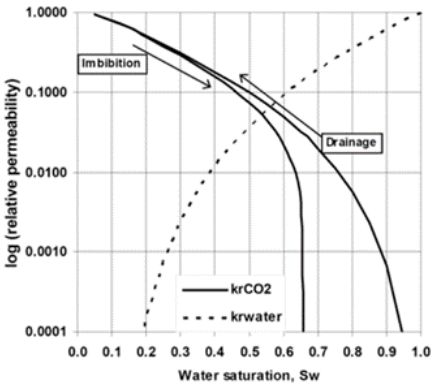

Figure 4.22: Relative CO_2-Water permeability curves [21]

Parameters	Values
Reservoir thickness	H=150 m
Injection well-completion interval	Hw=100 m
reservoir length	L=30,000 m
Depth	1,500 m
Angle	3.64°
Prosity	$\varphi = 0.22$
Horizontal permeability	$k_h = 500mD$
Vertical permeability	$k_v = 100mD$
Temperature	50°C
CO_2 saturation	$S_{gf} = 0.905$
Average CO_2 saturation	$S_g = 0.6$
Water viscosity	$\mu_w = 0.00043Pa.s$
CO_2 viscosity	$\mu_g = 0.000043Pa.s$
CO_2 solubility	$53.4kg/m^3$
CO_2 density	$634kg/m^3$
Water and CO_2 density difference	$\Delta\rho = 350kg/m^3$
CO_2 injection rate	200kg/s
Period	100 years
Diffusivity	$D = 1.00E-09m^2s^{-1}$

Table 4.6: The results for the base case

Zone	Values
Permeable zone	
Distance to injector (Dp)	1,000 m
Intrinsic permeability (Kp)	10 mD
Radius of the zone (rp)	100 m
Thickness of the zone (Lp)	500 m
Fault	
Distance to injector (Df)	2,000 m
Aperture(df)	100 μm
Width (wf)	10 m
Length (Lf)	500 m
Abandoned well	
Distance to injector (Dw)	3,000 m
Radius of Gas channel (rg)	110 μm
Length of Gas channel (Lg)	50 m
Aperture of Fracture	30 μm
Width of Fracture	0.75 m
Length of Fracture	50 m

Table 4.7: The results for the base case.

Now is the time to investigate the base case for the case study in order to analyze impact assessment and the subsequent relative features. This is achieved by examining three main research: [20], [141], and [21].

According to the LCI model results, the radius of the injected CO_2 distributes around 10 km, with 14.74% of the injected CO_2 dissolved during the injection. Capillary trapping is the major way to reduce free phase CO_2 during a 1,000-year period, and it will absorb approximately 67% of the remaining free phase CO_2. In terms of CO_2 leakage, when considering the three pathways described for a CO_2 injection well, it is vital to note that the permeable zone, with an initial leakage rate of 0.23 kg/s, is the principal source of CO_2 to the environment.

Other pathways' leakage rates gradually decrease with time, notably during 900 years, since capillary trapping and convective mixing effect immobilize the free phase CO_2, reducing the thickness of the CO_2 layer beneath the caprock (Figure 4.23). Table 4.8 summarizes the findings for the base case scenario based on the three studies indicated.

Characteristics	**Values**
CO_2 injection Radial Distribution|	10 km
CO_2 dissolved rate	14.74 %
CO_2 **Convective Mixing**	
t_c	0,23 year
t_{on}	32.49 year
t_{slow}	889.82 year
t_{sat}	13347.23 year
Dissolution rate	4.13E+07 kg/year
CO_2 **Capillary Trapping**	
N_{gv}	22.57
Trapping rate	67 %
Trapping period	900 years
Average annual trapping	4.70E+08 kg

Table 4.8: The results for the base case.

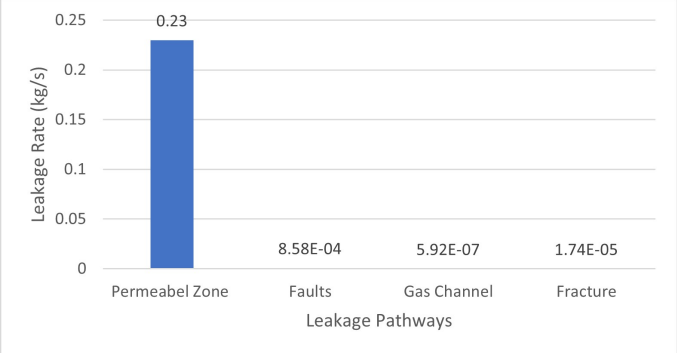

Figure 4.23: CO_2 leakage rate through different pathways.

According to the IPCC (2005) [4], around 3.0109 kg CO_2 leaks throughout the 1,000 year after injection, accounting for approximately 0.8% of the total CO_2 injected (Figure 4.24).

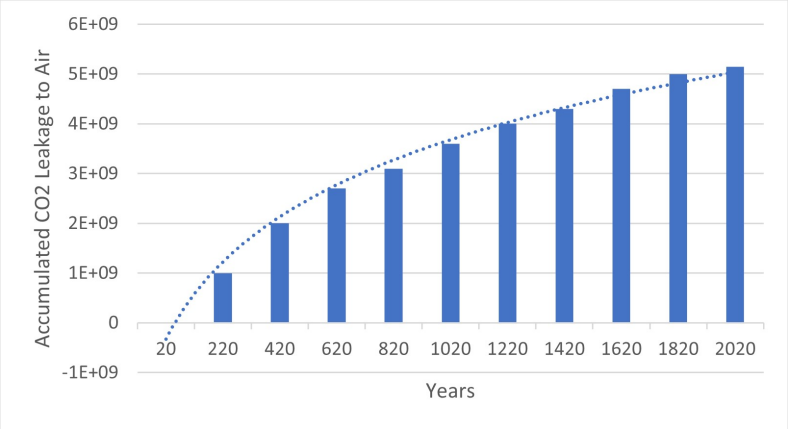

Figure 4.24: CO_2 leakage to the atmosphere.

4.4.3 Sensitivity Analysis

The purpose of the sensitivity analysis is to determine the operational and reservoir parameters, as well as the leakage pathways parameters, that have substantial effects on CO_2 leakage. The difference between the base case and sensitivity analysis was summarized in Table 4.9.

Keep in mind that chapter 3 has a thorough discussion of all of the input data, formulas, and parameters required by the LCI. Furthermore, Table 4.9 demonstrates the connection between each characteristic and certain chapter 3 sections.

Type	Characteristics	Base Case	Sensitivity Analysis	Research Reference	Chapter 3 Reference Part
Operational and reservoir parameters	Injection rate	200 kg/s	50-150	[20, 141]	3.3.2
	Permeability	500 mD	1000-2000		3.4.1
	Aquifer depth	1500 m	1200-2000		3.4.1
	Injection period	100 years	25-50		3.3.2
Leakage pathways parameters	Permeable zone: Permeability	10 mD	1-100	[21, 4]	3.4.1
	Fault: Width	10 m	1-20		3.4.1
	Gas channel: Radius	1 mm	11-55		3.4.1

Table 4.9: The Base case scenario and sensitivity analysis data of the storage.

4.4.3.1 Operational and Reservoir Parameters

The sensitivity analysis of operational and reservoir factors, including injection period, injection rate, reservoir permeability, and reservoir depth.Figure 4.25a and Figure 4.25d demonstrate that the injection period and injection rate have a substantial effect on the CO_2 leakage to total CO_2 injected proportion. A thicker CO_2 layer forms beneath the caprock as a result of higher injection rates or longer injection periods, which increases the ratio of CO_2 leakage to total CO_2 injected. On the other hand, Figure 4.25b and Figure 4.25c show that reservoir permeability and reservoir depth have little effect on the ratio of CO_2 leakage to total CO_2 injected.

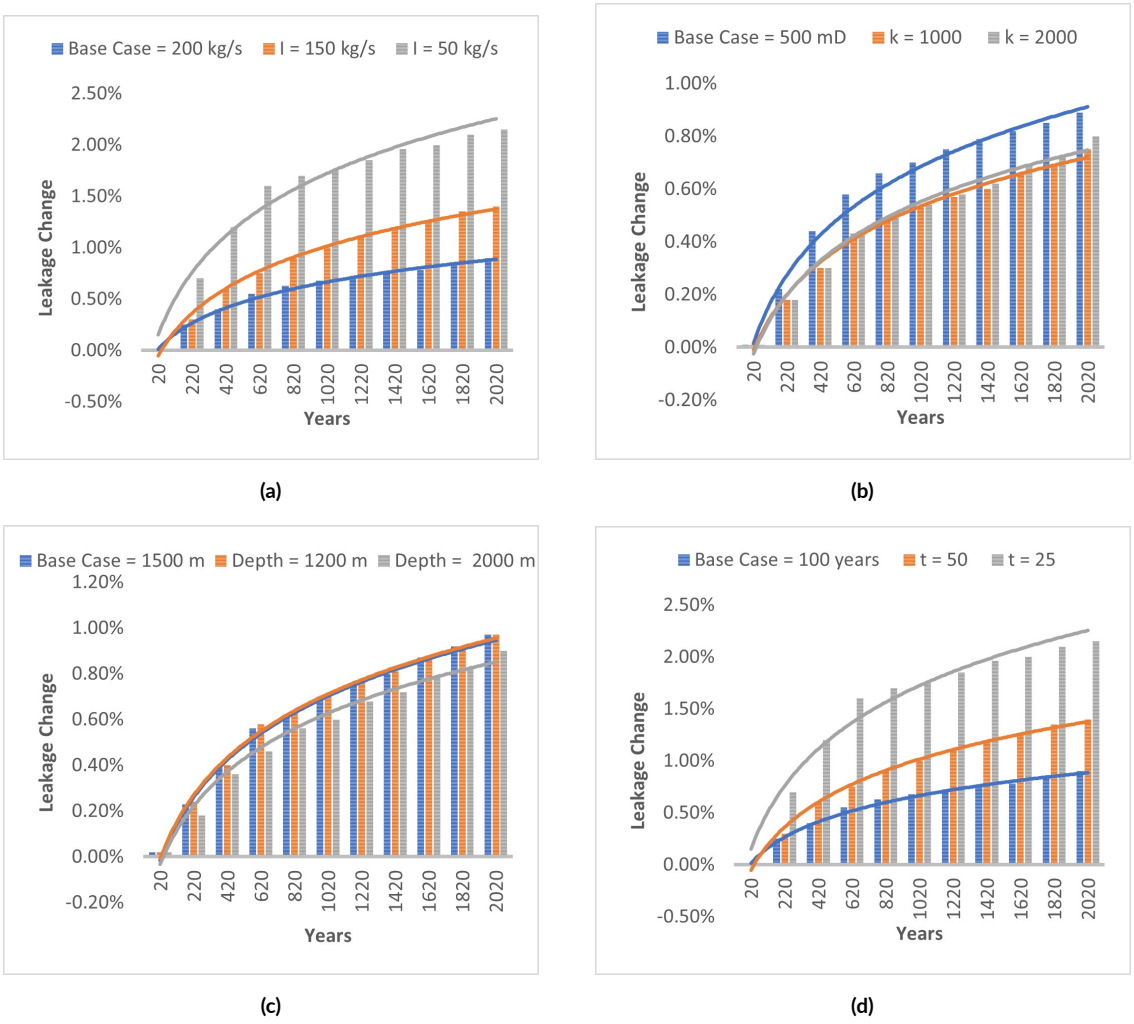

Figure 4.25: Sensitivity analysis of operational parameters and reservoir parameters: (a) injection period; (b) permeability; depth of the saline aquifer; (d) injection rate.

4.4.3.2 Leakage Pathways Parameters

Increased permeability of the permeable zone can greatly increase the ratio of CO_2 leakage to total CO_2 injected, as shown in Figure 4.26a. Figure 4.26b indicates that a change in the fault's width can result in a considerable change in the ratio of CO_2 leakage to total CO_2 injected, but with a low impact. Figure 4.26c demonstrates that a significant change in the ratio of CO_2 leakage to total CO_2 injected can arise from a change in the radius of the gas channel in an abandoned wellbore.

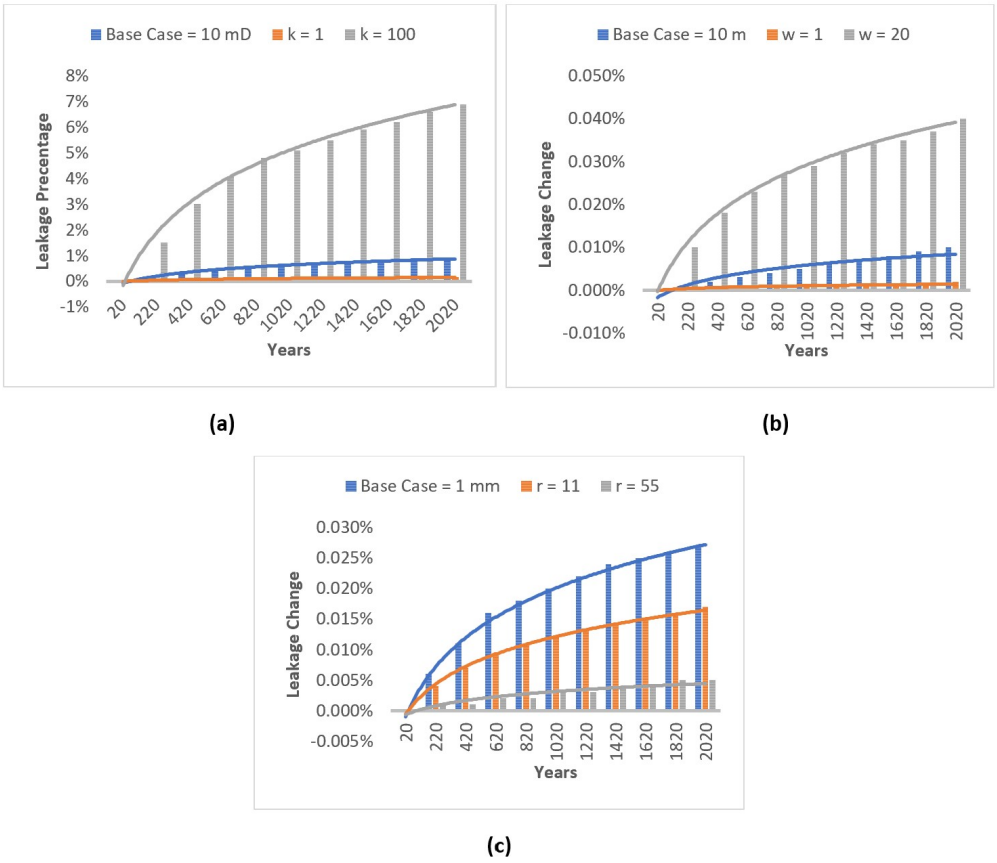

Figure 4.26: Sensitivity analysis of parameters of a: the permeability of a permeable zone; b: the width of the fault; c: the radius of the gas channel.

4.5 Summary

In this study, a life cycle inventory (LCI) model was created to calculate the direct emissions of the Asnaes coal power plant in Kalundborg, Denmark, equipped with post-combustion CO_2 capture, CO_2 conditioning, CO_2 pipeline transport, and CO_2 injection into the saline storage formation of the Havnsø structure. This study shows that post-combustion capture systems are the primary contributors to direct air emissions. A CO_2 capture unit that captures 95% of the CO_2 in the flue gas can further reduce PM_{10}, SO_2, SO_3, NO_2, HCl, HF, Hg vapour, and other trace metals present in flue gases after FGD. Due to the fact that the majority of trace motels are present naturally in coal and its combustion, this research did not take that into

consideration in detail.

The outcomes of life-cycle environmental impacts of power generation with post-combustion CO_2 capture with MEA, transport, and injection indicate that the post-combustion capture system generates all impact categories with the exception of HTP, which is dominated by MEA production. Emissions into the atmosphere are the main cause of AP, EP, GWP, HTP, and POCP. Both FAETP and TETP can be traced back to air or soil trace metal emissions. The results of the sensitivity analysis indicate that the life-cycle impacts in all categories are sensitive to changes in the CO_2 capture rate and energy consumption of CO_2 capture, since these parameters have a major impact on energy consumption. Moreover, the results indicate that the life-cycle impacts in the categories are not affected by changes in pipeline length or the needed CO_2 pressure for transportation. The findings of uncertainty analysis reveal that direct emissions of CO, NH_3, NO, NO_2, N_2O, and CO_2 are less uncertain than emissions of HF, HCl, SO_2, and SO_2 because emissions of HF, HCl, SO_2, and SO_2 are impacted by emission control mechanisms, which often increase uncertainty in emissions. In addition, the uncertainty of AP, EP, GWP, and POCP is lower than that of TETP, FAETP, and HTP because the first group is dependent on air emissions, which have a lower degree of uncertainty than emissions of trace metals, which dominate the second group.

Analyzed in the section on storage are operational and reservoir factors, as well as leakage pathway parameters, which have a substantial influence on CO_2 leakage. The results indicate that the injection period and injection rate significantly impact the ratio of CO_2 leakage to total CO_2 injected, while reservoir permeability and reservoir depth have little effect. Also, the CO_2 leakage rate is greatly affected by characteristics such as the permeability of the permeable zone, the width of the fault, and the radius of the gas channel.

5

Conclusion

Through this study, a comprehensive and adaptable LCA framework was created for the "Gate-to-Gate" assessment of possible CCS technology alternatives. The LCI models developed for the post-combustion capture system included the models chemical absorption CO_2 capture, CO_2 conditioning unit, CO_2 pipeline transport, CO_2 injection, and saline storage formation, which account for technological and geographical differences and generate reliable LCI data in a transparent manner.

This study tracked the final destination of direct emissions and trace metals of concern in CCS systems by using LCI models created for such a goal. In addition, it can also predict potential leakage paths for CO_2 and analyze the movement of injected CO_2 inside the reservoir. To quantify flows of materials, natural resources, energy, intermediate products, or emissions at the component unit process level, an LCI model was conducted using the case study, the Asnaes coal power plant in Kalundborg, Denmark, with post-combustion capture using MEA, transport and injection, and saline storage of the Havnsø structure. This model was developed

using basic chemical principles or empirical relationships that, to a greater extent, account for the technological, spatial, and temporal scales.

Post-combustion chemical absorption (MEA) CO_2 capture unit captures 95% of the CO_2 and emits less PM-10, SO_2, SO_3, NO_2, HCl, HF, mercury (Hg) vapor, and trace metals than conventional power plants. The percentage of trace metals released into the environment within a thousand years is less than 0.5% for most trace metals except As, Hg, and Se. It is surface impoundments that are the primary sources of soil contamination from trace metal emissions. Emissions from the post-combustion CO_2 capture system predominate throughout all impact categories and throughout the life cycle, with the exception of HTP, where emissions from MEA production play a larger role. There are very modest life-cycle environmental effects from the other upstream operations, such as MEA production, MEA transport, ammonia production, ammonia transport, power plant infrastructure, CO_2 pipeline infrastructure, CO_2 capture facility infrastructure, and compressor infrastructure. Emissions into the atmosphere are a major contributor to the AP, EP, GWP, HTP, and POCP. The FAETP and TETP are mainly due to trace metal emissions to air or soils.

Changes in the CO_2 capture rate and the amount of energy needed to capture CO_2 can have a sensitive impact on all of the categories. On the other hand, the length of the pipeline and the amount of CO_2 pressure needed for transport do not change the life-cycle impacts in most categories. Using K PZ or KS1 to chemically absorb CO_2 has a lower impact on the environment over its entire life cycle than using MEA to do the same thing. Moreover, the post-combustion CO_2 capture plant's direct emissions of CO, NH_3, NO, NO_2, $N2_O$, and CO_2 are less uncertain than the emissions of HF, HCl, and SO_2 and SO_3. The levels of uncertainty associated with TETP, FAETP, and HTP are higher than those associated with AP, EP, GWP, or POCP.

The results of this study show that the ratio of potential CO_2 leakage to total CO_2 injected is sensitive to changes in the injection period and injection rate. This is because a thicker CO_2 layer beneath the caprock is the result of either high injection rates or long injection durations,

both of which increase the risk of CO_2 leakage. In addition, the CO_2 leakage rate is significantly influenced by factors including the permeability of the permeable zone, the width of the fault, and the radius of the gas channel.

There is still an opportunity for future advancements towards enhancing the effectiveness of LCA on CCS technology. thus add some remarks and questions that might be advantageous here:

1. The time period during which the Global Warming Potential (GWP) of greenhouse gases (e.g. CO_2, CH_4, etc.) is computed affects the GWP of these gases. A gas that is rapidly evacuated from the atmosphere may initially have a significant impact, but its significance diminishes with time. For example, methane has a GWP100 of 25 (CO_2-equivalent) over 100 years, whereas its GWP20 is 72 over 20 years [142].

2. Current and predicted CCS systems make CO_2 capture and storage energy-intensive. Should power generating CO_2 be captured and stored in geological formations at the cost of abiotic resources? The answer dependents upon the comparative valuation of the impacts of climate change against the impact of abiotic resource depletion. The IPCC Fourth Assessment Report (2007) states that climate change will have uncertain impacts on systems of nature and humanity over a multi-century timescale and that most of the observed increase in global average temperatures since the mid-20th century is likely due to anthropogenic GHG concentrations.

3. Some kinds of life cycle effects, such as AP, EP, and so on, are increased by post-combustion CCS. However, in a global perspective, the emissions contributing to these categories come mostly from other industries (upstream processes) rather than power stations. This suggests that the rise in other types of environmental impacts produced by CCS can be mitigated by lowering emissions from other sectors where advanced pollution control technology can be easily implemented at lower prices.

4. Despite numerous research, the processes and mechanisms involved in CO_2 storage in saline aquifers and potential CO_2 leakage through other pathways are still poorly understood. Impurities in CO_2 geological storage formations (such as SOx, NOx, H2S, and trace elements) have unknown environmental impacts that must be investigated. Once the CO_2 storage processes and CO_2 leakage mechanisms are better known, it is desirable to improve the CO_2 storage LCI model further. Numerical simulations are the way to go if exact prediction of CO_2 migration or assessment of CO_2 leakage is required.

Appendices

Appendix I

LCI data for the upstream processes

Material & Process	Amount	Unit
Steel (High alloyed)	307	T
Concrete	1	m^3
Transport	9.5	kt.km
Tot CO_2 Capture	94	Mt
Lifetime	30	Year

Table 1: LCI data for CO_2 capture System [32].

Material & Process	Amount	Unit
Steel (Low alloyed)	65	T
Concrete	65	m^3
Diesel	1978	Gj
Electricity	61	MWH
Copper	7	T
Polyethylene	20	T
Capacity	40	MW
Tot CO_2 Compressed	62	Mt
Lifetime	30	Yt
Tot CO_2 Leakage	18	Kt

Table 2: LCI data for CO_2 compressor infrastructure [33] [34].

Material & Process	Amount	Unit
Sand	1.0372	kg
Diesel	1.7606	MJ
Steel	0.2554	kg
Bitumen	0.00123	kg
Polyethylene	0.00247	kg
Transportation	121.4362	kg.km
Tot CO_2 transported	1000	kg
Wastes	0.5914	kg

Table 3: LCI data for onshore CO_2 pipeline infrastructure [33, 32].

Material & Process	Amount	Unit
Well	18	k3
Sand	712,000	t
Steel (High and un-alloyed)	11,900	t
Concrete	10,463	m^3
Transportation	74,922,800	t.km
Copper	425	t
Tot CO_2 Injection	219	Mt
Lifetime	30	Year

Table 4: LCI data for CO2 injection facility [32].

Material & Process	Amount	Unit
Input		
Ethylene oxide	816	g
Ammonia)	788	g
Electricity	0.333	KWH
Natural gas	2	MJ
Transport	11.23	t.km
Infrastructure chemical plant	4E10	p
Output		
Monoethanolamine	1	kg
Waste heat	1.2	MJ
Ethylene oxide to air	1.63	g
Ethylene oxide to water	1.47	g
Ammonium to water	1.58	g
CO_2	26.5	g
Nitrate to water	6.97	g
Ammonia to air	3.04	g
COD, BOD	21.3	g
TOC, DOC	8.02	g

Table 5: LCI data for MEA production [35, 32].

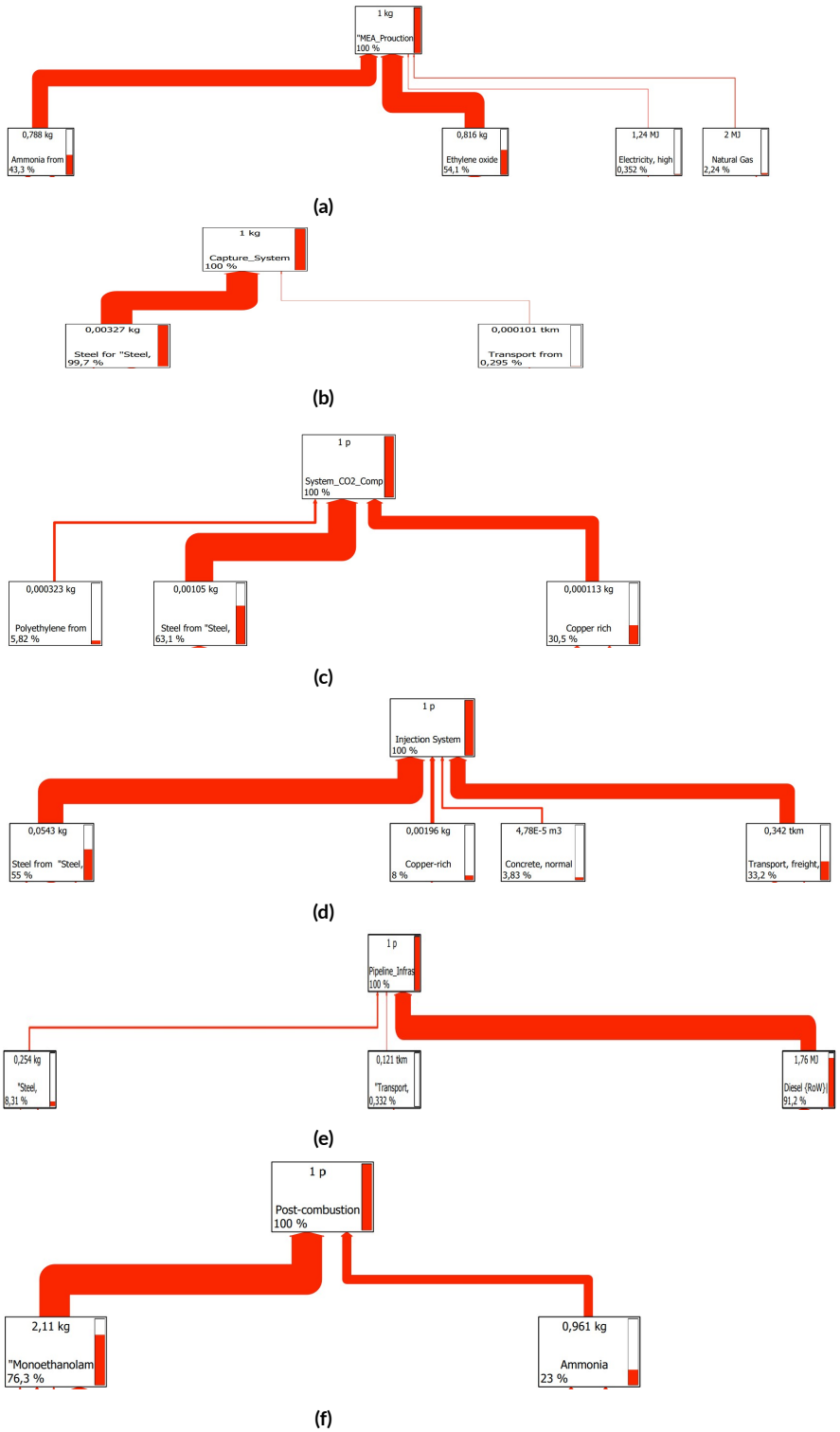

Figure A.1: LCI data by using Sima Pro software; a. MEA production; b. capture construction; c. compressor system; d. pipeline infrastructure; e. injection infrastructure; f. post-combustion system.

Appendix II

Parameters and Data Relating to Post-Combustion Carbon Dioxide Capture Life Cycle Assessment Results ; US EPA, 1998 [24]

Type of emissions (or Resources)		Emissions (or resources)	Total	Post-combustion CCS (MEA)	Upstream processes												
					Hard coal production (EU-15 mix)	Coal transport railway	MEA production	MEA transport truck	Limestone transport truck	Limestone Production	Ammonia transport truck	Ammonia Production	Natural gas production (GB mix)	CO_2 capture infrastructure	Compressor infrastructure	Injection infrastructure	Power plant construction	Transport infrastructure
Energy and Material Resources	Energy resources	Crude oil (resource)	9.505494	0	5.448331	0.026929	1.669811	0.00516	0.016147	0.006025	0.002346	0.055141	0.00382	0.000222	0.077106	0.004765	0.161134	2.028556
		Hard coal (resource)	352.4548	0	351.2464	0.117374	0.13095	2.24E-05	6.99E-05	0.0079	1.02E-05	0.035538	0.005238	0.003049	0.091984	0.047863	0.513162	0.255227
		Lignite (resource)	2.836084	0	2.567273	0.154374	2.00E-07	2.20E-05	6.88E-05	0.025226	1.00E-05	6.27E-08	0.000108	0.000272	0.009294	0.004206	0.046429	0.0288
		.....																
	Material resources	Chromium	1.66E-12	0	0	0	1.29E-12	0	0	0	0	3.55E-13	0	0	2.09E-14	0	0	0
		Copper	1.10E-10	0	0	0	3.47E-11	0	0	0	0	9.60E-12	0	0	6.56E-11	0	0	0
		Iron	0.00042	0	2.20E-10	7.02E-12	0.000393	2.90E-15	9.06E-15	8.37E-11	1.32E-15	2.29E-05	7.47E-13	0	3.57E-06	5.47E-09	6.67E-14	1.71E-08
		.....																
		Zinc - lead - copper ore (12%-3%-2%)	0.057908	0	0.000116	6.96E-06	0	6.56E-08	2.05E-07	6.35E-07	2.98E-08	0	5.27E-06	0	0.045216	0.012535	1.49E-06	2.62E-05
		Zinc - lead ore (4.21%-4.96%)	5.35E-16	0	0	1.98E-16	0	5.88E-19	1.84E-18	7.44E-18	2.67E-19	0	4.79E-17	0	1.76E-17	6.32E-18	1.34E-17	2.42E-16
		Zinc ore (sulphide)	3.49E-13	0	3.28E-13	7.28E-15	0	2.81E-17	8.79E-17	4.62E-16	1.28E-17	0	3.51E-16	0	3.81E-16	1.14E-16	6.39E-16	1.13E-14
Emissions to air	Heavy metal emissions to air	Antimony	4.82E-07	1.66E-08	4.56E-07	7.24E-09	6.41E-15	2.00E-12	6.27E-12	3.18E-10	9.11E-13	2.31E-15	3.87E-10	0	1.01E-09	1.51E-10	6.13E-11	9.77E-10
		Arsenic	9.59E-06	7.57E-06	1.92E-06	6.57E-08	1.75E-10	4.93E-11	1.54E-10	1.84E-09	2.24E-11	1.42E-11	2.82E-09	0	7.89E-09	1.27E-09	1.23E-09	2.10E-08
		....																
	Inorganic emissions to air	Ammonia	0.127391	0.122626	0.001375	3.77E-06	0.003362	1.24E-07	3.89E-07	1.54E-06	5.65E-08	1.36E-05	1.46E-07	6.08E-09	5.68E-07	4.99E-07	1.30E-06	7.01E-06
		Ammonium	9.96E-11	0	8.32E-11	1.35E-11	0	1.72E-15	5.40E-15	1.54E-12	7.84E-16	0	7.57E-14	0	2.42E-13	7.30E-14	4.26E-14	8.42E-13
		...																
	Organic emissions to air (group VOC)	Organic emissions to air (group VOC)	3.137117	0.091086	2.973052	0.00164	0.042294	2.69E-05	8.42E-05	0.000163	1.22E-05	0.009141	0.002551	3.03E-05	0.001487	0.000327	0.005655	0.009567
	Organic emissions to air	Group NMVOC to air	0.118134	0.083945	0.027502	0.000119	0.003678	1.12E-05	3.49E-05	3.49E-05	5.07E-06	1.01E-06	0.000218	2.65E-06	0.000121	4.20E-05	0.000627	0.001792
		....																
	Other emissions to air	Exhaust	66.47702	0	61.64545	3.524762	0	0.00085	0.00266	0.248717	0.000386	0	0.109013	0	0.291195	0.09076	0.023488	0.539733
		....																
	Particles to air	Dust (combustion)	0.000179	0.000179	0	0	0	0	0	0	0	0	0	0	0	0	0	0
		Dust (PM10)	0.007412	0.004341	0.0015	1.06E-05	0.001223	9.12E-08	2.85E-07	2.58E-06	4.15E-08	0.000278	1.99E-06	0	1.54E-05	6.37E-07	2.08E-06	3.69E-05
		...																

Figure A.2: The calculations of life cycle emissions of power plant with post-combustion CO_2 capture, transport and injection

Type of emissions (or Resources)		Emissions (or resources)	Total	Post-combustion CCS (MEA)	Upstream processes													
					Hard coal production (EU-15 mix)	Coal transport railway	MEA production	MEA transport truck	Limestone transport truck	Limestone Production	Ammonia transport truck	Ammonia Production	Natural gas production (GB mix)	CO_2 capture infrastructure	Compressor infrastructure	Injection infrastructure	Power plant construction	Transport infrastructure
Emissions to fresh water	Analytical measures to fresh water	Adsorbable organic halogen compounds (AOX)	6.88E-06	0	4.79E-06	6.53E-08	1.41E-12	3.88E-09	1.21E-08	9.89E-09	1.76E-09	2.80E-13	1.70E-08	1.32E-09	7.37E-08	1.23E-08	3.09E-07	1.58E-06
		Biological oxygen demand (BOD)	0.000184	0	2.88E-05	3.74E-07	3.37E-05	1.81E-08	5.66E-08	5.54E-08	8.22E-09	1.64E-07	1.82E-08	4.36E-07	1.21E-05	3.44E-06	7.35E-05	3.09E-05
		Chemical oxygen demand (COD)	0.054731	0	0.007186	0.000185	0.046246	3.71E-07	1.16E-06	1.59E-05	1.69E-07	0.000584	8.19E-06	1.19E-06	5.37E-05	1.44E-05	0.000211	0.000223
		Solids (dissolved)	0.0007	0	0.000113	1.81E-05	0.000369	2.64E-09	8.25E-09	8.37E-07	1.20E-09	0.000196	2.88E-07	0	1.07E-06	7.76E-08	7.18E-08	1.19E-06
		Total dissolved organic bounded carbon	2.88E-05	0	0	4.35E-11	2.73E-05	6.24E-17	1.95E-16	4.08E-12	2.84E-17	8.28E-08	4.06E-15	4.28E-09	3.39E-07	2.97E-08	8.02E-07	2.69E-07
		Total organic bounded carbon	0.017204	0	0.000125	8.99E-07	0.016945	7.87E-08	2.46E-07	9.96E-08	3.58E-08	0	1.18E-07	3.82E-07	1.07E-05	2.79E-06	6.80E-05	5.08E-05
	Heavy metals to fresh water	Antimony	7.69E-13	0	6.76E-13	7.33E-14	0	1.91E-17	5.97E-17	1.61E-15	8.67E-18	0	2.58E-16	0	4.03E-15	2.17E-15	4.44E-16	1.17E-14
		Arsenic	4.11E-06	0	1.28E-06	2.43E-08	5.64E-10	7.14E-10	2.23E-09	4.28E-09	3.25E-10	6.46E-11	7.33E-10	9.87E-09	2.64E-07	6.92E-08	1.67E-06	7.84E-07
		…																
		Zinc	4.99E-05	0	3.57E-05	6.29E-08	5.43E-07	2.72E-10	8.51E-10	5.23E-09	1.24E-10	2.14E-07	2.14E-09	4.95E-08	1.80E-06	4.86E-07	8.31E-06	2.64E-06
	Inorganic emissions to fresh water	Acid (calculated as H+)	4.15E-05	0	0	4.58E-08	2.69E-05	2.19E-11	6.85E-11	4.20E-09	9.95E-12	1.45E-05	1.36E-10	0	4.14E-08	2.40E-10	5.39E-08	9.07E-09
		Aluminium	0.001667	0	0.00041	9.52E-06	8.52E-07	1.39E-09	4.36E-09	4.43E-07	6.34E-10	3.43E-08	1.55E-07	4.92E-06	0.000128	3.42E-05	0.000827	0.000252
		….																
		Sulphuric acid	8.34E-08	0	6.93E-08	4.07E-09	0	1.81E-11	5.67E-11	2.44E-10	8.24E-12	0	1.44E-09	0	3.98E-10	1.20E-10	4.13E-10	7.33E-09
	Organic emissions to fresh water	Halogenated organic emissions to fresh water	3.04E-08	0	2.52E-08	3.61E-10	1.21E-11	3.90E-13	1.22E-12	2.81E-11	1.77E-13	3.35E-12	4.28E-11	1.49E-11	4.20E-10	2.06E-10	2.74E-09	1.31E-09
		….																
	Particles to fresh water	…																
		Solids (suspended)	0.218527	0	0.213288	0.000308	0.00019	9.87E-06	3.09E-05	3.84E-05	4.49E-06	1.52E-05	9.14E-06	1.00E-06	0.000187	5.04E-05	0.000408	0.003988
Emissions to industrial soil	Heavy metals to industrial soil	…																
		Zinc	6.13E-06	6.03E-06	7.34E-08	9.72E-10	0	5.58E-11	1.75E-10	1.42E-10	2.54E-11	0	2.64E-10	0	5.73E-10	5.76E-11	1.27E-09	2.19E-08
	Inorganic emissions to industrial soil	Aluminium (3+)	9.99E-07	0	7.42E-07	9.72E-09	0	5.66E-10	1.77E-09	1.43E-09	2.57E-10	0	2.70E-09	0	5.80E-09	5.80E-10	1.28E-08	2.22E-07
		…																
	Organic emissions	Oil (unspecified)	8.28E-06	0	6.63E-06	1.04E-06	0	1.33E-10	4.15E-10	7.98E-09	6.03E-11	0	7.90E-09	0	3.53E-08	1.20E-07	3.02E-09	4.35E-07

Figure A.3: Figure A.2 continued

continued

Type of emissions (or Resources)		Emissions (or resources)	Total	Post-combustion CCS (MEA)	Upstream processes													
					Hard coal production (EU-15 mix)	Coal transport railway	MEA production	MEA transport truck	Limestone transport truck	Limestone Production	Ammonia transport truck	Ammonia Production	Natural gas production (GB mix)	CO_2 capture infrastructure	Compressor infrastructure	Injection infrastructure	Power plant construction	Transport infrastructure
Emissions to sea water	Analytical measures to sea water	Absorbable organic halogen compounds (AOX)	4.96E-12	0	2.89E-12	5.85E-14	0	2.15E-15	6.73E-15	2.24E-15	9.77E-16	0	1.07E-12	0	2.98E-14	3.86E-15	4.89E-14	8.45E-13
		….																
	Heavy metals to sea water	Arsenic	2.10E-06	0	1.71E-06	8.49E-09	0	8.80E-10	2.75E-09	4.29E-10	4.00E-10	0	2.35E-09	0	8.87E-09	7.05E-10	2.00E-08	3.44E-07
		Cadmium	3.18E-06	0	3.00E-06	6.72E-09	0	3.99E-10	1.25E-09	3.30E-10	1.82E-10	0	4.15E-09	0	4.21E-09	9.48E-10	9.06E-09	1.58E-07
		…																
	Inorganic emissions to sea water	…																
		Sulphide	0.000845	0	0.000596	2.06E-06	0	5.66E-07	1.77E-06	4.37E-07	2.57E-07	0	4.50E-06	0	5.67E-06	2.01E-07	1.28E-05	0.000221
		Sulphur	3.71E-08	0	3.60E-08	2.32E-11	0	2.20E-13	6.89E-13	1.32E-12	1.00E-13	0	1.17E-12	0	3.67E-10	2.17E-10	5.02E-12	4.88E-10
	Organic emissions to sea water	Hydrocarbons to sea water	0.000208	0	0.000147	5.53E-07	0	1.39E-07	4.34E-07	1.29E-07	6.30E-08	0	9.60E-07	0	1.39E-06	5.27E-08	3.15E-06	5.41E-05
		Naphthalene	2.31E-06	0	1.58E-06	5.46E-09	0	1.68E-09	5.24E-09	1.98E-09	7.62E-10	0	7.45E-09	0	1.67E-08	5.47E-10	3.80E-08	6.53E-07
	Particles to sea water	Solids (suspended)	0.004356	0	0.002536	5.14E-05	0	1.89E-06	5.91E-06	1.97E-06	8.58E-07	0	0.000944	0	2.62E-05	3.39E-06	4.29E-05	0.000742

Figure A.4: Figure A.2 continued

Resources required/Sources of impacts	Amount (kg)	Emissions to Air	Amount (kg)	Trace metal emissions to air	Amount (kg)	Trace metal emissions to soils	Amount (kg)
Coal	347.89	CO_2	48.96	Antimony (Sb)	6.65E-08	Antimony (Sb)	3.65E-08
Natural gas	1.63	PM	0.0047	Arsenic (As)	3.02E-05	Arsenic (As)	2.77E-06
Limestone	6.61	PM-10	0.0046	Beryllium (Be)	1.62E-06	Beryllium (Be)	7.08E-08
Ammonia	0.93	SO_2	0.0010	Cadmium (Cd)	6.39E-07	Cadmium (Cd)	1.89E-08
MEA	2.04	SO_3	0	Chromium (Cr)	2.75E-06	Chromium (Cr)	1.25E-07
Energy consumption equivalence (kwh)	351.79	NO	0.4580	Cobalt (Co)	2.33E-07	Cobalt (Co)	1.82E-07
Solid wastes	34.77	NO_2	0.0181	Lead (Pb)	6.56E-06	Lead (Pb)	1.94E-06
Liquid wastes	2.11	N_2O	0.0052	Manganese (Mn)	1.88E-06	Manganese (Mn)	2.55E-06
		CO	0.0870	Nickel (Ni)	1.37E-06	Nickel (Ni)	4.29E-07
		HCl	1.04E-04	Selenium (Se)	1.97E-05	Selenium (Se)	7.81E-06
		HF	3.92E-05	Zinc (Zn)	3.58E-05	Zinc (Zn)	6.03E-06
		CH_4	0.0070	Copper (Cu)	1.29E-05	Copper (Cu)	4.17E-07
		NH_3	0.1230	Thallium (Tl)	2.78E-07	Thallium (Tl)	3.63E-08
		MEA	0.0119	Vanadium (V)	8.92E-06	Vanadium (V)	3.02E-05
				Barium (Ba)	8.63E-05	Barium (Ba)	5.17E-06
				Silver (Ag)	2.78E-08	Silver (Ag)	3.63E-09
				Hg0	1.12E-07	Mercury (Hg)	1.62E-09
				Hg++	1.25E-06		
				Hg particulate	0.00E+00		

Figure A.5: The direct emissions and the consumption of resources in power plant with post-combustion (MEA) capture, transport and injection (per 1 MWh electricity generated).

Appendix III

The input parameters for uncertainty analysis : U.S. Environmental Protection Agency (USEPA), 1998c [24]

Emissions	Base case scenario	Mean	Standard deviation (% of base case scenario)	10% Percentile	25% Percentile	Median	75% Percentile	90% Percentile
Carbon monoxide	0.10354	0.10378	5%	0.097333	0.10018	0.10349	0.10711	0.11053
Ammonia	0.14598	0.14664	7.05%	0.13367	0.13963	0.14631	0.15343	0.16019
Nitrogen monoxide	1.1938	1.2	10.80%	1.0355	1.1104	1.1964	1.2852	1.3667
Nitrous oxide	0.000639	0.000644	19.70%	0.000484	0.000558	0.000644	0.000727	0.000808
Nitrogen dioxide	0.022575	0.022736	19.90%	0.016958	0.019666	0.022603	0.025767	0.028571
Carbon dioxide	57.218	57.468	35.60%	31.488	43.746	57.203	70.965	84.075
Hydrogen fluoride	4.66E-05	5.95E-05	67.70%	1.31E-05	2.92E-05	5.25E-05	8.32E-05	0.000115
Sulphur dioxide	0.001203	0.00155	69.80%	0.000353	0.000739	0.001347	0.002149	0.003023
Hydrogen chloride	0.000124	0.000164	82.30%	2.68E-05	6.41E-05	0.000135	0.000223	0.000339
Sulphur trioxide	0	1.81E-06	187%	0	0	0	2.28E-06	5.95E-06

Figure A.6: Statistical outputs of air emissions at direct emission level

Impact Category	Base case scenario	Mean	Standard deviation (% of base case)	10% Percentile	25% Percentile	Median	75% Percentile	90% Percentile
GWP	57.601	57.849	35.30%	31.854	44.124	57.601	71.343	84.454
TETP	0.089082	0.19092	49.70%	0.08793	0.12326	0.17434	0.24121	0.31571
MAETP	2571.4	4182.8	48.30%	1886.7	2712.8	3886.3	5299.1	6893
HTP	4.127	8.6838	84.50%	2.4472	3.8385	6.4862	10.963	17.686
FAETP	0.17793	0.39573	68.60%	0.12018	0.20043	0.33406	0.52079	0.74449
POCP	-0.50621	-0.50882	-10.90%	-0.57975	-0.54503	-0.5073	-0.47048	-0.43874
EP	0.29279	0.29428	9.69%	0.2586	0.27453	0.29331	0.3127	0.33098
ADP	5.2729	5.2851	5%	4.9566	5.1013	5.2708	5.4543	5.6284
AP	1.569	1.5774	9.68%	1.3865	1.4715	1.5721	1.676	1.774

Figure A.7: Statistical outputs of environmental impact at direct emission level

Bibliography

[1] I. P. O. C. Change, "Carbon dioxide capture and storage," *Published in the United States of America by Cambridge University Press, New York*, 2005.

[2] M. Bui, I. Gunawan, V. Verheyen, Y. Artanto, E. Meuleman, and P. Feron, "Dynamic modeling and validation of post-combustion co2 capture plants in australian coal-fired power stations," *Energy Procedia*, vol. 37, pp. 2694–2702, 2013.

[3] S. M. Nazir, J. H. Cloete, S. Cloete, and S. Amini, "Efficient hydrogen production with co2 capture using gas switching reforming," *Energy*, vol. 185, pp. 372–385, 2019.

[4] B. Metz, O. Davidson, H. De Coninck, M. Loos, and L. Meyer, *IPCC special report on carbon dioxide capture and storage*. Cambridge: Cambridge University Press, 2005.

[5] W. L. Theo, J. S. Lim, H. Hashim, A. A. Mustaffa, and W. S. Ho, "Review of pre-combustion capture and ionic liquid in carbon capture and storage," *Applied energy*, vol. 183, pp. 1633–1663, 2016.

[6] G. C. institute, "Global status of ccs report: 2019," https://www.globalccsinstitute.com/resources/publications-reports-research/global-status-of-ccs-report-2019/, Dec 2019, accessed: 2023-02-10.

[7] "Cooperative research centre for greenhouse gas technologies," 2005.

[8] G. Finnveden and Å. Moberg, "Environmental systems analysis tools–an overview," *Journal of cleaner production*, vol. 13, no. 12, pp. 1165–1173, 2005.

[9] J. Guinée, "Lca and mfa/sfa: Analytical tools for industrial ecology," *Centre of Environmental Science (CML) Leiden. Holanda*, 2001.

[10] L. Strömberg, "Encap integrated project," in *Presentation held at ENCAP–CASTOR Training Seminar*, vol. 16, 2006.

[11] G. Göttlicher, *The energetics of carbon dioxide capture in power plants*. National Energy Technology Laboratory, 2004.

[12] A. Aspelund and K. Jordal, "Gas conditioning—the interface between co2 capture and transport," *International Journal of Greenhouse Gas Control*, vol. 1, no. 3, pp. 343–354, 2007.

[13] M. A. Abdi, "Design of natural gas handling equipment, lecture note," *Memorial University of Newfoundland*, 2007.

[14] D. L. McCollum and J. M. Ogden, "Techno-economic models for carbon dioxide compression, transport, and storage & correlations for estimating carbon dioxide density and viscosity," 2006.

[15] S. D. Hovorka, M. Holtz, S. Sakurai, P. Knox, D. Collins, P. Papadeas, and D. Stehli, "Report to the texas commission on environmental quality to accompany a class v application for an experimental technology pilot injection well," *Bureau of Economic Geology, USA*, 2003.

[16] M. Bentham and M. Kirby, "Co2 storage in saline aquifers," *Oil & gas science and technology*, vol. 60, no. 3, pp. 559–567, 2005.

[17] S. Ide, K. Jessen, and F. Orr Jr, "Time scales for migration and trapping of co2 in saline aquifers," *Internation Journal of Greenhouse Gas Control*, 2006.

[18] S. T. Ide, K. Jessen, and F. M. Orr Jr, "Storage of co2 in saline aquifers: Effects of gravity, viscous, and capillary forces on amount and timing of trapping," *International journal of greenhouse gas control*, vol. 1, no. 4, pp. 481–491, 2007.

[19] C. Oldenburg and J. Lewicki, "On leakage and seepage of co 2 from geologic storage sites into surface water," *Environmental Geology*, vol. 50, pp. 691–705, 2006.

[20] M. Larsen, N. Bech, T. Bidstrup, N. P. Christensen, T. Vangkilde-Pedersen, and O. Biede, "Kalundborg case study, a feasibility study of co2 storage in onshore saline aquifers," *CO2STORE. GEUS Report*, vol. 2, p. 2007, 2007.

[21] I. Akervoll, P. Zweigel, and E. Lindeberg, "Co2 storage in open, dipping aquifers," in *Proceedings of GHGT-8 8th international conference on greenhouse gas control technologies, Trondheim, Norway*, 2006, pp. 19–22.

[22] G. Rochelle, "Co2 capture by aqueous absorption/stripping opportunities for better technology," in *Workshop on Carbon Sequestration Science, Washington, DC*, 2001.

[23] C. R. Bozzuto, N. Nsakala, G. Liljedahl, M. Palkes, J. Marion, D. Vogel, J. Gupta, M. Fugate, and M. Guha, "Engineering feasibility and economics of co2 capture on an existing coal-fired power plant," *Alstom Power Inc., Ohio Coal Development Office, and US DOE NETL (June 2001). See: http://www. netl. doe. gov/coal/Carbon% 20Sequestration/pubs/analysis/AlstomReport. pdf*, 2001.

[24] U. E. P. A. (USEPA), "Ap 42, volume i, fifth edition, chapter 1: External combustion sources, 1.4 natural gas combustion," https://www.epa.gov/, 1998, accessed: 2023-02-13.

[25] R. Turner, N. Hardy, and B. Hooper, "Quantifying the risks associated with a co2 sequestration pipeline: a methodology & case study," https://extra.co2crc.com.au/, 2007, accessed: 2023-02-13.

[26] U. E. P. A. (USEPA), "Volume i, fifth edition, chapter 3: Stationary internal combustion sources, 3.2 natural gas-fired reciprocating engines," https://www.epa.gov/, 2000, accessed: 2023-02-12.

[27] S. Eggleston, L. Buendia, K. Miwa, T. Ngara, and K. Tanabe, "Ipcc 2006, 2006 ipcc guidelines for national greenhouse gas inventories," *Prepared by the National Greenhouse Gas Inventories Program me*, 2006.

[28] D. Epperson, "Protocol for equipment leak emission estimates, 1995," Radian Corp., Research Triangle Park, NC (United States), Tech. Rep., 1995.

[29] G. Heddle, H. Herzog, and M. Klett, "The economics of co2 storage," *Massachusetts Institute of Technology, Laboratory for Energy and the Environment*, 2003.

[30] T. Shires and C. Loughran, "Compendium of greenhouse gas emissions estimation methodologies for the oil and gas industry," 2004.

[31] N. Huerta, S. Bryant, S. Minkoff, and C. Oldenburg, "Well leakage pathways and their importance to co2/cement reactions: analysis of long-term cement competence as part of a certification framework for co2 sequestration," in *Sixth annual conference on carbon capture & sequestration: expediting deployment of industrial scale systems: can it be done*, 2007, pp. 7–10.

[32] J. Koornneef, T. van Keulen, A. Faaij, and W. Turkenburg, "Life cycle assessment of a pulverized coal power plant with post-combustion capture, transport and storage of co2," *International journal of greenhouse gas control*, vol. 2, no. 4, pp. 448–467, 2008.

[33] M. Faist Emmenegger, T. Heck, N. Jungbluth, and M. Tuchschmid, "Erdgas," *Sachbilanzen von Energiesystemen: Grundlagen für den ökologischen Vergleich von Energiesystemen und den Einbezug von Energiesystemen in Ökobilanzen für die Schweiz*, 2007.

[34] A. Röder, C. Bauer, and R. Dones, "Sachbilanzen von energiesystemen," Final report No. 6 ecoinvent 2000, Tech. Rep., 2004.

[35] H. Althaus, M. Chudacoff, R. Hischier, N. Jungbluth, M. Osses, A. Primas *et al.*, "Life cycle inventories of chemicals," *Ecoinvent report*, vol. 2, 2007.

[36] K. Elsaid, M. Kamil, E. T. Sayed, M. A. Abdelkareem, T. Wilberforce, and A. Olabi, "Environmental impact of desalination technologies: A review," *Science of The Total Environment*, vol. 748, p. 141528, 2020.

[37] M. A. Abdelkareem, K. Elsaid, T. Wilberforce, M. Kamil, E. T. Sayed, and A. Olabi, "Environmental aspects of fuel cells: A review," *Science of The Total Environment*, vol. 752, p. 141803, 2021.

[38] R. Ben-Mansour, M. Habib, O. Bamidele, M. Basha, N. Qasem, A. Peedikakkal, T. Laoui, and M. Ali, "Carbon capture by physical adsorption: materials, experimental investigations and numerical modeling and simulations–a review," *Applied Energy*, vol. 161, pp. 225–255, 2016.

[39] M. Plaza, A. González, C. Pevida, J. Pis, and F. Rubiera, "Valorisation of spent coffee grounds as co2 adsorbents for postcombustion capture applications," *Applied Energy*, vol. 99, pp. 272–279, 2012.

[40] J.-S. Bae and S. Su, "Macadamia nut shell-derived carbon composites for post combustion co2 capture," *International Journal of Greenhouse Gas Control*, vol. 19, pp. 174–182, 2013.

[41] R. Carlson and A.-C. Pålsson, "Industrial environmental information management for technical systems," *Journal of Cleaner Production*, vol. 9, no. 5, pp. 429–435, 2001.

[42] M. Akai, N. Nomura, H. Waku, and M. Inoue, "Life-cycle analysis of a fossil-fuel power plant with co2 recovery and a sequestering system," *Energy*, vol. 22, no. 2-3, pp. 249–255, 1997.

[43] "Coal in sustainable society (ciss), 2003, case study b17: electricity from co2 recovery type igcc," http://www.ciss.com.au/, assessed 6 December 2004.

[44] L. Lombardi, "Life cycle assessment comparison of technical solutions for co2 emissions reduction in power generation," *Energy conversion and management*, vol. 44, no. 1, pp. 93–108, 2003.

[45] A. Corti and L. Lombardi, "Biomass integrated gasification combined cycle with reduced co2 emissions: Performance analysis and life cycle assessment (lca)," *Energy*, vol. 29, no. 12-15, pp. 2109–2124, 2004.

[46] N. A. Odeh and T. T. Cockerill, "Life cycle ghg assessment of fossil fuel power plants with carbon capture and storage," *Energy Policy*, vol. 36, no. 1, pp. 367–380, 2008.

[47] F. Birol *et al.*, "World energy outlook," *Paris: International Energy Agency*, vol. 23, no. 4, p. 329, 2008.

[48] J. F. Contadini, R. M. Moore, and P. L. Mokhtarian, "Life cycle assessment of fuel cell vehicles a methodology example of input data treatment for future technologies," *The International Journal of Life Cycle Assessment*, vol. 7, pp. 73–84, 2002.

[49] J.-M. G. Amann and C. Bouallou, "A new aqueous solvent based on a blend of n-methyldiethanolamine and triethylene tetramine for co2 recovery in post-combustion: Kinetics study," *Energy Procedia*, vol. 1, no. 1, pp. 901–908, 2009.

[50] D. Bonenfant, M. Mimeault, and R. Hausler, "Comparative analysis of the carbon dioxide absorption and recuperation capacities in aqueous 2-(2-aminoethylamino) ethanol

(aee) and blends of aqueous aee and n-methyldiethanolamine solutions," *Industrial & engineering chemistry research*, vol. 44, no. 10, pp. 3720–3725, 2005.

[51] T. C. Drage, A. Arenillas, K. M. Smith, C. Pevida, S. Piippo, and C. E. Snape, "Preparation of carbon dioxide adsorbents from the chemical activation of urea–formaldehyde and melamine–formaldehyde resins," *Fuel*, vol. 86, no. 1-2, pp. 22–31, 2007.

[52] W.-J. Son, J.-S. Choi, and W.-S. Ahn, "Adsorptive removal of carbon dioxide using polyethyleneimine-loaded mesoporous silica materials," *Microporous and Mesoporous Materials*, vol. 113, no. 1-3, pp. 31–40, 2008.

[53] R. Davies, G. Foulger, A. Bindley, and P. Styles, "Induced seismicity and hydraulic fracturing for the recovery of hydrocarbons," *Marine and petroleum geology*, vol. 45, pp. 171–185, 2013.

[54] B. Dou, Y. Song, Y. Liu, and C. Feng, "High temperature co2 capture using calcium oxide sorbent in a fixed-bed reactor," *Journal of hazardous materials*, vol. 183, no. 1-3, pp. 759–765, 2010.

[55] Z. H. Ban, L. K. Keong, and A. Mohd Shariff, "Physical absorption of co2 capture: a review," *Advanced Materials Research*, vol. 917, pp. 134–143, 2014.

[56] C.-H. Yu, C.-H. Huang, C.-S. Tan *et al.*, "A review of co2 capture by absorption and adsorption," *Aerosol and Air Quality Research*, vol. 12, no. 5, pp. 745–769, 2012.

[57] N. A. Rashidi and S. Yusup, "An overview of activated carbons utilization for the post-combustion carbon dioxide capture," *Journal of CO2 utilization*, vol. 13, pp. 1–16, 2016.

[58] C. A. T. Force, "Advanced post-combustion co2 capture," *Freund, H., J. Bauer, T. Zeiser and G. Emig (2005)." Detailed simulation of transport processes in fixed-beds." Industrial & engineering chemistry research*, vol. 44, no. 16, pp. 6423–6434, 2009.

[59] A. Wahby, J. Silvestre-Albero, A. Sepúlveda-Escribano, and F. Rodríguez-Reinoso, "Co2 adsorption on carbon molecular sieves," *Microporous and Mesoporous Materials*, vol. 164, pp. 280–287, 2012.

[60] R. Khalilpour, K. Mumford, H. Zhai, A. Abbas, G. Stevens, and E. S. Rubin, "Membrane-based carbon capture from flue gas: a review," *Journal of Cleaner Production*, vol. 103, pp. 286–300, 2015.

[61] I. In, B. Metz, O. Davidson, H. Coninck, M. Loos, and L. Meyer, "Special report on carbon dioxide capture and storage," *Metz, B., Davidson, O., Coninck, HC, Loos, M., Meyer, LA, Eds*, 2005.

[62] C. M. White, D. H. Smith, K. L. Jones, A. L. Goodman, S. A. Jikich, R. B. LaCount, S. B. DuBose, E. Ozdemir, B. I. Morsi, and K. T. Schroeder, "Sequestration of carbon dioxide in coal with enhanced coalbed methane recovery a review," *Energy & Fuels*, vol. 19, no. 3, pp. 659–724, 2005.

[63] T. Ajayi, J. S. Gomes, and A. Bera, "A review of co 2 storage in geological formations emphasizing modeling, monitoring and capacity estimation approaches," *Petroleum Science*, vol. 16, pp. 1028–1063, 2019.

[64] J. Linßen, P. Markewitz, D. Martinsen, and M. Walbeck, "Zukünftige energieversorgung unter den randbedingungen einer großtechnischen co2-abscheidung und speicherung," *Abschlussbericht des Forschungsvorhabens FKZ*, vol. 326889, 2006.

[65] R. P, C. C, W. S, G. P, M. Dr. F, and K. S, "Uba 2006: Umweltbundesamt (ed.)," 2006.

[66] S. Salvi, F. Quattrocchi, C. Brunori, F. Doumaz, M. Angelone, A. Billi, F. Buongiorno, R. Funiciello, M. Guerra, G. Mele *et al.*, "A multidisciplinary approach to earthquake research: implementation of a geochemical geographic information system for the gargano site, southern italy," *Natural Hazards*, vol. 20, pp. 255–278, 1999.

[67] C. Nelson, J. Evans, J. Sorensen, and E. Steadman, "Factors affecting the potential for co2 leakage from geologic sinks, plain co2 reduction (pcor) partnership, 2005," *Available only online at http://www. undeerc. org/PCOR/newsandpubs/pdf/FactorsAffectingPotential. pdf (accessed June 30, 2010)*.

[68] C. M. White, B. R. Strazisar, E. J. Granite, J. S. Hoffman, and H. W. Pennline, "Separation and capture of co2 from large stationary sources and sequestration in geological formations—coalbeds and deep saline aquifers," *Journal of the Air & Waste Management Association*, vol. 53, no. 6, pp. 645–715, 2003.

[69] N. Fan, J. Wang, C. Deng, Y. Fan, Y. Mu, and T. Wang, "Numerical study on enhancing coalbed methane recovery by injecting n2/co2 mixtures and its geological significance," *Energy Science & Engineering*, vol. 8, no. 4, pp. 1104–1119, 2020.

[70] S. Bachu, J. C. Shaw, and R. M. Pearson, "Estimation of oil recovery and co2 storage capacity in co2 eor incorporating the effect of underlying aquifers," in *SPE/DOE symposium on improved oil recovery*. OnePetro, 2004.

[71] R. Hadlow, "Update of industry experience with co2 injection," in *SPE annual technical conference and exhibition*. OnePetro, 1992.

[72] D. J. Stephenson, A. G. Graham, and R. W. Luhning, "Mobility control experience in the joffre viking miscible co2 flood," *SPE Reservoir Engineering*, vol. 8, no. 03, pp. 183–188, 1993.

[73] T. Holt, J.-I. Jensen, and E. Lindeberg, "Underground storage of co2 in aquifers and oil reservoirs," *Energy Conversion and Management*, vol. 36, no. 6-9, pp. 535–538, 1995.

[74] N. NETL, "Carbon dioxide enhanced oil recovery-untapped domestic energy supply and long term carbon storage solution," *The Energy Lab*, 2010.

[75] D. LAW, S. HUANG, N. FREITAG, E. PERKINS, F. WASSMUTH, B. DUNBAR, and K. ASGHARI, "Theme 3: Co2 storage capacity and distribution predictions and the application of economic limits," *IEA GHG WEYBURN CO2 MONITORING & STORAGE PROJECT SUMMARY REPORT 2000-2004*, p. 149.

[76] J. Shi and S. Durucan, "Co2 storage in deep unminable coal seams," *Oil & gas science and technology*, vol. 60, no. 3, pp. 547–558, 2005.

[77] R. M. Flores, *Coal and coalbed gas: fueling the future*. Newnes, 2013.

[78] M. Hightower and A. Sattler, "Managing coal bed methane produced water for beneficial uses, initially using the san juan and raton basins as a model," 2006.

[79] M. Taulis and M. Milke, "Chemical variability of groundwater samples collected from a coal seam gas exploration well, maramarua, new zealand," *Water research*, vol. 47, no. 3, pp. 1021–1034, 2013.

[80] R. Hunt and E. Franklin, "How it came about—personal reflections on the origin and the development of lca in the usa," *Int J Life Cycle Assess*, vol. 1, pp. 4–7, 1996.

[81] O. Bonifaz, H. Nikodem, and W. Klopper, "Lca-how it came about: An early systems analysis of packaging for liquids," *The International Journal of Life Cycle Assessment*, vol. 1, no. 2, pp. 62–65, 1996.

[82] I. Boustead, "Lca—how it came about: The beginning in the uk," *The International Journal of Life Cycle Assessment*, vol. 1, no. 3, pp. 147–150, 1996.

[83] L. Hoffman and A. Schmidt, "Life cycle assess-ment. a guide to approaches, experiences and in-formation sources," *Man. of Environ. Quality: an int. Jour*, vol. 17, no. 4, pp. 490–507, 1997.

[84] "Environmental management – life cycle assessment – principles and framework," 1997.

[85] H. Vagt, F. Rubik, K. Jacob, G. Huppes, and T. Ekvall, "Lca options for sustainable governance assessed," 2009.

[86] "American center for life cycle assessment (aclca), 2004, increasing knowledge and promoting the use of life cycle assessment in the united states." https://lcacenter.org/pdf/ACLCAplan.pdf, 2004, assessed at 21 March 2007.

[87] E. C. (EC), ", european platform on life cycle assessment website," http://lca.jrc.ec.europa.eu/EPLCA/index.htm, 2008, assessed at 18 December 2008.

[88] J. Reap, F. Roman, S. Duncan, and B. Bras, "A survey of unresolved problems in life cycle assessment: Part 2: Impact assessment and interpretation," *The International Journal of Life Cycle Assessment*, vol. 13, pp. 374–388, 2008.

[89] A. Zamagni, P. Buttol, P. Porta, R. Buonamici, P. Masoni, J. Guinee, R. Heijungs, T. Ekvall, R. BERSANI, A. Bienkowska *et al.*, *Critical review of the current research needs and limitations related to ISO-LCA practice*, 2008.

[90] S. Durucan, A. Korre, and G. Munoz-Melendez, "Mining life cycle modelling: a cradle-to-gate approach to environmental management in the minerals industry," *Journal of Cleaner production*, vol. 14, no. 12-13, pp. 1057–1070, 2006.

[91] J. Wainwright and M. Mulligan, *Environmental modelling: finding simplicity in complexity*. John Wiley & Sons, 2013.

[92] B. Weidema, N. Fress, E. Petersen, and H. Ølgaard, "Reducing uncertainty in lci: Developing a data collection strategy," *Environmental project*, vol. 862, p. 2003, 2003.

[93] A. Korre, J. Q. Shi, C. Imrie, C. Grattoni, and S. Durucan, "Coalbed methane reservoir data and simulator parameter uncertainty modelling for co2 storage performance assessment," *international journal of greenhouse gas control*, vol. 1, no. 4, pp. 492–501, 2007.

[94] P. W. Riemer and W. G. Ormerod, "International perspectives and the results of carbon dioxide capture disposal and utilisation studies," *Energy Conversion and Management*, vol. 36, no. 6-9, pp. 813–818, 1995.

[95] B. Sass, B. Monzyk, S. Ricci, A. Gupta, B. Hindin, and N. Gupta, "Impact of sox and nox in flue gas on co2 separation, compression, and pipeline transmission," *Carbon dioxide capture for storage in deep geologic formations*, vol. 2, pp. 955–981, 2005.

[96] I.-Y. Lee, D.-W. Kim, J.-B. Lee, and K.-O. Yoo, "A practical scale evaluation of sulfated v205/tio2 catalyst from metatitanic acid for selective catalytic reduction of no by nh3," *Chemical Engineering Journal*, vol. 90, no. 3, pp. 267–272, 2002.

[97] R. Dugas, G. T. Rochelle, and F. Seibert, "Co2 capture performance of a monoethanolamine pilot plant," in *Proceedings of the 8th international conference on Greenhouse Gas Control Technologies. Norway*, 2006.

[98] P. Feron, "Progress in post-combustion co_2 capture," in *First Regional Carbon Management Symposium, Dharan, Saudi Arabia, 2006*, vol. 19, 2006.

[99] D. G. Chapel, C. L. Mariz, and J. Ernest, "Recovery of co2 from flue gases: commercial trends," in *Canadian society of chemical engineers annual meeting*, vol. 4. Citeseer, 1999.

[100] O. Bolland and P. Mathieu, "Comparison of two co2 removal options in combined cycle power plants," *Energy Conversion and Management*, vol. 39, no. 16-18, pp. 1653–1663, 1998.

[101] A. B. Rao, E. S. Rubin, and M. B. Berkenpas, "An integrated modeling framework for carbon management technologies," Carnegie Mellon University (US), Tech. Rep., 2004.

[102] H. Nalbandian, "Air pollution control technologies and their interactions," 2004.

[103] A. O. Alawode, "Oxidative degradation of piperazine in the absorption of carbon dioxide," Ph.D. dissertation, 2005.

[104] N. Imai, "Advanced solvent to capture co2 from flue gas," in *2nd International forum on geological sequestration of CO2 in deep, unmineable coal seams*, 2003.

[105] G. S. Goff, "Oxidative degradation of aqueous monoethanolamine in co2 capture processes: iron and copper catalysis, inhibition, and o2 mass transfer," Ph.D. dissertation, University of Texas at Austin Austin, TX, 2005.

[106] I. GHG, "Environmental impact of solvent scrubbing of co2," *TNO Science and Industry, IEA Greenhouse Gas R&D Programme*, vol. 14, p. 2006, 2006.

[107] "Transmission of co2 and energy," 2002.

[108] G. Heggum, T. Weydahl, R. Mo, M. Mølnvik, and A. Austegaard, "Chapter 15—co2 conditioning and transportation, carbon dioxide capture for storage in deep geologic formations, vol 2, dc thomas and sm benson, ed," 2005.

[109] M. Seiersten and K. Kongshaug, "Materials selection for capture, compression, transport and injection of co2," *Carbon Dioxide Capture for Storage in Deep Geologic Formations*, vol. 2, p. 937, 2005.

[110] J. Marion, C. Bozzuto, N. Nsakala, and G. Liljedahl, "Evaluation of advanced coal combustion & gasification power plants with greenhouse gas emission control," *Topical Phase-I DOE-NETL Report, Prepared by ALSTOM Power Inc*, 2003.

[111] M. Anheden, J. Yan, and G. De Smedt, "Denitrogenation (or oxyfuel concepts)," *Oil & gas science and technology*, vol. 60, no. 3, pp. 485–495, 2005.

[112] B. Guo, A. Ghalambor, and C. Xu, "A systematic approach to predicting liquid loading in gas wells," in *SPE production operations symposium*. OnePetro, 2005.

[113] A. B. Rao and E. S. Rubin, "A technical, economic, and environmental assessment of amine-based co2 capture technology for power plant greenhouse gas control," *Environmental science & technology*, vol. 36, no. 20, pp. 4467–4475, 2002.

[114] A. Kohl and R. Nielsen, "Gas purification, 1997," *Houston: Elsevier*, 2011.

[115] C. Hamelinck, H. Schreurs, A. Faaij, G. Ruijg, D. Jansen, H. Pagnier, F. v. Bergen, K.-H. Wolf, O. Barzandji, and H. Bruining, "Potential for co2 sequestration and enhanced coalbed methane production in the netherlands," 2006.

[116] J. Heller and J. Taber, "Influence of reservoir depth on enhanced oil recovery by co2 flooding," in *Permian Basin Oil and Gas Recovery Conference*. OnePetro, 1986.

[117] S. T. McCoy, "The economics of co2, transport by pipeline and storage in saline aquifers and oil reservoirs," Ph.D. dissertation, Sean T. McCoy, 2008.

[118] D. H.-S. Law and S. Bachu, "Hydrogeological and numerical analysis of co2 disposal in deep aquifers in the alberta sedimentary basin," *Energy conversion and management*, vol. 37, no. 6-8, pp. 1167–1174, 1996.

[119] A. Carcoana, "Applied enhanced oil recovery," 1992.

[120] J. Ennis-King and L. Paterson, "Engineering aspects of geological sequestration of carbon dioxide," in *SPE Asia Pacific Oil and Gas Conference and Exhibition*. OnePetro, 2002.

[121] P. Saripalli and P. McGrail, "Semi-analytical approaches to modeling deep well injection of co2 for geological sequestration," *Energy Conversion and Management*, vol. 43, no. 2, pp. 185–198, 2002.

[122] M. Hesse, A. Riaz, and H. Tchelepi, "Resolving density fingering during co2 sequestration: A challenge for reservoir simulation," *CO2SC 2006*, 2006.

[123] A. Riaz, M. Hesse, H. Tchelepi, and F. Orr, "Onset of convection in a gravitationally unstable diffusive boundary layer in porous media," *Journal of Fluid Mechanics*, vol. 548, pp. 87–111, 2006.

[124] D. B. Silin, T. W. Patzek, and S. M. Benson, "Exact solutions in a model of vertical gas migration," in *SPE Annual Technical Conference and Exhibition*. OnePetro, 2006.

[125] J.-P. Nicot, R. Bouroullec, H. Castellanos, S. Hovorka, S. Lakshminarasimhan, and J. Paine, "Development of science-based permitting guidance for geological sequestration of co2 in deep saline aquifers based on modeling and risk assessment," Univ. of Texas, Austin, TX (United States), Tech. Rep., 2006.

[126] A. Brown, "Evaluation of possible gas microseepage mechanisms," *AAPG bulletin*, vol. 84, no. 11, pp. 1775–1789, 2000.

[127] M. A. Celia, D. Kavetski, J. M. Nordbotten, S. Bachu, and S. Gasda, "Implications of abandoned wells for site selection," in *Proceedings CO2SC*, 2006, pp. 20–22.

[128] M. Y. Corapcioglu, A. Cihan, and M. Drazenovic, "Rise velocity of an air bubble in porous media: Theoretical studies," *Water resources research*, vol. 40, no. 4, 2004.

[129] C. M. Oldenburg and A. J. Unger, "On leakage and seepage from geologic carbon sequestration sites: unsaturated zone attenuation," *Vadose Zone Journal*, vol. 2, no. 3, pp. 287–296, 2003.

[130] A. S. Altevogt and M. A. Celia, "Modeling carbon dioxide transport in unsaturated soils," in *Developments in Water Science*. Elsevier, 2002, vol. 47, pp. 41–47.

[131] G. Bozzano and M. Dente, "Shape and terminal velocity of single bubble motion: a novel approach," *Computers & chemical engineering*, vol. 25, no. 4-6, pp. 571–576, 2001.

[132] P. G. Brewer, E. T. Peltzer, G. Friederich, and G. Rehder, "Experimental determination of the fate of rising co2 droplets in seawater," *Environmental science & technology*, vol. 36, no. 24, pp. 5441–5446, 2002.

[133] N. Christensen and S. Holloway, "Geological storage of co2 from combustion of fossil fuel. summary report of the gestco project. geological survey of denmark and greenland," *British Geological Survey*, 2003.

[134] M. Corsten, A. Ramírez, L. Shen, J. Koornneef, and A. Faaij, "Environmental impact assessment of ccs chains–lessons learned and limitations from lca literature," *International Journal of Greenhouse Gas Control*, vol. 13, pp. 59–71, 2013.

[135] B. Singh, A. H. Strømman, and E. G. Hertwich, "Comparative life cycle environmental assessment of ccs technologies," *International Journal of Greenhouse Gas Control*, vol. 5, no. 4, pp. 911–921, 2011.

[136] "Ieaghg, 2010. environmental evaluation of ccs using life cycle assessment (lca)," *UK,International EnergyAgency Greenhouse Gas R&D Programme*, 2010.

[137] M. R. Abu-Zahra, L. H. Schneiders, J. P. Niederer, P. H. Feron, and G. F. Versteeg, "Co2 capture from power plants: Part i. a parametric study of the technical performance based on monoethanolamine," *International Journal of Greenhouse gas control*, vol. 1, no. 1, pp. 37–46, 2007.

[138] C. Wildbolz, "Life cycle assessment of selected technologies for co2 transport and sequestration," *Diplom Thesis. Zurich: Swiss Federal Institute of Technology*, 2007.

[139] ——, "Life cycle assessment of selected technologies for co2 transport and sequestration," *Diplom Thesis. Zurich: Swiss Federal Institute of Technology*, 2007.

[140] D. J. Griggs and M. Noguer, "Climate change 2001: the scientific basis. contribution of working group i to the third assessment report of the intergovernmental panel on climate change," *Weather*, vol. 57, no. 8, pp. 267–269, 2002.

[141] N. Bech and M. Larsen, "Storage of co2 in the havnsø aquifer-a simulation study," *A CO2STORE contribution. Danmarks*, vol. 2, 2005.

[142] B. Metz, O. Davidson, R. Swart, and J. Pan, *Climate change 2001: mitigation: contribution of Working Group III to the third assessment report of the Intergovernmental Panel on Climate Change*. Cambridge university press, 2001.